LEVEL III

12 B.S.

CERAMIC PIEZOELECTRIC TRANSDUCERS.

Annual Summary Report.
1 Jan - 31 Dec 77,

Period Jan. 1, 1977 to Dec. 31, 1977

Contract No. N00014-76-C-0515, ARPA Order-3203

Project No. 3203

12 157p.

Sponsored by 11 Jan 78

Advanced Research Projects Agency (DOD)

ARPA Order No. 3203

Office of Naval Research

Contract No. N00014-76-C-0515

Monitored by ONR

APPROVED FOR PUBLIC RELEASE: DISTRIBUTION UNLIMITED

L.E. Cross,
J.V. Biggers
R.E. Newnham

MATERIALS RESEARCH LABORATORY

THE PENNSYLVANIA STATE UNIVERSITY

UNIVERSITY PARK, PENNSYLVANIA 16802

LEVEL II

(12)

CERAMIC PIEZOELECTRIC TRANSDUCERS

Annual Summary Report

to the

Office of Naval Research
Arlington, Virginia 22217

Contract No. N00014-76-C-0515

January 1978

L.E. Cross
J.V. Biggers
R.E. Newnham

CONTENTS

ABSTRACT

This report documents work performed during the period January 1 to December 31, 1977 under joint ONR-DARPA sponsorship. This period covers the second year of a three year program focused upon the tasks associated with the development of new and improved materials for ceramic piezoelectric transducers, and with improving the understanding of the processing and properties of present PZT ceramics.

A major part of the effort has been concerned with the development of new techniques for the fabrication of diphasic ceramic and ceramic:plastic composites and with investigation of the manner in which local and macroscopic symmetry and phase interconnection (connectivity) controls the coupled elasto-electric (piezoelectric) and thermo-elasto-electric (pyroelectric) properties of the composite. Replicating a natural microstructure of desired connectivity, a new type of flexible ceramic elastomer composite has been developed which exhibits g_{33} constants over an order of magnitude larger than PZT and has interesting potential for many passive voltage generation applications such as in hydrophones and towed arrays.

Tape casting (doctor blade) methods are being used to explore a wide range of potentially interesting lamellar heterogeneous systems with ferroelectric, antiferroelectric and interleaved electrode configurations. New pretreatments of the cast tapes are being studied to equalize shrinkage in the different compositions during firing and poling and property studies are now in progress for a number of these new composite systems.

Electrostriction transducers in the ferroelectric relaxor family $Pb_3MgNb_2O_9$:$PbTiO_3$ have been studied, and in cooperation with Corning Research Center extruded multi-element transducer structures incorporating these materials are being investigated.

The ADAGE computer graphics faciilty at Penn State is being used to develop a family of Elastic Gibbs functions for the PZT solid solution system and to study the full three dimensional polarization surfaces in the vicinity of the morphotropic phase boundary.

Processing studies have been performed on PZT and on various relaxor ferroelectric formulations. Preparation, calcining, fabrication and densification procedures have had to be developed both for conventional single phase, and for the more unusual diphasic systems presently under study.

1. INTRODUCTION

This report documents work performed during the period January 1 to December 31, 1977 under joint ONR-DARPA sponsorship. This period covers the second year of a three year program focused upon the tasks associated with the development of new and improved materials for ceramic piezoelectric transducers, and with improving the understanding of the processing and properties of present PZT ceramics.

Over the past year a major part of the effort has been concerned with developing techniques for the fabrication of diphasic and polyphasic ceramics and ceramic:plastic composites, and with investigating both theoretically and experimentally the manner in which local and macroscopic symmetry and the mode of phase interconnection (connectivity) controls the coupled elasto-electric (piezoelectric) and thermo-elasto-electric (pyroelectric) properties of the composites.

A special ceramic replication has been developed which enables a natural micro structure with the desired form of phase connection to be replicated in PZT, yielding a completely new type of ceramic:elastomer composite in which the PZT phase can be poled to saturation remanence from simple surface electrodes. This material exhibits g_{33} constants over an order of magnitude larger than the present PZT, is highly flexible and robust to handle. This material appears to have very interesting potential for many passive voltage generation applications such as in hydrophones and in towed arrays. A patent application has been submitted to cover the special replication procedure used.

Tape casting (doctor blade) methods are being used to explore a wide range of potentially interesting lamellar heterogeneous systems with ferroelectric, antiferroelectric and interleaved electrode configurations. New pretreatments of the cast tapes are being studied to equalize shrinkage in the

different compositions during firing and poling and property studies are now in progress for a number of these new composite systems.

For more specialized applications, where a transducer is used for "slow" precise position control, as in optical interferometers, phase correction mirrors and multiposition mirrors, high permittivity compositions in the $BaTiO_3$: $CaZrO_3$ and $Pb_3MgNb_2O_9$:$PbTiO_3$ systems are being studied. These materials are dominantly in the paraelectric phase, and dimension control is obtained through the high intrinsic quadratic electrostrictive effect. Since stable ferroelectric domain structures do not occur, the problems of dimensional creep and non-reproducibility (aging and de-aging effects) of the conventional piezoceramic are largely eliminated. Current studies suggest that for suitably chosen compositions in the $Pb_3MgNb_2O_9$:$PbTiO_3$ family "effective" electrostriction constants may be more than 10 times those of the conventional $BaTiO_3$ based ceramics. We are now working with Corning Research Center to exploit these larger electrostriction properties in extruded multi-element transducer structures.

A second major part of this program is aimed at achieving a better understanding of the very complex interactions between single domain, domain wall and phase boundary contributions which control the electrical, mechanical and electromechanical properties of the present PZT materials, and particularly with the manner in which processing and the resultant ceramic microstructure modulate these interactions. To this end, we have used the ADAGE computer graphics system at Penn State to develop computational techniques to handle and display the phenomenological Elastic Gibbs functions for perovskite ferroelectrics. In specializing the function to the PZTs, we use those facets of the behavior which are least likely to be grossly perturbed by the ceramic microstructure, namely the phase transition temperatures and the spontaneous strains as a function of temperature in the ferroelectric phases. This work is now at the stage where

the whole phase diagram for the "single cell" pure PZTs is adequately described by the function, and the parameters are in the final stage of refinement to fit the spontaneous strains with temperature independent electrostriction constants. The ADAGE graphics capability allows a simple visualization of the three dimensional polarization surfaces at any energy level and a direct method of viewing the possible switching trajectories between rhombohedral and tetragonal phases under elastic or electric stress. It is our intention to use the refined energy function to compute single domain dielectric and piezoelectric properties and to ascertain the manner in which these properties may be perturbed by realizable elastic and electric stress fields in the ceramic.

Considerable work on the processing of PZT and of various electrostrictor formulations has been required to underpin the whole materials effort. Preparation, calcining, fabrication and densification procedures have had to be developed both for the single phase, and for the more unusual mixed phase materials.

For the conventional mixed oxide starting materials, problems associated with the variability of the ZrO_2 powders available to the PZT manufacturers have been studied, and new evidence adduced as to the influence of the state of aggregation of the ZrO_2 upon calcining behavior and upon sintering and resultant microstructure.

Work on the contract has been described in the following papers presented at National and International Meetings (page iv) and in the papers which have been published or are accepted for publication (page v).

In the following report, a very brief narrative description is given of the present ongoing work in the areas of electrostrictors, diphasic materials, phenomenological studies, processing work, and amorphous materials. Studies which have been written up for publication are included as appendices to the report and are referred to in the text in the appropriate sections.

Papers Presented at National and International Meetings

1. L. E. Cross and H. A. McKinstry. A Computer Graphic Presentation of the Polarization Surface of Constant Elastic Gibbs Free Energy in Perovskite-Type Ferroelectrics. American Ceramic Society Meeting, Chicago, 1977.

2. R. E. Newnham, J. J. Kramer, A. SaNeto and T. Cline. Second Harmonic Generation by Ceramic Materials. American Ceramic Society Meeting, Chicago, 1977.

3. W. A. Schulze, J. V. Biggers and L. E. Cross. Aging of Dielectric Dispersion in PLZT Relaxor Ceramics. American Ceramic Society Meeting, Chicago, 1977.

4. D. P. Skinner, R. E. Newnham and L. E. Cross. Dielectric and Piezoelectric Studies on Layer Structure Titanates. American Ceramic Society Meeting, Chicago, 1977.

5. R. C. Pohanka and L. E. Cross. Inorganic Glass and Glass-Ceramic Ferroelectric Dielectrics. American Ceramic Society Meeting, Chicago, 1977.

6. L. E. Cross and H. McKinstry. Analysis of Phenomenological Energy Functions for Perovskite Ferroelectrics using an ADAGE Computer Graphics System. *IV International Meeting on Ferroelectrics* (IMF4), Leningrad, Sept. 1977.

7. S. Venkataramani, L. J. Tarhay and J. V. Biggers. Role of Chemically Prepared ZrO_2 on Properties of PZT Ceramics. American Ceramic Society, Fall Meeting, Montreal, 1977.

8. K. A. Klicker and J. V. Biggers. Control of Lead Atmosphere During Sintering of PZT Ceramics. American Ceramic Society, Fall Meeting, Montreal, 1977.

9. T. R. Shrout, W. A. Schulze and J. V. Biggers. Processing Effects on Microstructure of Tape Cast PZT Ceramics. American Ceramic Society, Fall Meeting, Montreal, 1977.

10. D. L. Hankey, L. J. Tarhay and J. V. Biggers. Commercial Powder Characteristics of ZrO_2 and Their Effect on PZT Processing. American Ceramic Society, Fall Meeting, Montreal, 1977.

11. D. P. Skinner, R. E. Newnhan and L. E. Cross. Diphasic Transducers. American Ceramic Society, Fall Meeting, Montreal, 1977.

12. W. A. Schulze, L. E. Cross and W. R. Buessem. Degradation of $BaTiO_3$ Ceramic Under High AC Electric Fields. American Ceramic Society, Fall Meeting, Montreal, 1977.

Papers Published

1. A. S. Bhalla, L. E. Cross. A Simple Technique for Decorating Ferroelectric Domains in Gadolinuim Molybdate. J. Mat. Sci. 12:2364 (1977).

2. S. T. Liu, L. E. Cross. Primary Pyroelectricity in Strontium Barium Niobate $(Sr_{0.5}Ba_{0.5})Nb_2O_6$ Single Crystals. Phys. Stat. Sol. (a) 41:K83 (1977).

3. J. V. Biggers, D. L. Hankey, L. Tarhay. The Role of ZrO_2 Powders in the Microstructural Development of PZT Ceramics. Proc. Int. Conf. on Ceramic Processing, Raleigh, NC (Nov. 1977).

4. W. A. Schulze, J. V. Biggers, L. E. Cross. Aging of Dielectric Dispersion in PLZT Relaxor Ceramics. J. Am. Ceram. Soc. (Accepted).

5. T. W. Cline, L. E. Cross, S. T. Liu. Dielectric Behavior of Strontium Barium Niobate ($Sr_{0.5}Ba_{0.5}Nb_2O_6$) Single Crystals. J. Appl. Phys. (Accepted).

2. CERAMICS FOR ELECTROSTRICTION TRANSDUCERS

2.1 INTRODUCTION

Very early in the evolution of piezoceramic materials, "soft" low coercivity ferroelectric ceramics were often used under DC bias for piezoelectric applications. However, with the evolution of the PZT family, where the effective coercivity could be controlled by suitable 'doping' systems the present generation of poled piezoceramics completely replaced these early electrostrictive devices. Over the last ten years, however, the rapid development of tape cast multilayer technology, and the ensuing development of new high K low saturation anhysteretic capacitor dielectric formulations has considerably changed the situation.

The observation of very efficient ultrasound generation from simple high K multilayer chip capacitors by G. Kino and colleagues at Stamford suggested that a new look at electrostrictive devices based on the multilayer configuration would be most desirable. Earlier work (*1976 Report*) confirmed the large strain effects in commercial $BaTiO_3$ based capacitor formulations, and the potential utility of these electrostrictive effects for certain device configurations.

Over the past year, the major effort on materials for potential application in electrostriction transducer systems has focused upon a study of the ferroelectric relaxor dielectrics. It has been proposed (1,2,3) that in these systems there is a spatially inhomogeneous distribution of cations in the crystal lattice, giving rise to a broad spatial distribution of ferroelectric Curie temperature and the coexistence of ferroelectric and paraelectric phases over a wide temperature range. Lead magnesium niobate (PMN)($Pb_3MgNb_2O_9$) is perhaps the most thoroughly studied example in the perovskite family of ferroelectrics, and a very extensive literature documents structure, dielectric, optical, electrooptical and nonlinear optical properties of this compound. Surprisingly little, however, appears to have been reported on the electromechanical properties of this or of other relaxor materials, although PMN itself is quite widely used in Japan as one component in ternary $PbTiO_3$:$PbZrO_3$:$Pb_3MgNb_2O_9$ ceramic transducer formulations.

Early optical studies show clearly that above -20°C PMN has no stable remanent polarization, even though large polarization levels can be field induced, with corresponding high stable quadratic electrooptic response. Clearly if the quadratic electrostriction constants in this structure are "normal" high stable quadratic electrostriction should also occur. This was shown to be the case, and PMN itself is superior to modified $BaTiO_3$ in its electrostrictive response. The response can be further improved if the Curie range, which is below room temperature in PMN, could be shifted to slightly higher temperature, and our major effort has been focused on solid solution systems based upon PMN which might accomplish this goal.

Initial studies have been focused on the following solid solution systems:

(1) $PbMg_{1/3}Nb_{2/3}O_3$:$Pb(Mg_{1/2}W_{1/2})O_3$

This system was selected to investigate the evolution of properties across a solid solution field between a disordered relaxor (PMN) and a cation ordered antiferroelectric (PMW).

(2) $Pb(Mg_{1/3}Nb_{2/3})O_3$:$Pb(Zn_{1/3}Nb_{2/3})O_3$

Selected to study the evolution from a relaxor of lower Curie range (PMN) to a relaxor with a higher Curie range (PZnN).

(3) $Pb(Mg_{1/3}Nb_{2/3})O_3$:$PbTiO_3$

A solid solution between the relaxor and a simple tetragonal ferroelectric (abrupt transition) material.

(4) $PbMg_{1/3}Nb_{2/3}O_3$:$PbTiO_3$:$BaZn_{1/3}Nb_{2/3}O_3$

When it became apparent in the studies under (2) above that we could not stabilize the PZnN against the pyrochlore alternative structure, even in solid solution with PMN, this sequence was chosen as a possible indirect route to stabilizing the higher temperature relaxor, with, we believe, most interesting results.

In parallel with these extensive material studies, a lower level program has been carried on in cooperation with Corning Research Center to investigate the possibility of using the extrusion techniques developed at Corning for

exhaust catalyst support structures to fabricate electrostriction transducer arrays for possible optical applications.

2.2 STUDIES OF RELAXOR FERROELECTRICS

2.2.1 Lead Magnesium Niobate: Lead Magnesium Tungstate

Initial dielectric studies showed that this system was not promising for transducer applications, since both the Curie range and the absolute level of the permittivity are reduced by PMW solid substitution, even though the antiferroelectric Curie point of PMW (39°C) is above room temperature. Nonetheless, work on the system has been actively pushed forward because of the high potential which we believe it holds for answering some of the more intractable general questions relating to the origin of the relaxor response in all systems.

Preparation, preliminary characterization and dielectric studies on this system have been written up for publication and are attached as Appendix 1 to this report. The basis for our continuing interest may be briefly summarized as follows:

(i) Complete solid solution between the two endmembers has been clearly demonstrated.

(ii) Relaxor character (a diffuse phase change) is preserved in compositions up to 80 mole % PMW.

(iii) Clear superlattice lines begin to appear in the x-ray spectrum which correspond with the superstructure observed in pure PMW, at compositions containing more than 20% PMW.

(iv) There is clear evidence of line broadening in the superstructure lines at low PMW concentrations which is not evident in the base structure lines. This broadening decreases steadily with increasing PMW concentration.

One of the most intractable problems in the relaxor systems is that of the scale of the compositional inhomogeneity which gives rise to the Curie point distribution in these crystals. For the PMN:PMW solid solutions the

dielectric data suggest a heterogeneity in the Nb^{5+}:W^{6+} distribution, but now W^{6+} rich regions are clearly labeled by the W^{6+}:Mg^{2+} structural ordering. We believe that both the size and the strain in these W^{6+}:Mg^{2+} ordered regions can be determined by intercomparison of the line broadening, and the position of the superstructure lines with respect to the base lattice reflections, and this work is now in progress.

2.2.2 $PMg_{1/3}Nb_{2/3}O_3$:$PbZn_{1/3}Nb_{2/3}O_3$

A number of compositions in this system were made up by solid state reaction of the constituent oxides (PbO, MgO, ZnO, Nb_2O_5) using a wide range of calcining temperature, with repeated calcining and regrinding, in an attempt to achieve homogeneous single phase perovskite compositions. In every case, however, even small additions of the PZnN to PMN resulted in the appearance of a significant pyrochlore structure phase.

We believe that, as in pure PZnN, it would be possible to suppress the pyrochlore structure phase by reacting under high pressure, but since the primary object of these studies was to examine systems which could be of practical interest, higher pressure studies were not carried out. We chose rather to try to induce a higher temperature relaxor phase through solid solution with $BaZn_{1/3}Nb_{2/3}O_3$, which is known to have a stable perovskite structure.

2.2.3 Lead Magnesium Niobate:Lead Titanate (PMN:PT)

2.2.3.1 Sample Preparation and Characterization

Ceramic samples of pure PMN, and of PMN:PT solid solutions were prepared from reagent grade oxides using techniques similar to those given in Appendix 1. Calcining schedules for the different compositions are given in Table 2.1, and the sintering conditions used and final densities achieved are given in Table 2.2. X-ray powder diffraction was used to confirm that all samples had the simple single cell cubic perovskite structure. Slow scan techniques were used for a precise measurement of the lattice spacing with composition in the short range of PT solid solution of interest to confirm proper formation.

TABLE 2.1

Composition	Calcining Time 15 Hours		
Mole Fraction PMN:PT	First	Second	Third
1.0:0.0	850°C	870°C	900°C
0.95:0.05	900°C	920°C	950°C
0.90:0.10	950°C	950°C	950°C

Calcining schedule for compositions in the PMN:PT solid solution system

TABLE 2.2

Composition	Sintering Temperature	Time	Fired Density
Mole Fraction PMN:PT			
1.0:0.0	1280°C	2 hours	7.40 gm/cc
0.95:0.05	1300°C	2 hours	7.45 gm/cc
0.90:0.10	1320°C	2 hours	7.41 gm/cc

Sintering conditions and fired densities for PMN:PT solid solutions

2.2.3.2 Dielectric Measurements

Pure PMN: Weak field dielectric permittivity as a function of frequency and temperature (Fig. 2.1) confirm the broad diffuse character of the ferroelectric phase change in this material, giving data in good agreement with earlier published values. Low frequency (0.1 Hz) hysteresis measurements taken by the modified Sawyer Tower method (Fig. 2.2) also confirm the absence of any true remanent polarization in PMN at room temperature. In exploring the high field dielectric saturation under large DC bias voltages, a new and interesting phenomenon was observed which appears to be characteristic of the ferroelectric relaxors. For temperatures above 25°C the measured permittivity decreases continuously with bias with ascending and descending fields tracing the same path (Fig. 2.3a). Below 25°C, however, in the relaxation region, an unusual inverse hysteresis is observed (Fig. 2.3b). At lower temperatures, the behavior again becomes largely anhysteretic then finally at still lower temperature, the expected butterfly curve of conventional ferroelectric behavior is observed (Fig. 2.3c,d).

This unusual saturation behavior was first observed in pure PMN ceramics, but has now been confirmed in PMN:PMW solid solutions with relaxor character and in the PMN:PT solid solutions to be described. Thus we are tempted to believe that it may be a phenomenon occurring in all ceramic relaxation dielectrics when measured within the dispersion range.

PMN:PT Solid Solutions: For compositions containing up to 10% PT, which are of most interest technologically, the dielectric relaxation character associated with diphase transition behavior is preserved, though the dispersion range decreases continuously with PT addition (Fig. 2.4). Hysteresis measurements confirm that compositions containing up to 10 mole % PT remain essentially anhysteretic under low frequency cycling fields. Under DC bias, the inverse hysteresis phenomenon in the dielectric saturation is observed in all compositions, although as the PT content increases the temperature range over which "inverse" loops are observed contracts (Fig. 2.5).

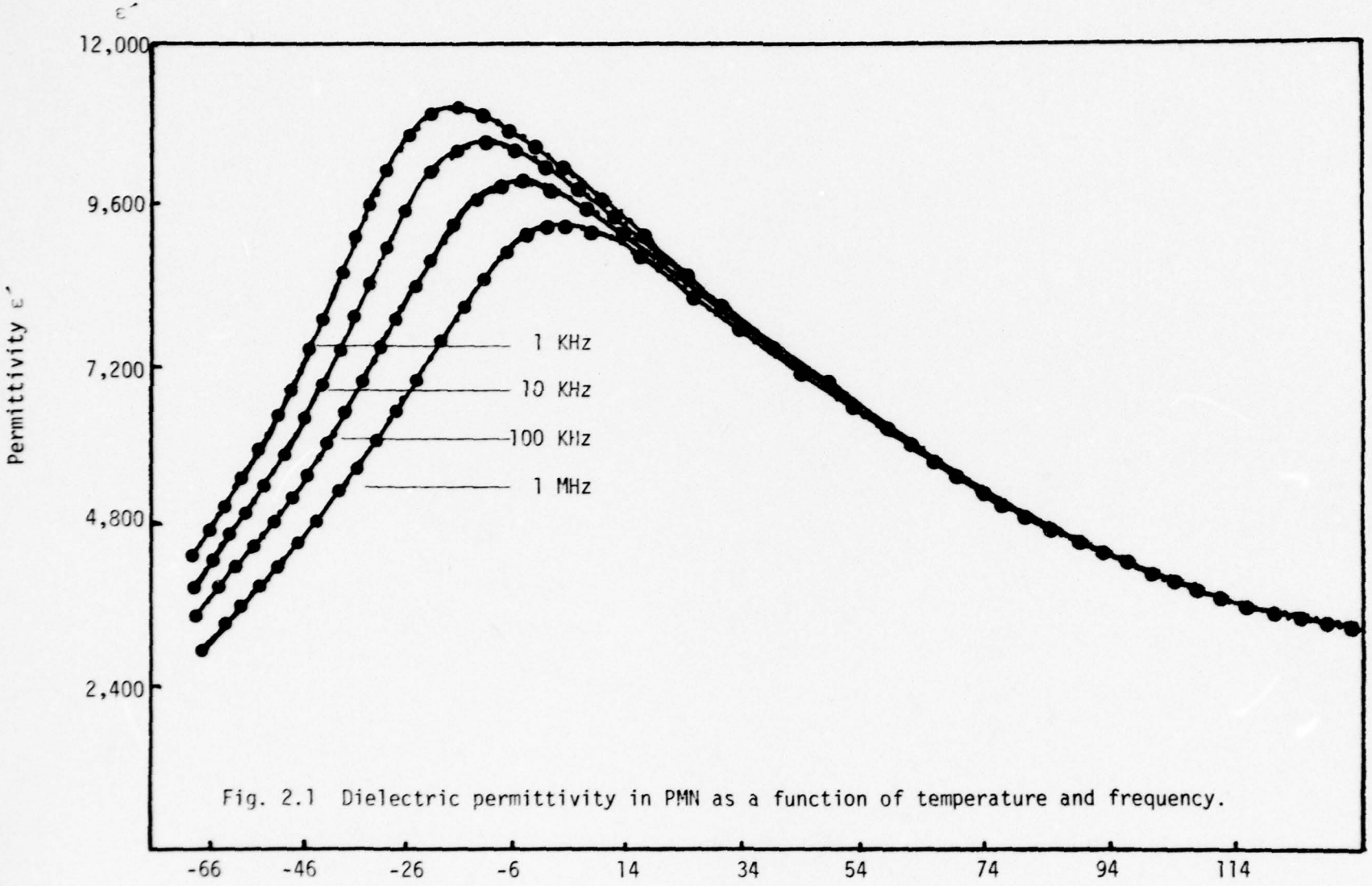

Fig. 2.1 Dielectric permittivity in PMN as a function of temperature and frequency.

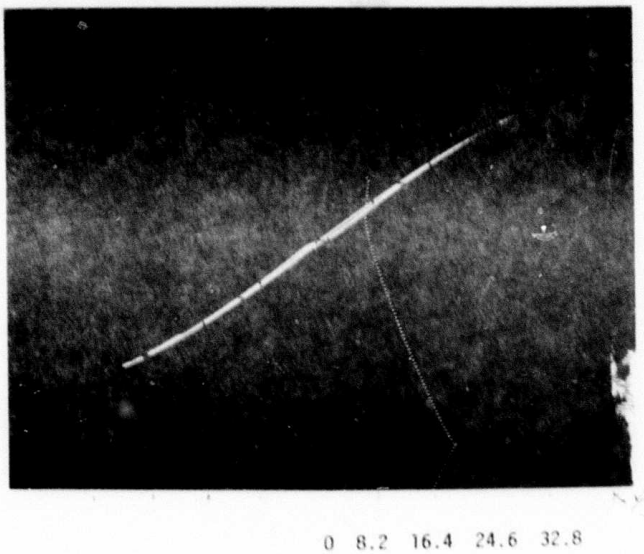

Fig. 2.2 Dielectric hysteresis in PMN at a frequency of 0.05 Hz (24°C)

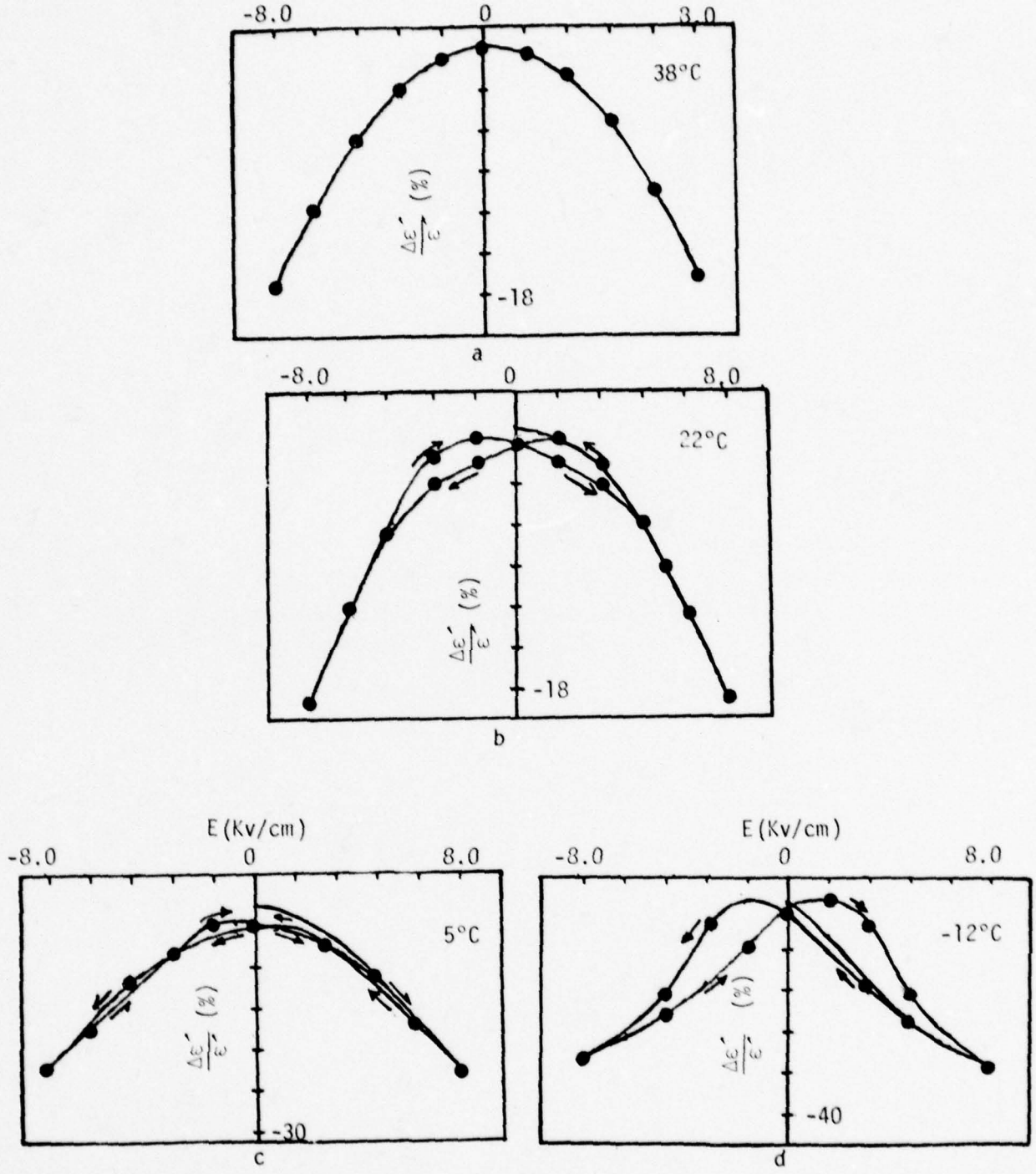

Fig. 2.3 Dielectric saturation as a function of electric field in 0.9XPMN-0.1XPT.

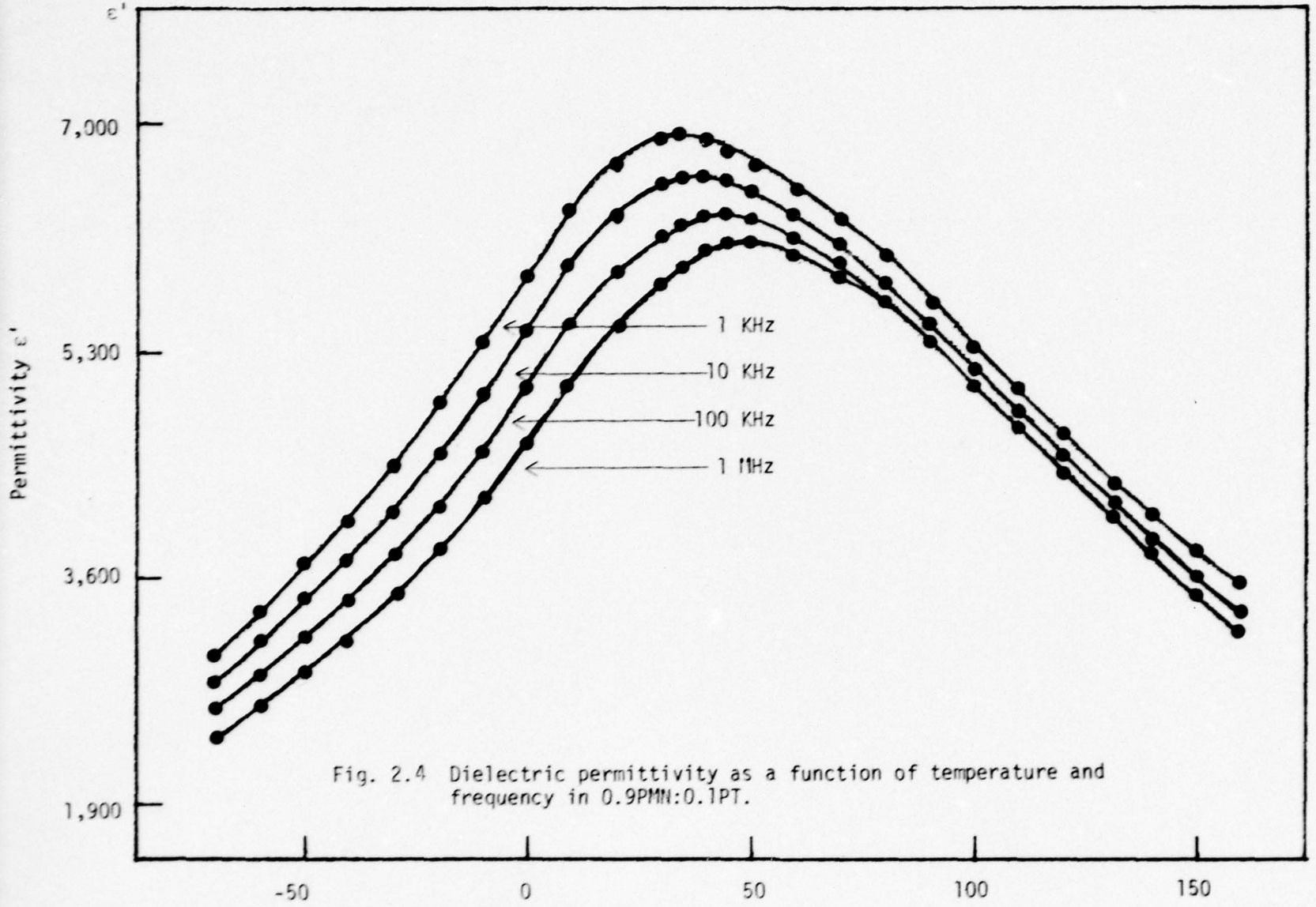

Fig. 2.4 Dielectric permittivity as a function of temperature and frequency in 0.9PMN:0.1PT.

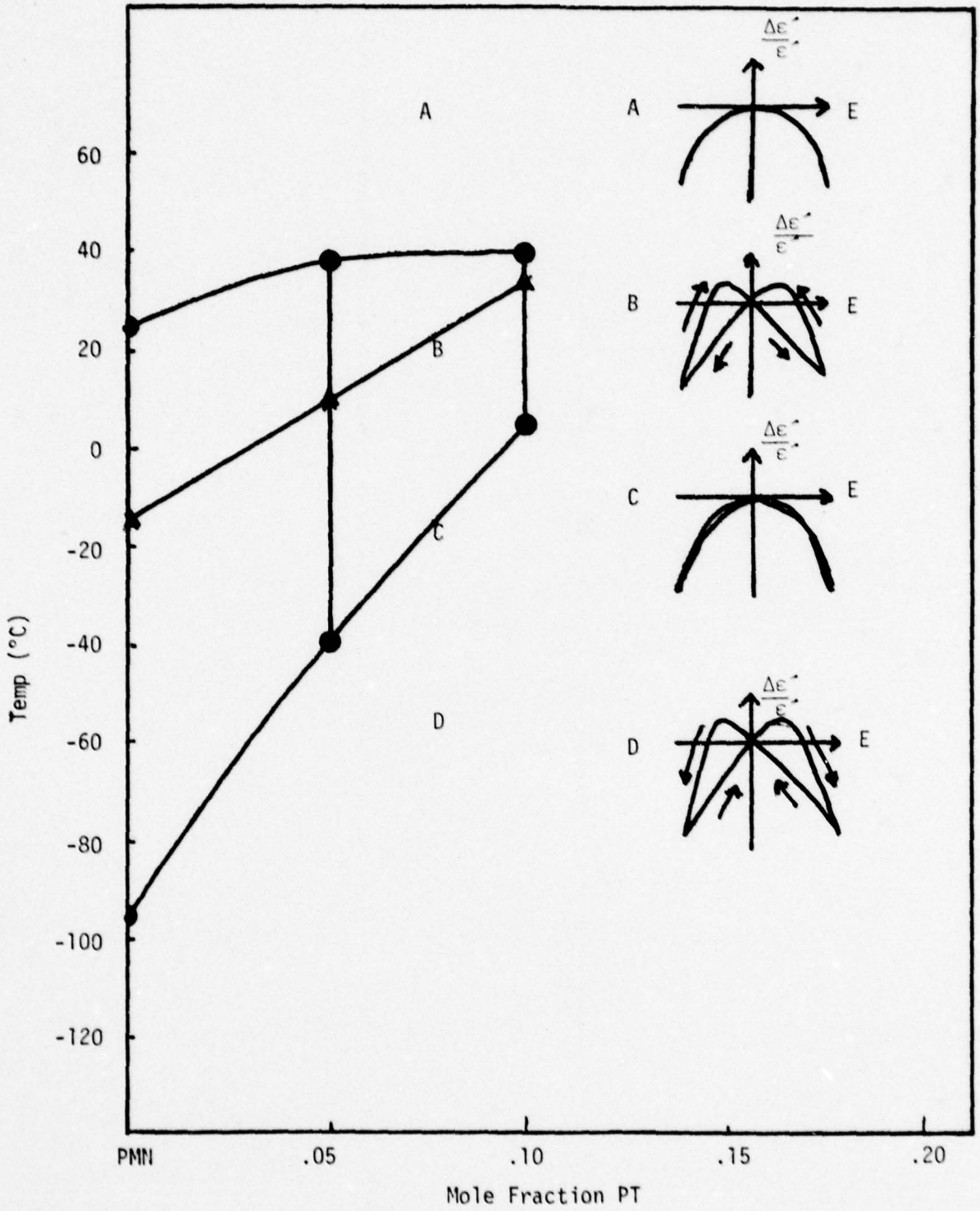

Fig. 2.5 Curie range in PMN:PT solid solutions.

2.2.3.3. Electrostriction Measurements

The quadratic electrostriction constant Q_{12} was determined from measurements of the transverse contraction in thin ceramic disks subjected to DC bias fields applied in a direction normal to the plane of the disk. The dimension change was measured using a differential transformer dilatometer at the larger dilatation levels, and a high sensitivity capacitance dilatometer at the lower strain level.

Transverse contraction as a function of bias field for PMN, PMN 5 mole % PT and PMN 10 mole % PT are shown in Fig. 2.6. For comparison the comparable data for a $BaTiO_3$ type K6,000 formulation is also shown. The PMN compositions are anhysteretic, and retrace the same curve both with rising and falling fields. The $BaTiO_3$ based composition shows a weak remanence, and only the data for rising fields are reproduced here.

Data for several other PMN solid solutions which have been studied are also included in Fig. 2.6 for reference.

At present we are constructing a more sensitive dilatometer with better absolute precision, so that the temperature and time dependence of the dilatation levels can be completely documented.

2.3 $PbMg_{1/3}Nb_{2/3}O_3$:$PbTiO_3$:$BaZn_{1/3}Nb_{2/3}O_3$

In an attempt to circumvent the instability in the PMN:PZnN phase system, several compositions in the PMN:PT:BaZnN solid solution system were fabricated. For this system, the compositions studied showed no tendency to develop pyrochlore structure phases and "solid solution" formation was evidenced in the continuous change of lattice parameters with composition.

Dielectric data, however, suggest the coexistence of two relaxation regions: one centered near 0°C which increases in magnitude with the mole fraction of PMN, the second near 110°C which increases with mole fraction of BaZnN (Fig. 2.7). The net result in intermediate regions appears to be a rather flat temperature dependence in the average permittivity over a very wide temperature range.

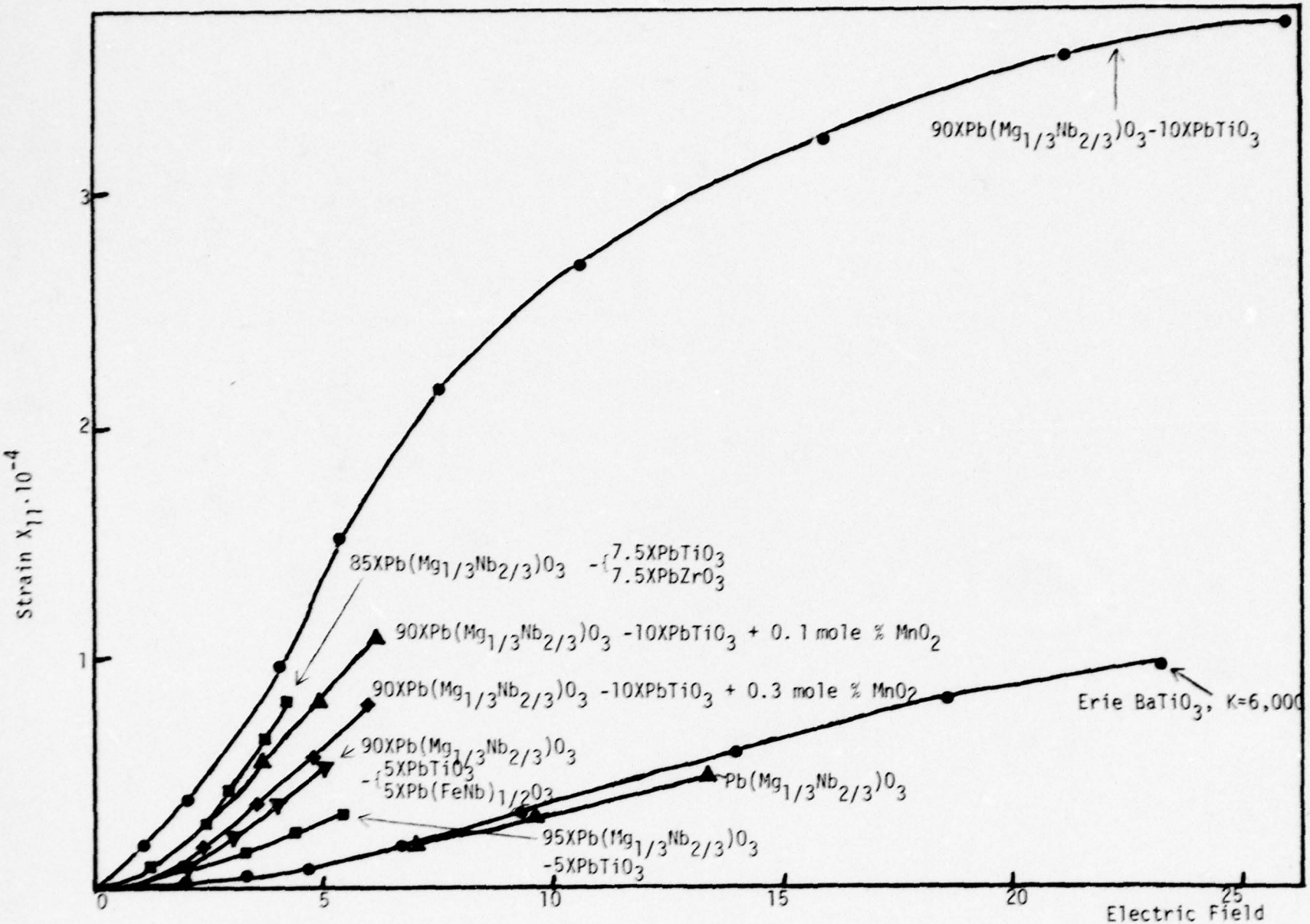

Fig. 2.6 Electrostrictive strain X_{11} as a function of electric field.

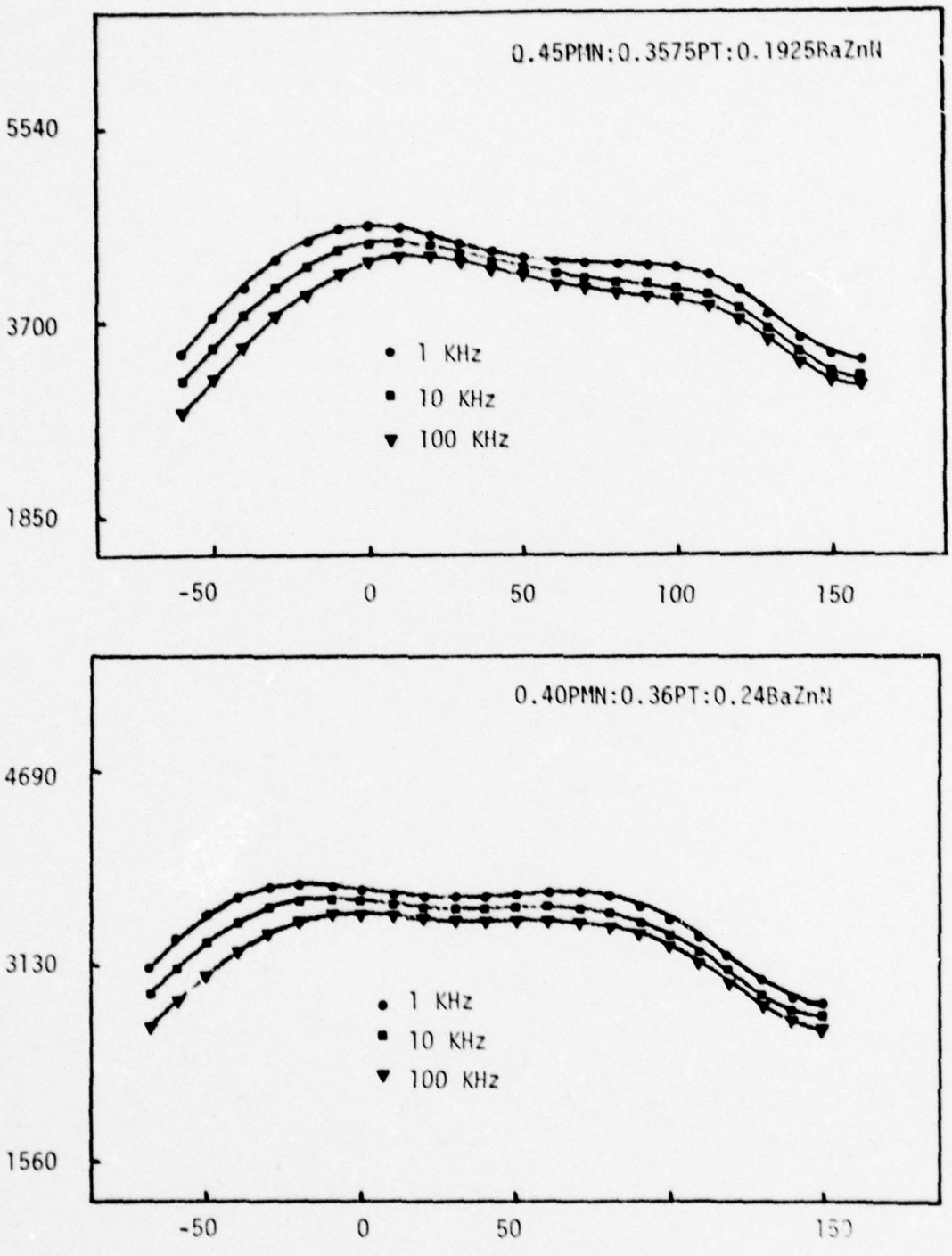

Fig. 2.7 Dielectric permittivity in PMN:PT:BaZnN solid solutions.

Since BaZnN shows low dielectric permittivity with no relaxor character, we believe that in these complex compositions there is partial conversion to PbZnN, stabilized in a perovskite form by the residual Ba^{2+}. The unexpected finding is that in these solid solutions, the two Curie ranges apparently do not amalgamate to a single diffuse relaxor peak, but to some extent retain their individual character more like a mixture of two separate phases.

This unexpected result does, however, suggest that with more study, we may be able to stabilize high permittivity behavior over a very broad temperature range and probably also enhance the temperature stability of the electrostriction behavior by using mixed systems of this type.

Dilatation studies are now proceeding on these more complex relaxor systems.

References

2.1 G.A. Smolenskii, A.I. Agronosvskaya. Soviet Phys. Tech. Phys. 3, 1380 (1958).

2.2 V.A. Bokov, I.E. Mylnikova. Soviet Phys.-Solid State 3 613 (1961).

2.3 L.E. Cross, J.W. Smith. Ferroelectrics 1, 137 (1970).

3. DIPHASIC MATERIALS

3.1 INTRODUCTION

The basic thinking which led to the expectation that two-phase systems might offer significant advantage for certain types of transducer applications has been summarized for publication and is attached as Appendix II to this report. Exploitation of these basic concepts has so far concentrated on two areas of study.

(1) The development of two-phase ceramic:plastic composites, using natural template microstructures to control the connectivity between phases so as to be able to produce PZT:plastic composites which could be poled to full saturation remanence from simple surface electrodes, then processed to give a mechanically flexible transducer with very high $\tilde{g}_{33}$ and $\tilde{g}_h$ coefficients which might find application in hydrophones and in towed array systems.

(2) Development of techniques to produce ceramic:ceramic composites with lamellar heterogeneous structures, which might exploit the wide range of phases available in the PZT and PSnZT family. To integrate noble metal electrodes interleaving the lamellae for impedance control, and to explore the consequences upon the high field poling and depoling character of the mutual influence between the phases upon both the electrical and elastic boundary conditions in each phase.

Using a modification of the "replamine process" developed by E.W. White and colleagues at MRL, new transducer materials have been fabricated which replicate a natural coral microstructure, and exhibit a number of the expected features, i.e. ease of poling, high flexibility, large $\tilde{g}_{33}$ coefficients and very high $\tilde{g}_h$ coefficients. This work is presented in Appendix III.

For the lamellar heterogeneous systems, the effort needed to co-process different PZT and PSnZT composites to high density monolithic structures has

required considerable work upon preparation, tape casting, assembly and densification. This work is reported in section 5 of the report, which contains the preliminary electrical and piezoelectric data for several of the composites which have been fabricated to date.

3.2 PZT:PLASTIC COMPOSITES

Work of the past year using the replamine process to develop a PZT:elastomer composite polable from simple surface electrodes, highly flexible and with large $\bar{g}_{33}$ coefficients is contained in Appendix III*.

Current work in this area is concerned with:

(i) Developing a suite of PZT:elastomer samples of size and shape suitable for more extensive and detailed evaluation of the parameters.

(ii) Further studies of the preparation techniques, in particular for the re-impregnation step when the unpolymerized elastomer is introduced into the fixed ceramic replica. It is this step which at present gives the major problem in scaling up the processing to produce larger samples.

(iii) Application of the processing to develop hard PZT:plastic composites using a "hard" epoxy as the plastic phase.

(iv) Evaluation of the pyroelectric response of the hard epoxy PZT composites, as a model system to explore the modification of the pyroelectric figure of merit between single and diphasic systems.

(v) Examination of the piezoelectric resonance spectra for the hard composites, to enable characterization of the leastic anisotropy, the mechanical Q and the piezoelectric coupling coefficients under AC drive fields.

(vi) Determination of the temperature coefficients of resonance for simple extensional resonance modes to explore the influence of material parameters symmetry and connectivity, and assess the possibility of using two-phase structures for temperature compensated resonators.

*Complementary work at the Naval Research Laboratory, using a different approach, has confirmed the piezoelectric parameters for series and parallel connected composites, and has led to the development of a new type of flexible macrocomposite which shows considerably enhanced voltage sensitivity.

3.3 LAMELLAR DIPHASIC CERAMIC:CERAMIC COMPOSITES

Over the past year a very heavy emphasis in our processing studies has been upon generating the necessary background to be able to assemble and densify these structures. This work is covered in Section 5 of this report.

Based on these studies we believe that by using pressure densification of the green ceramic tapes before assembly, we shall be able to balance shrinkage between tapes of different composition and thus avoid the porosity problems which plagued initial fabrication. Coupled with the ability to hot isostatically press the presintered monolithic assemblages, present evidence suggests that it will be possible to achieve adequate density and phase connectivity without too much interdiffusion between the constituent phases.

Platinum electrodes have been successfully cofired into several of the proprietary PZT compositions, and data are now being obtained on the modifications which can be effected both in the poling characteristics and in the piezoelectric performance using these integrated electrode structures.

4. PHENOMENOLOGICAL STUDIES

4.1 INTRODUCTION

Over the first year of this contract the ADAGE computer graphics system was used to explore the possibility of computer solution and display of the Elastic Gibbs Free Energy for simple perovskite type (single cell) ferroelectrics. Two problems were initially tackled.

(I) Using the imaging capability of the ADAGE to explore the three dimensional polarization surfaces of constant ΔG, near the phase stability limits for the simple Devonshire function, so as to be able to delineate minimum energy trajectories for cubic-tetragonal, tetragonal-orthorhombic, and orthorhombic-rhombohedral switching.

(II) The evolution of a more complete energy function which would mimic the tetragonal-rhombohedral morphotropic phase boundary so important in the PZT piezoceramics.

During the past year, task I has been essentially completed. All three phase transitions accessible with the simple Devonshire function have been explored in detail, and a motion picture describing this study is almost complete. Preliminary work has been started to explore the deformation of the polarization surface by electric fields and mechanical stress to examine field forced ferroelectric switching trajectories,but the detailed examination is being postponed until the energy function for PZT is available.

The major part of our effort is now focused onto the task II, and progress on this topic will be discussed in the following section.

4.2 DEVELOPMENT OF AN ELASTIC GIBBS FUNCTION FOR PZT

In a simple ferroelectric crystal, derived from the cubic m3m prototype, the increment in the elastic gibbs free energy associated with the onset of a polarization P, with components P_1, P_2, P_3 may be written:

$$\Delta G_1 = A(P_1^2+P_2^2+P_3^2) + B(P_1^4+P_2^4+P_3^4) + C(P_1^2P_2^2+P_2^2P_3^2+P_3^2P_1^2)$$

$$+D(P_1^6+P_2^6+P_3^6) +E(P_1^2P_2^4+P_1^2P_3^4+P_2^2P_1^4+P_2^2P_3^4+P_3^2P_1^4+P_3^2P_2^4)$$

$$+F(P_1^2P_2^2P_3^2) - 1/2\ s_{11}\ (X_1^2+X_2^2+X_3^2) - s_{12}\ (X_1X_2+X_2X_3+X_3X_1)$$

$$- 1/2\ s_{44}\ (X_4^2+ X_5^2+ X_6^2) - Q_{11}\{X_1P_1^2+ X_2P_2^2+X_3P_3^2\}$$

$$- Q_{12}\ \{X_1(P_2^2+P_3^2) +X_2(P_1^2+P_3^2) +X_3(P_1^2+P_2^2)\}$$

$$-Q_{44}\ \{X_4P_2P_3+X_5P_1P_3+X_6P_1P_2\}$$

where the A,B,C,D,E,F are dielectric stiffness, and higher order stiffness coefficients, s_{11}^P, s_{12}^P, s_{44}^P the elastic compliances (measured at constant polarization), Q_{11}, Q_{12}, Q_{44} the cubic electrostriction constant.

The A,B... may be functions of both temperature and composition, but in any solid solution system it is expected that the variation would be continuous across the phase diagram. To give Curie Weiss behavior in the paraelectric phase,A must necessarily be a linearly decreasing function of temperature passing through zero at the Curie Weiss temperature θ which is at or below the temperature of onset of the first ferroelectric phase (T_c).

Initial studies had shown that even if the parameters A,B,C,D are given continuous temperature dependence a simple tetragonal:rhombohedral morphotropy could not be developed from the simple Devonshire function (E=F=0). However, by adding a positive E parameter to destabilize the orthorhombic and rhombohedral phase, then restabilizing the rhombohedral phase with a negative F parameter, tetragonal and rhombohedral phases could be made coincident over a wide temperature range without any interleaving orthorhombic regions.

To permit ready visualization of the influence of the A → F parameters on the resulting phase stabilities, the ADAGE has now been programmed to

operate in a split screen mode. The right hand half of the screen plots ΔG_1 vs T for all possible stable phases. ΔG_1 is derived from a computer solution of the polynomial equations

$$\frac{\partial \Delta G_1}{\partial P_i} = 0$$

which yield the appropriate values of P_i at each temperature. On the ADAGE the A → F are under dial control and linear temperature coefficients can be added to any of the parameters B → F. Markers are inserted at each of the intersections of the different phase stabilities, marking the equilibrium transition temperatures. This information on phase stabilities is then transferred to the left portion of the screen, the parameters A → F are incremented to new values under machine control and the process is repeated. In this manner, a hypothetical phase diagram can be rapidly built up for any given initial choice of parameters, and any chosen scheme of parameter increments. Since the starting values and progression increments are under analog control on the ADAGE system, new combinations can be "dialed" in at the start of each run and a wide range of parameter combinations can be tested in quite a short period.

Experience using this plotting program has confirmed our earlier expectations in that:

(1) We cannot reproduce morphotropy with the simple Devonshire function.

(2) In the Devonshire formalism, as expected, the parameter $\emptyset = C/B$ controls the relative stability of tetragonal to orthorhombic and rhombohedral phases; however the orthorhombic phase always interleaves or is degenerate with the rhombohedral.

(3) To generate a near vertical tetragonal-rhombohedral boundary requires a positive value of E, and a negative value of F.

(4) For all parameter combinations which generate a near vertical (morphotropic boundary) the orthorhombic phase is always very close to (but metastable with respect to) the overlaying tetragonal and rhombohedral stability curves.

Having developed a small family of dimensionless parameters which mimic morphotropy, the necessary task is now to scale and refine the fitting to describe real PZT compositions as accurately as possible. This task clearly requires additional experimental data, and we are proceeding as follows:

(1) Reprogramming the incremental behavior of T_c to reflect the nonlinear behavior of T_c vs composition in the known PZT phase diagram.

(2) Measuring the spontaneous strains $X_{11(s)}$, $X_{22} = X_{33(x)}$ as a function of temperature, by x-ray methods on a series of carefully prepared compositions in the tetragonal phase field.

(3) Measuring $X_{44(s)}$ vs T for compositions in the single cell rhombohedral field.

(4) Calculating P_s vs T for each of the combinations of parameters which exhibit morphotropy.

(5) Using the relations $X_{11} = Q_{11}P_s^2$ $X_{22} = Q_{12}P_s^2$ to fit the measured strain behavior with $P_s(T_c)$, θ and Q_{11} and Q_{12} as fitting parameters.

(6) Re-calculating the phase diagram for the new T_c and θ values to confirm that the minor changes in these parameters do not degrade the initial fitting of the phase diagram.

The best fitting to date has been obtained with the following parameters:

Ao = 1 (no scaling for Xo)

$\emptyset$ = C/B = -1.20 in $PbZrO_3$ changing linearly to
+0.80 in $PbTiO_3$

E = 80×10^{-6}

F = -450.10^{-6} in $PbZrO_3$ changing linearly to
-200.10^{-6} in $PbTiO_3$

The temperature behavior of T_c (Fig. 4.1) is chosen to fit the phase diagram given by Jaffe Cook and Jaffe.

The trend of $T_c - \theta$ from $PbTiO_3$ to $PbZr_{0.5}Ti_{0.5}O_3$ required for fitting is shown also in Fig. 4.1. The resulting values for Q_{11} vs composition are shown in Fig. 4.2 together with the calculated values of P_s (25°C) vs composition. The fitting of the observed and calculated spontaneous strains for pure $PbTiO_3$ and for $PbZr_{0.5}Ti_{0.5}O_3$ are shown in Fig. 4.3. For intermediate compositions, the fitting is very similar. To obtain this fitting, however, it is necessary to assume that Q_{11} and Q_{12} decrease continuously with increasing Zr content as shown in Fig. 4.2.

The difficulty of proceeding from the measured single crystal data is admirably shown in Fig. 4.2. The triangular data points for P_s are taken from the compilation by Landolt Bornstein. The scatter for pure $PbTiO_3$ is immediately evident, the very low value for single crystals of $PbZr_{0.4}Ti_{0.6}O_3$ is clearly incorrect, while the corrected ceramic value (assuming perfect poling) at the rhombohedral 44:56 composition is very close to the predicted curve.

The next step in refinement will be to select a χ_o value so as to scale the dielectric permittivity. Here again, the quality of the available single crystal data leaves much to be desired. Normally it is a trivial task to select χ_o to fit the Curie Weiss behavior above T_c; however in both ceramics and single crystals values of the Curie constant C have been quoted which range from less than 1.5×10^5 to greater than 14×10^5. Since usually the lowest values of C are most reliable, we propose to select initially $C = 1.5 \times 10^5$. For our values of $T_c - \theta$ this gives

$K = 10{,}000$ at T_c for $PbTiO_3$

$K = 30{,}000$ at T_c for $PbZr_{0.5}Ti_{0.5}O_3$

which are not unrealistic as compared to the best measured single crystal values.

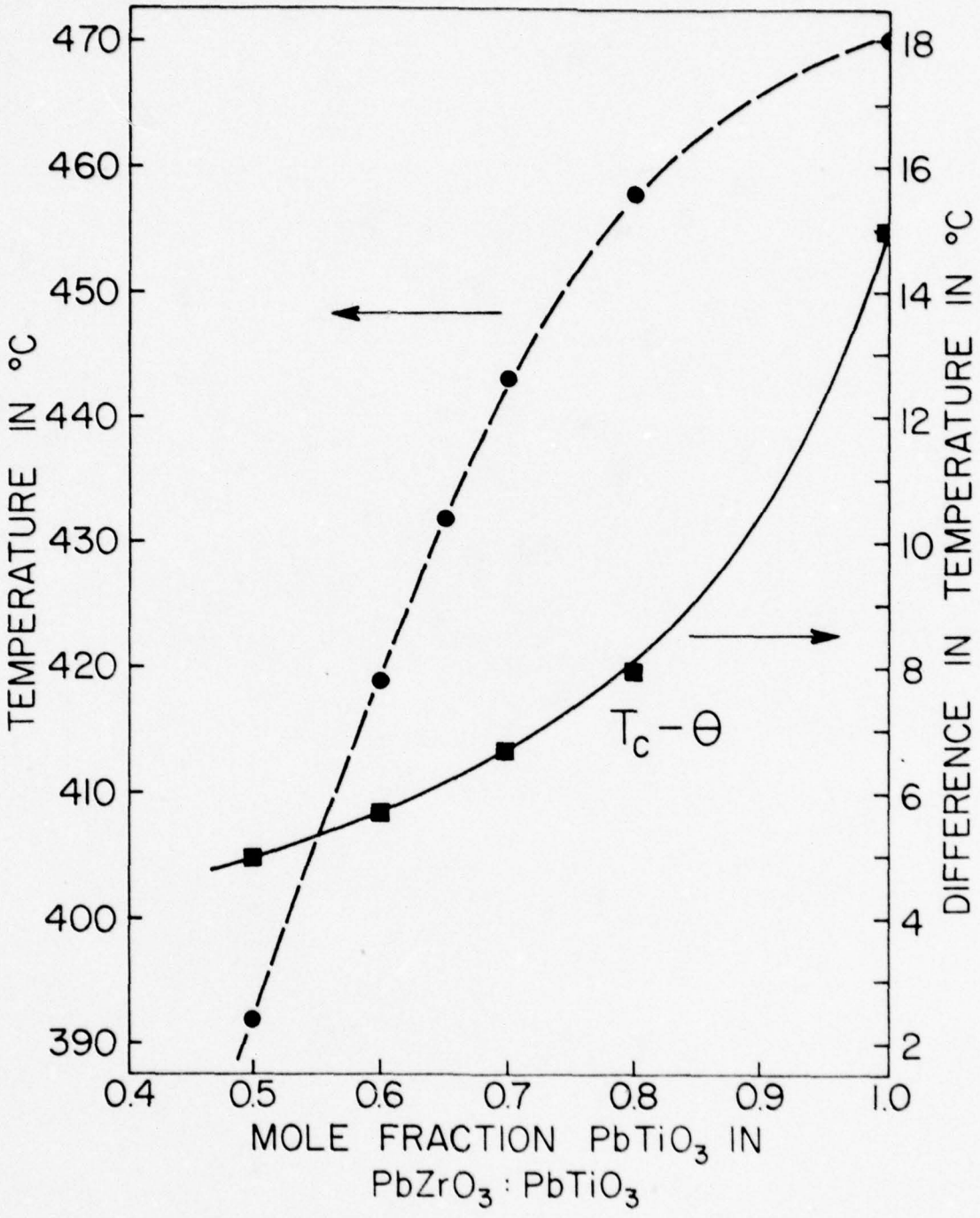

Fig. 4.1 Curie temperature and Curie Weiss temperature as a function of composition in PZT.

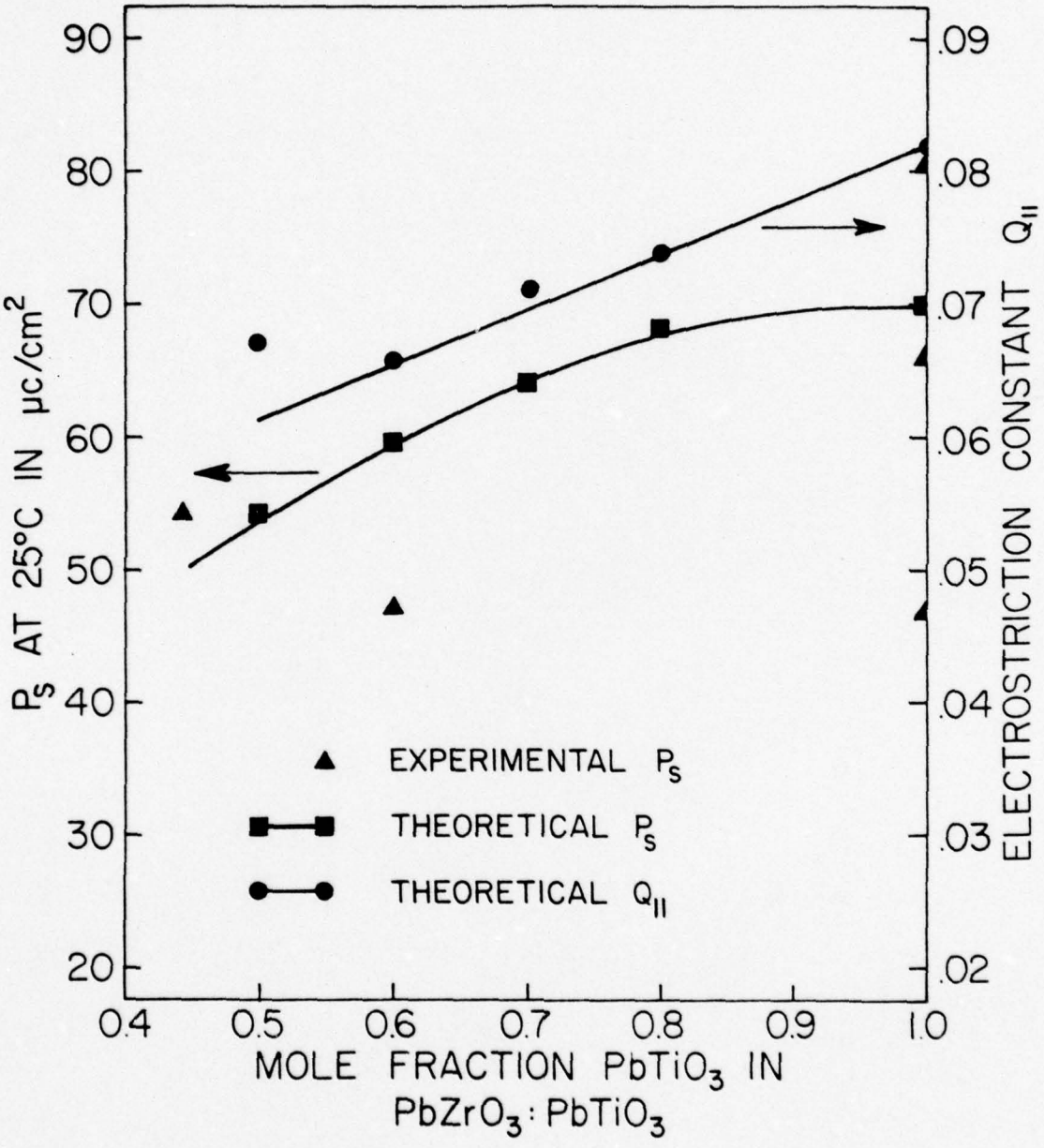

Fig. 4.2 Calculated values of Q_{11} and of P_s(25°C) as a function of composition in PZT.

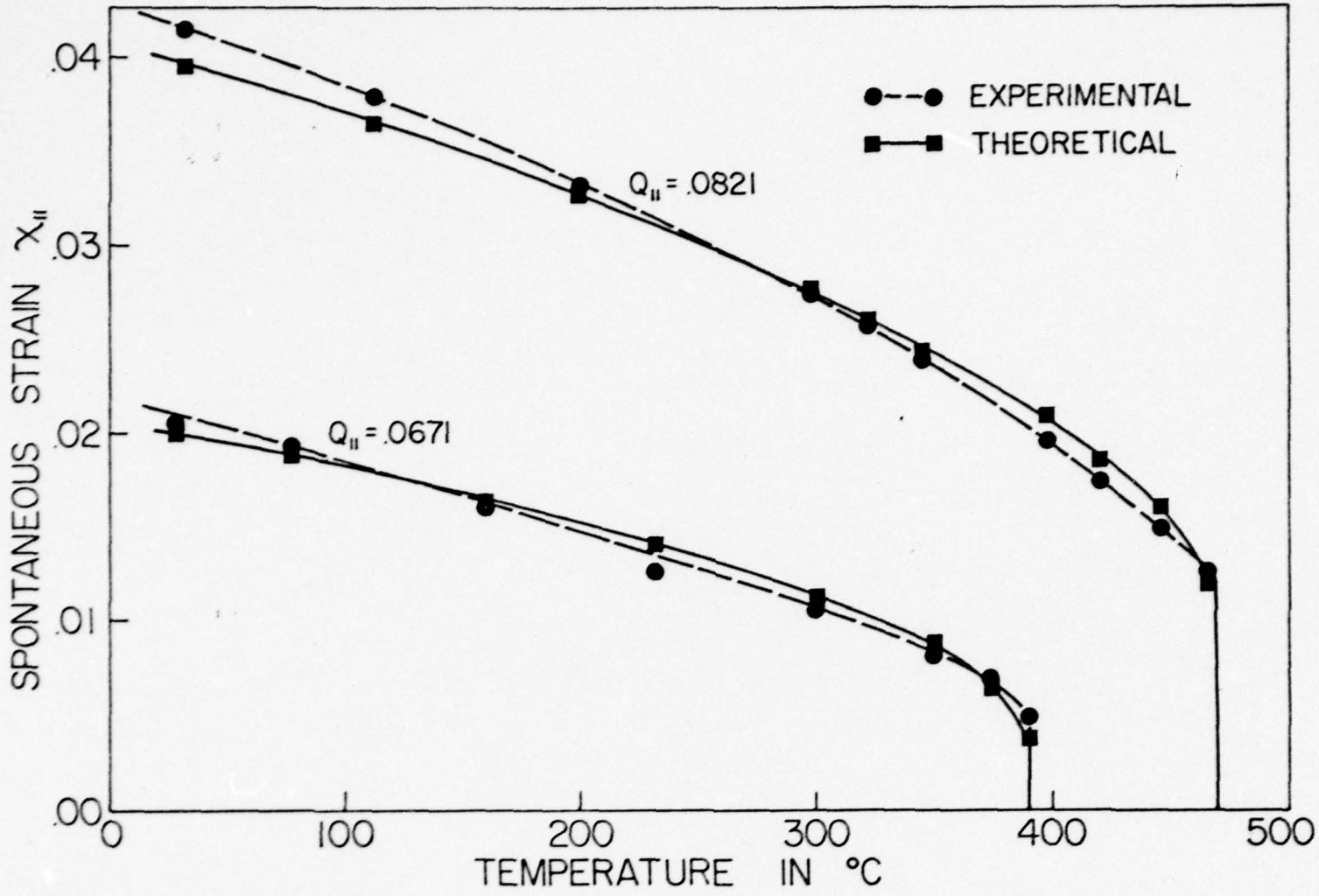

Fig. 4.3 Comparison of measured and calculated spontaneous strain $x_{11}(s)$ in $PbTiO_3$ and in $Pb(Ti_{0.5}Zr_{0.5})O_3$.

Calculations of the anisotropic dielectric permittivities and the piezoelectric d, g, a, b parameters for the single domain states are now proceeding.

5. PROCESSING STUDIES

5.1 INTRODUCTION

The majority of the processing work described in previous reports has been completed. Our goal of developing "standardized" processes that allow us to duplicate industrial practice in batching, calcining, forming, and sintering mixed oxide compositions and processing precalcined commercial formulations has been attained. Four papers prepared for publication describing the different aspects of this work are included in the appendix.

In the past 6 month period we have concentrated our efforts on the problems associated with the fabrication of lamellar heterogeneous devices (LHD's). The topics include:

A. Powder Preparation

B. Tape Casting

C. Fabrication of Devices

D. Dielectric Measurements

E. Hot Isostatic Pressing

5.2 POWDER PREPARATION

The fabrication of many of the LHD's will require chemically prepared precursors for control of reactivity during sintering.

The preparation and reactivity evaluations of chemically prepared oxides and PZT compositions are described in the appendix.

At present we are continuing our investigations of the reactivity of these materials. The goal of the work is the development of a one-step process in which chemically prepared powders can be introduced into tape without prior calcining. Rate controlled sintering will be used to fire the tapes to produce the right phase prior to the high temperature densification period.

5.3 TAPE CASTING

Work is continuing on using the technique of post casting pressing (PCP) to increase the green tape density. In previous work we have demonstrated that PCP can be used to increase the green density by as much as 30%. This increase in density significantly alters the sintering kinetics of the tape. A very interesting trend has been noted where the green density and fired density have a linear relationship over a range of green densities from 3.5 to 4.7 gm/cc (See paper by Biggers, Shrout and Schulze in appendix).

In addition the PCP tape fires to acceptable densities at temperatures 100°C lower than a pressed disc of the same composition. The PCP process appears to have great utility in the fabrication of LHD's. With this process it was possible to lower the sintering temperatures and control firing shrinkages. The control of shrinkage is a critical problem in the fabrication of the LHD's described in later sections of the report.

Work in progress includes extension of the green density-fired density data to lower and possibly higher values of green density. We are also building a warm rolling apparatus that will enable us to densify larger quantities of tape with more reproducibility than is currently achieved with batch uniaxial pressing.

5.4 FABRICATION OF DEVICES

We are presently building the following LHD configurations:

A. Multiple layers of ceramics with the same composition and external electrodes.

B. Multiple layers of ceramics with different compositions and external electrodes.

C. Multiple layers of ceramics with the same composition and internal electrodes.

D. Multiple layers of ceramics with different composition and internal electrodes.

Many variables are encountered in the fabrication of the devices. The most important under investigation are:

A. Reactivity of oxides or compounds and the effect on sintering.

B. Effect of tape green density on sintering.

C. Fabrication techniques required to electrode, assemble multilayers.

D. Binder burnout of tape and electrodes.

E. Sintering including electrode compatibility and interaction of ceramic layers of different compositions.

5.5 DIELECTRIC MEASUREMENTS

Dielectric measurements are being conducted to compare the effect of various fabrication methods on the electrical properties of commercial material. Initial studies have been limited to four compositions from Ultra Sonics (401-888, 401, 501, and U5H-32).

A comparison is to be made between conventionally pressed and tape cast single phase material. These results will be used to study the interactions in cofired composites of one or more ceramic compositions and internal platinum electrodes. The primary measurements will be d_{33} and complex permittivity as a function of temperature and frequency.

The devices were prepared from tape produced as described in the paper by Biggers, Shrout and Schulze included in the appendix.

The multiple layer devices were built up from one-inch squares cut from green tape. After stacking the composites were uniaxially pressed at 50°C and 5000 psi.

The parts with internal electrodes were fabricated from one-inch squares of green tape on which the platinum electrode patterns were screen printed. The platinum ink was allowed to air dry and the requisite number of layers was stacked and uniaxially pressed at 50°C and 5000 psi.

For binder burnout the parts were placed on a zirconia setter and fired in air. A typical binder burnout schedule for the parts was one hour heat-up to 110°C hold for 2 hours, 2 hours to 280°C with a 3-hour hold followed by one hour change to 350°C with a one-hour hold.

Firing was done in alumina containers. The parts were placed on setters of their own composition. The setters were stacked together with a PbO source at the top and bottom of the stack. A silicon carbide resistance furnace was used for sintering. The firing schedule included a 200°C/hr heat-up to 1330°C with a 2-hour hold followed by cooling with the power off.

Initial measurements indicate that there is essentially no difference (tolerance ±5%) in the electrical characteristics of ceramic prepared by cold pressing or tape casting. It is, however, necessary to consider the density and microstructural difference that may occur when sintering from these two fairly different green states.

Tables 5.5.1 and 5.5.2 may be used to compare fired single tape layers and pressed multilayer ceramic bodies with the typical values obtained from conventionally cold pressed ceramic. The reduction in K and to a lesser extent d_{33} in the single layers can be attributed mainly to a reduced density (see appendix on pressing effects on tape). The samples produced from pressing and cofiring 10 layers had higher densities which resulted in higher K and lower tan δ (1).

Some two layer composites have been prepared using a "hard" and "soft" PZT to explore the possibility of producing a composite with improved high drive field stability. Results of tests on the first two composites are listed in Table 5.5.2. The calculated values were derived using the experimental values in Table 5.5.3 and the following series mixing equations.

$$K = \frac{(t_1+t_2)(K_2t_1+K_1t_2)}{K_1K_2}$$

$$d_{33} = \frac{t_1d_1\varepsilon_2 + t_2d_2\varepsilon_1}{t_1\varepsilon_2 + t_2\varepsilon_1}$$

Table 5.5.1

Electrical Properties of Tape-Cast Single Layer PZT's.

Specimen Designation	Poling* Cond. (kV/m)	K† - (1kHz - 25°C) Comm. Data	Exp.	tan δ† 1kHz - 25°C	d_{33}† ($\times 10^{-12}$ C/N) - 25°C Comm. Data	Exp.
400	3000	1350	1100	0.0100	290	295
401-888	3000	1000	898	0.0045	215	230
501	3000	2000	1000	0.0237	400	370
U5H-32	3400	3200	2120	0.0340	590	510

*Specimens poled for 2 minutes at 100°C.
†24 hours after poling.

Table 5.5.2

Electrical Properties of Tape-Cast 10 Layer (Multi) PZT's.

Specimen Designation	Poling* Cond. (kV/m)	K† - (1kHz - 25°C) Comm. Data	Exp.	tan δ† 1kHz - 25°C	d_{33}† (10^{-12} C/N) - 25°C Comm. Data	Exp.
401	2600	1350	1180	0.0050	290	300
401-888	2600	1000	935	0.0027	215	225
501	2200	2000	1600	0.0180	400	425
U5H-32	2000	3200	2070	0.0298	590	580

*Specimens poled for 2 minutes at 100°C.
†24 hours after poling.

Table 5.5.3

Electrical Properties of Tape-Cast Multi (50/50) Layer PZT's.

Specimen Designation	Poling* Cond. (kV/m)	k† - (1kHz - 25°C) Cal.	Exp.	tan δ† 1kHz - 25°C	d_{33}† (10^{-12} C/N) 100Hz - 25°C Cal.	Exp.
401-888/501	3000	1180	1050	0.0100	299	275
401-888/U5H-32	2400	1288	969	0.0123	335	315

*Specimens poled for 2 minutes at 100°C.
†24 hours after poling.

where t = fraction of total thickness, K relative permittivity and d = d_{33} of component.

All experimental values fall below those calculated from dense tape cast material. The decreases are most likely the result of a decreased density in the soft phase (U5H-32 or 501) which has now been shown to have a greater linear shrinkage than the 401-888 material. It appears that the common surface is well bonded and the first layer to approach maximum shrinkage clamps the densification in the adjacent layer. The result is increased porosity in one layer along the interface. Experiments are now being conducted in pretreatment of the tapes to equalize the shrinkage.

Figure 5.5.1 illustrates the relaxations that occur when combining PZTs with quite different additions. The hard materials have modifications that cause oxygen vacancies which result in conductivities about three orders of magnitude greater than the materials with additives causing A-position vacancies. As the temperature is increased, the RC time constant of the hard layer is decreased and interfacial polarization contributes to the permittivity at higher frequencies. This is most apparent in the increase in the tan δ when the RC time constant becomes equal to the inverse of the frequency. At 1KHz the relaxation occurs at approximately the same temperature as the transition in the 401-888 material, resulting in a large tan δ peak at 265°C. When the resistivity decreases by an order of magnitude with increasing temperature, the relaxation occurs at 10 KHz (365°C). At higher temperature this again occurs for 100 KHz at 420°C.

The very nonuniform voltage distribution that may occur as a function of frequency suggests that very different poling conditions may be achieved depending on the application of field. A DC poling condition would apply most of the field across the insulating, soft layers and build up a space charge at the interface due to the conduction through the hard layer. Pulse poling would be temperature dependent and apply the voltage inversely proportional to the permittivities.

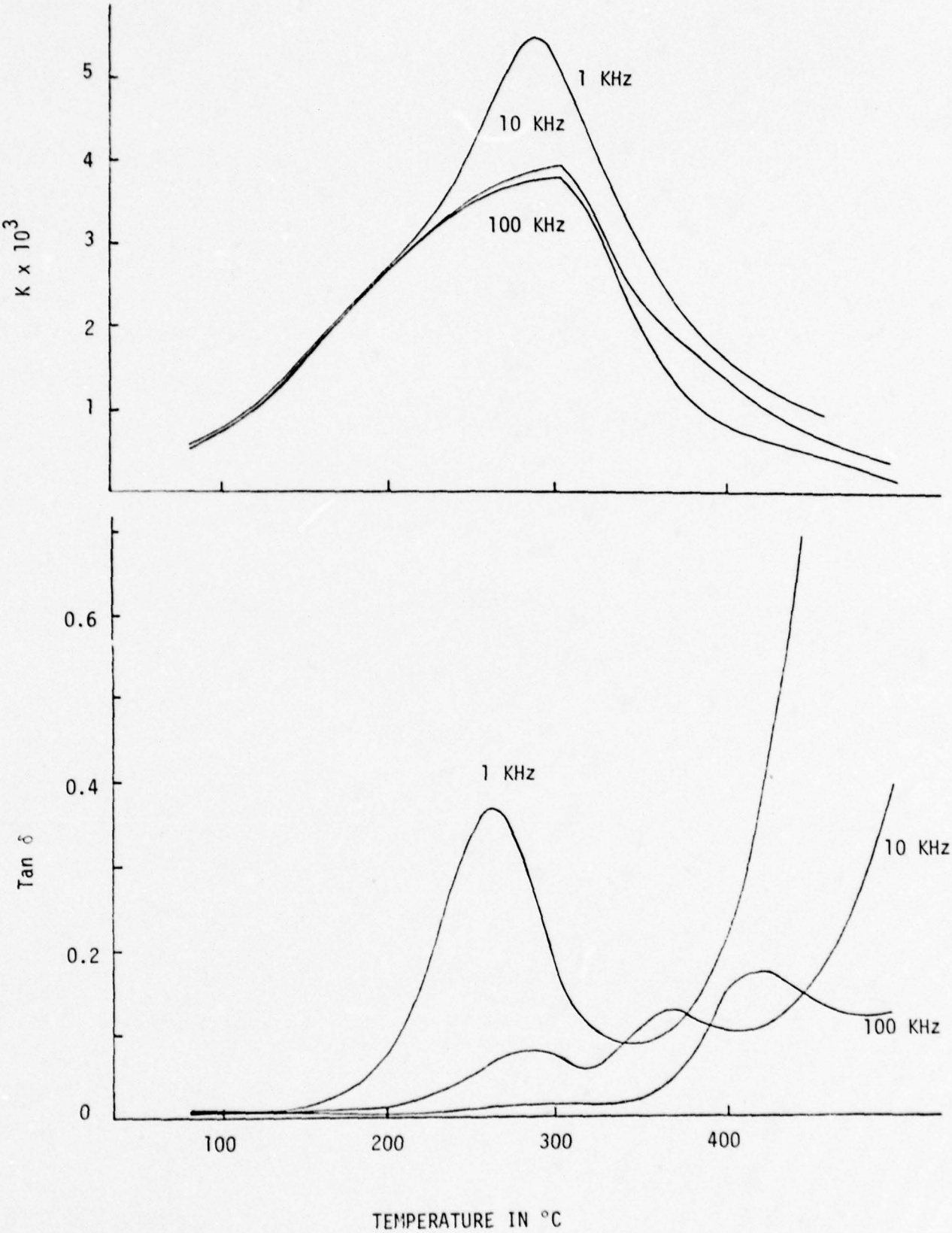

Fig. 5.5.1 Interfacial Polarization Relaxation in LHD 401-888/U5H-32 (Equal Thickness Layers).

5.6 HOT ISOSTATIC PRESSING

One of the most serious problems encountered in fabrication of the LHD's is difficulty in obtaining matched shrinkages and similar fired densities with layers of different composition.

The post casting pressing technique already described is one method of solving the problems of cofiring. It is possible that some variation of hot isostatic pressing in conjunction with PCP may produce the best LHD's.

In the HIP process it is necessary to achieve closed porosity (~92% theoretical density) by conventional sintering. The parts can then be hipped to nearly theoretical density at lower temperatures and times than the sintering process.

In the process envisioned substitution of chemically prepared oxides or compounds in the PZT compositions and pressing of the tape would be used to obtain the desired closed porosity state by sintering at low temperatures and short times. The parts would then be hipped to acceptable densities for electrical property evaluation. This combined process may be the only way of fabricating devices with ceramic layers of radically different compositions.

With the previous hot isostatic press design, problems associated with convectional heat loss at high gas pressures were encountered, leading to steep temperature gradients in the hot zone and excessive power input requirements. The temperature gradients have been largely eliminated by incorporating a hearth heater into the furnace structure. However, the low thermal efficiency (for example, with pure argon at 3000 psi the highest temperature attainable was only 1210°C for a power input of 7 KVA) has meant that conventional furnace designs based on conduction and radiation controlled heat transfer must be abandoned in favor of a system designed to eliminate convection.

Accordingly, in the present HIP design (Fig. 5.6.1) the heating element, a molybdenum-wound alumina crucible 4" high x 2" internal diameter, is enclosed

Figure 5.6.1 The Hot Isostatic Press

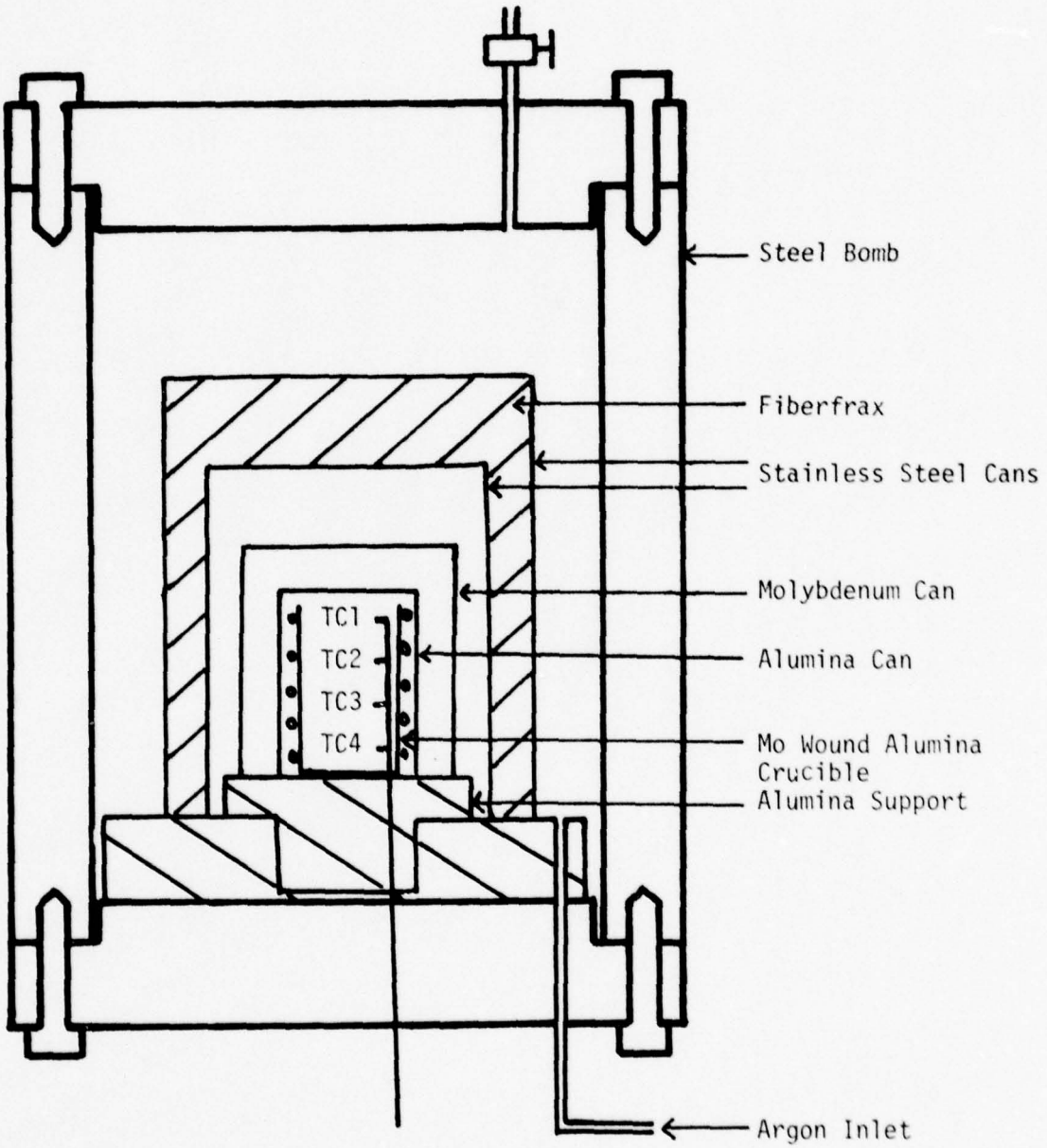

within four sealed concentric ceramic and metal cans which act as convection barriers. The innermost alumina barrier provides both thermal and electrical insulation. This arrangement, which can be readily assembled for rapid specimen turn-around, has proved to be very thermally efficient, requiring only 0.8 KVA of power to maintain the hot zone at 1300°C under 3000 psi argon pressure. Although these HIP conditions would be typical for the PZT compositions now under investigation, the equipment has been tested to 1700°C and 4,400 psi.

Hot zone temperature profiles at various pressures are shown in Figs. 5.6.2a and 5.6.2b. It has been found that the length of the constant temperature region is very dependent upon specimen size. Large specimens interrupt the convection path within the hot zone and reduce its ability to even out temperature gradients. Although a large temperature drop is observed in the lower part of the furnace, it should be noted that the temperature within the top inch of the hot zone is constant to within 10°C for small specimen size. The length of the constant temperature region can be increased if necessary by incorporating a hearth heater within the wound alumina crucible.

Characterization experiments are now in progress to determine the optimum HIP conditions for the various PZT compositions being studied. Preliminary work on a 95% dense $PbTi_{0.45}Zr_{0.55}O_3$ composition indicates that theoretical density can be obtained in this material after one hour at 1300°C under 3000 psi with approximately 1% weight loss due to lead oxide vaporization. Attempts to control this weight loss have included:

A. Encapsulating the specimens in platinum foil -- expensive and did not significantly reduce vaporization of PbO.

B. Incorporation of PbO source material within the hot zone. The excess lead oxide was reduced in the neutral HIP atmosphere and this led to degradation of the platinum thermocouples.

C. Minimizing the HIP time. This has proved to be the most successful method of avoiding weight loss.

Figure 5.6.2 Temperature Profiles at Various HIP Pressures

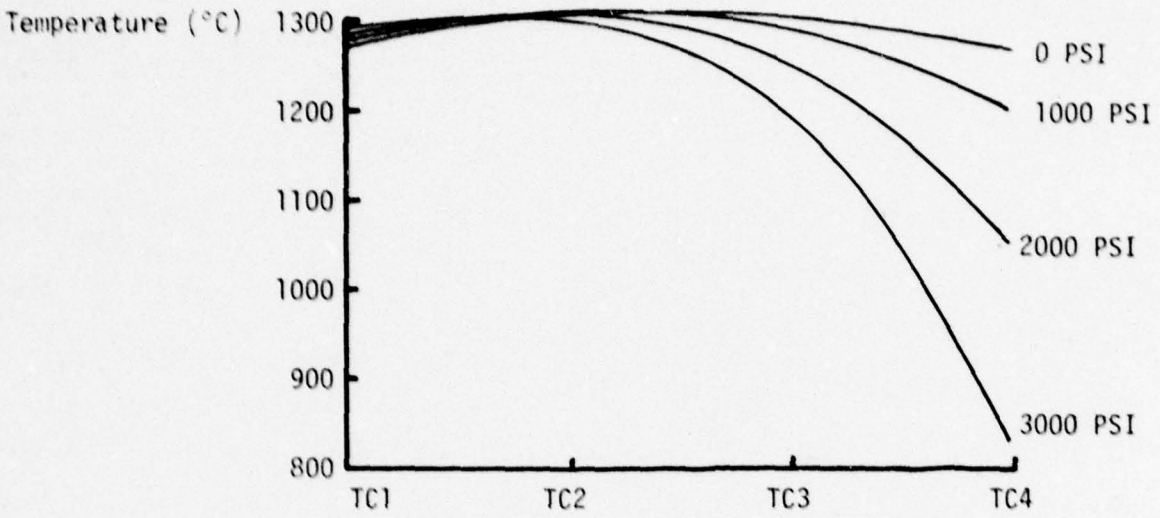

(a) Small Specimen Size (<1 cu in.)

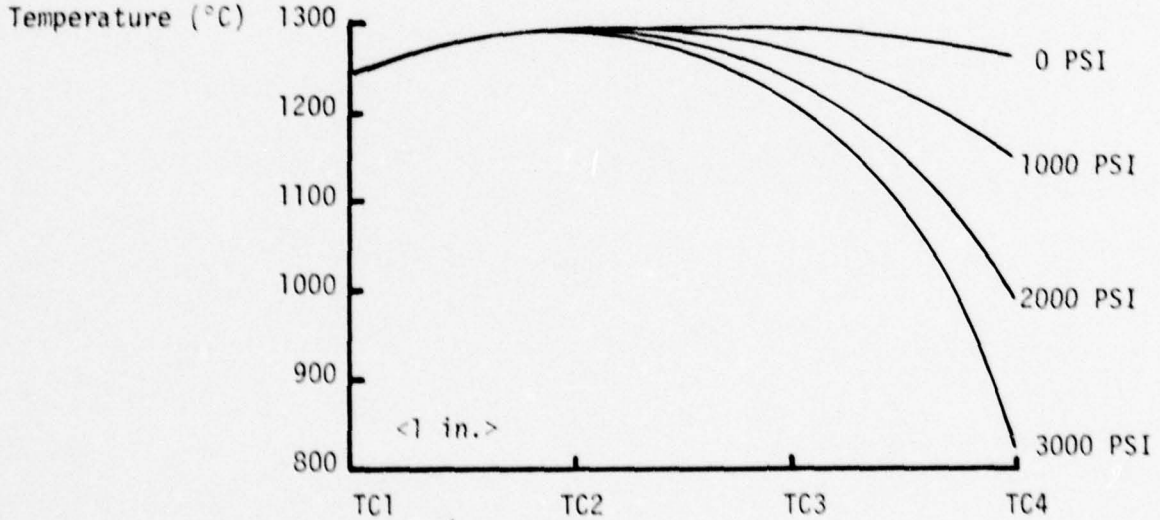

(b) Large Specimen Size

Discoloration has been observed in hot isostatically pressed specimens on removal from the press. This may be due to contamination by traces of volatile molybdenum oxides present within the furnace. However, it would seem more probable that slight surface reduction of the PZT occurred in neutral HIP atmosphere since the specimens regained their original colors when reheated to 1000°C in air. To eliminate this problem, the HIP furnace will be rewound with platinum and operated in a slightly oxidizing environment.

Measured dielectric constants and d_{33} values for this hot isostatically pressed composition show increases consistent with the increase in density (See Table 5.6.1). A comparison of micrographs of both the pre-sintered and the hot isostatically pressed materials (Fig. 5.6.3) indicates that the HIP process has virtually eliminated porosity without otherwise affecting grain morphology. A program of HIP experiments on other piezoelectric materials, e.g. tape-cast composites and Corning's "honeycomb" structured $BaTiO_3$ ceramic is now in progress.

Reference

1. K. Okazaki and K. Nagata. Effects of the Density and the Grain Size of Piezoelectric Ceramics Influencing Upon the Electrical Properties. Trans. Inst. Electronics Commun. Engrs. Japan 53C, 815-822 (1970).

Table 5.6.1 Comparison of Electrical Properties of Fired and Hipped PZT.

Specimen/relative density MRL $PbTi_{.45}Zr_{.55}O_3$	% Weight change on prefiring at 1330°C, 1-1/2 hrs PbO source present	% Weight change during HIP, at 1300°C, 1 hr No PbO source	Dielectric constant before poling (1 KHz)	Dielectric constant after poling (1 KHz)	d_{33} $CN^{-1} \times 10^{-12}$
I (prefired only) 0.94	-0.22	--	1129	1083	330
II (prefired only) 0.97	-0.22	--	1250	1267	360
III HIP 1.00	+0.13	-1.16	1298	1346	345
IV HIP 1.00	-0.14	-1.43	1342	1451	375

Figure 5.6.3

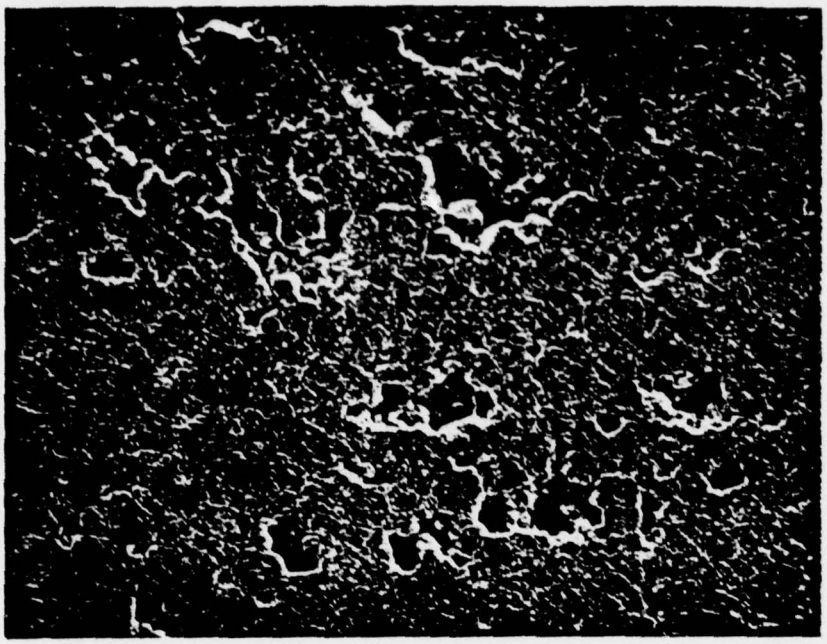

50 μm

(a) Prefired 1330°C, 1 hour, relative density 0.94

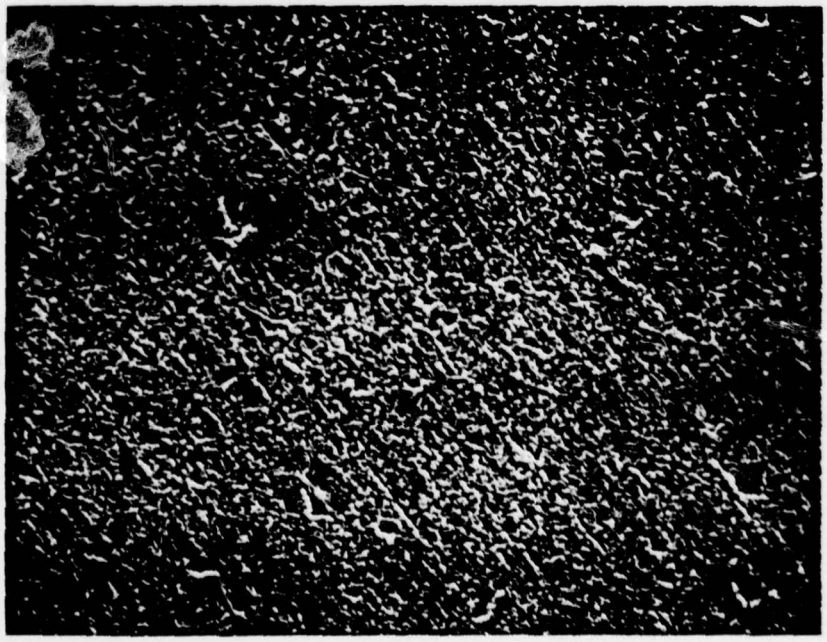

50 μm

(b) Hipped 1300°C, 3000 psi, 1 hour

6. AMORPHOUS FERROELECTRICS

6.1 INTRODUCTION

The theoretical studies of Lines (6.1) and initial experimental work at Bell Telephones by Nassau (6.2) and Glass (6.3) suggest the possibility of achieving ferroelectric properties in a glass. The theory suggests that for the possibility of ferroelectric ordering the network should incorporate highly polarizable ionic groupings such as the BO_6 octahedron and that for such compounds the network arrangement would always have a Curie point T_c significantly below that of the corresponding regularly ordered crystalline structures. Thus potential materials of interest should have very high proper ferroelectric Curie temperatures in the crystalline phase, with the possibility of multiaxial polar arrangements within the polarizable "sub units" of the regular ordered crystalline unit cell.

Lithium niobate satisfies these requirements and shows unusual properties in the splat quenched glass which could be attributed to a ferroelectric ordering.

Roller splat quenching is a difficult task with lower thermal conductivity inorganic liquids. The objective of our studies was to produce stoichiometric amorphous films of a very high T_c ferroelectric compound by the RF sputtering process, and to test the dielectric and related properties of these films for potential ferroelectric activity. For these studies, strontium pyroniobate, $Sr_2Nb_2O_7$, was selected as it has one of the highest known Curie temperatures of all oxide ferroelectrics. It was hoped that if the amorphous films themselves showed normal dielectric response, it might be possible, by suitable thermal annealing, to induce controlled recrystallization and thus explore the evolution of the properties of the crystalline phase for micro crystalline sizes.

6.2 SAMPLE PREPARATION

RF sputtering of insulators is itself a highly complex and difficult subject. Much progress has been made, particularly within the last 10 years in characterizing and correlating the release and deposition mechanisms, but it is still not possible to predict "ad initio" the required boundary conditions and much initial experimentation is required for each new compound to establish the choices of geometry, carrier gas species, pressure, power level, substrate requirements, substrate temperature, etc. for successful sputtering.

During the past year over 500 sputtering runs have been carried out to test out and optimize the parameters for $Sr_2Nb_2O_7$ so as to be able to reproducibly sputter stoichiometric films onto a range of different substrate materials.

Using a standard MRC model 8502 sputtering unit operating at 13.5 MHz with 2" diameter ceramic target and a target substrate spacing of the following optimum conditions were found.

(1) Carrier gas pure O_2 at pressure 30.10^{-3} torr.

(2) Power level 50 watts.

(3) Substrate recrystallized Al_2O_3.

(4) Target composition $2(SrO)_{1.05}.(Nb_2O_5)$.

The off stoichiometry in the target required to produce stoichiometric films on the substrate was traced to a high re-sputtering rate from the substrate, which also gives rise to an unusually low effective sputtering rate in this sytem. By redesigning the dark space shield on the target, it was found possible to improve the sputtering rate for oblique angles, and in this manner to achieve deposition rates of more than 50 Å/minute.

6.3 DIELECTRIC STUDIES

After considerable experimentation, pinhole free samples up to 10 μm in

thickness with stoichiometry corresponding to $Sr_2Nb_2O_7$ suitable for dielectric studies were obtained.

X-ray powder diffraction gave no discernible structure, but after heating to 1200°C for 4 hours a pattern corresponding to the polycrystal $Sr_2Nb_2O_7$ material prepared by conventional ceramic methods was obtained.

Dielectric measurements taken as a function of temperature and frequency on the amorphous films are shown in Fig. 6.1, and the corresponding loss tangent in Fig. 6.2. Unfortunately, the dielectric results do not provide any unequivocal evidence either for or against ferroelectricity. The frequency dependence of the higher temperature rise in ε' and the corresponding rapid rise in tan δ suggest that this is extrinsic, and associated with space charge deformation of the potential distribution (Maxwell-Wagner effect).

Attempts to pole the films with high DC fields at room temperature gave no residual pyroelectric effect, and there was no evidence of dielectric hysteresis. The films are too thin for proper bulk measurements of the optical properties but exhibit no starting birefringence, or substructure which could be associated with ferroelectric ordering. Thus we are tempted to believe that amorphous $Sr_2Nb_2O_7$, as fabricated by R.F. sputtering onto a cool (less than 400°C) substrate does not exhibit ferroelectricity.

6.4 PRELIMINARY ANNEALING STUDIES

Amorphous $Sr_2Nb_2O_7$ films deposited on recrystallized alumina proved remarkably stable under thermal annealing.

Initial runs were for 18 hours at 300, 500, 700 and 1000°C produced no observable change in the film under microscopic examination. Increasing the time at 1000°C from 36 hours even up to 148 hours, again showed unchanged amorphous films.

Raising the temperature to 1200°C collapsed the film into isolated islands, which showed the characteristic x-ray pattern for $Sr_2Nb_2O_7$.

References

6.1 M. Lines. Phys. Rev. B15, 388 (1977).

6.2 K. Nassau, J. Shiver. Bull. Am. Ceram. Soc. 56, 363 (1977).

6.3 M.E. Lines, A.M. Glass. Bull. Am. Ceram. Soc. 56, 363 (1977).

APPENDIX I

Structure and Dielectric Properties of Materials in the Solid Solution System $Pb(Mg_{1/3}Nb_{2/3})O_3$:$Pb(W_{1/2}Mg_{1/2})O_3$

S. Nomura, S.J. Jang, L.E. Cross and R.E. Newnham

Materials Research Laboratory
The Pennsylvania State University
University Park, Pennsylvania 16802

1. Introduction

Lead magnesium niobate (PMN) is a ferroelectric material with diffuse phase transition[1,2]. The structure is cubic (Pm3m) at room temperature, with no evidence of long-range ordering of the dissimilar B site cations in the ABO_3 perovskite structure. The weak field dielectric properties are strongly dispersive with a broad frequency dependent maximum in ε' in the range 0 to -15°C, and a corresponding broad maximum in ε'' at lower temperatures. A very extensive literature covering many of the properties of this compound is effectively summarized in Landolt Bornstein[3,4].

At room temperature $Pb(Mg_{1/2}W_{1/2})O_3$ (PMW) has an orthorhombically distorted perovskite structure, with a unit cell which is approximately 4a x 4a x 4a, where a is the dimension of the normal perovskite single cell (64 formula units/unit cell). The origin of this enlarged "supercell" has been traced to two phenomena[5]:

(i) A three dimensional ordering of the Mg^{2+} and W^{6+} cations in the B sites of the ABO_3 structure, producing a doubling of the unit cell edges.

(ii) Antipolar displacements of the ions, leading to an additional doubling.

PMW undergoes a transition from quadrupled to doubled cell parameters at 39°C, with a weak dielectric maximum at this phase change and a loss of the orthorhombic distortion[6]. Since the lower temperature phase does not exhibit dielectric hysteresis it has been classified as antiferroelectric.

The present work shows that PMN and PMW form a complete range of solid solu-

tions between the two endmember compositions. Of special interest for these studies was the manner in which the dielectric dispersion changes with composition in the solid solution range, the evolution of the ordered superstructures, and the modifications which occur in the higher field dielectric properties as the ordered cation arrangement becomes established. This paper is concerned primarily with the dielectric properties. A more detailed description of the structural work will be given in a subsequent paper.

2. Sample Preparation and Characterization

The required series of compounds were prepared from reagent grade PbO, MgO, Nb_2O_5 and WO_3. The constituent oxides were mixed in appropriate proportions, ball-milled in alcohol, then dried and calcined in air in a closed alumina crucible. Calcining temperatures ranged from 800 to 1,000°C depending on composition for a calcine time of 15 hours. The resulting calcine was ground and refired for two additional 15-hour periods to ensure complete reaction.

Ceramic samples were prepared by cold pressing into disks 2.54 cm diameter and firing on zirconia setters in air. Sintering temperatures ranged from 990°C to 1280°C depending on composition. A 2-hour sintering time was used. In the pure PMW ceramics, there was always a small amount of a second phase, probably stalzite ($PbWO_4$) as previously reported by Zaslavskii et al.[5].

X-ray powder diffraction patterns were taken at room temperature using Cu-Kα radiation. The samples were all of perovskite structure, and except pure PMW were all cubic. The lattice constants were determined from (200), (211), (220), (310) and (321) reflections, the indices being referred to the primitive perovskite cell. Superstructure reflections characteristic of a doubling of the perovskite subcell began to appear for compositions containing more than 20 mole% PMW, with intensities increasing continuously with increasing PMW content. The lattice constants and the x-ray diffraction intensity ratio $I(\frac{1}{2}\frac{1}{2}\frac{1}{2})/I(100)$ as a function of composition are shown in Fig. 1. To avoid

the complexities associated with the quadruple cell in PMW, the intensity ratios were taken at 50°C, which is in the cubic phase region for all compositions.

Dielectric Measurements

The general trends in the temperature dependence of the weak field dielectric permittivity ε'_w across the solid solution range can be seen in Fig. 2, which summarizes measurements taken at 100 kHz in a field of 100 volts/cm. It is evident that the maximum value of ε'_w decreases rapidly with increasing PMW content, but the broad maximum characteristic of a diffuse change is evident even up to 80 mole% PMW. This was confirmed by dielectric dispersion measurements on compositions taken at 10 mole% PMW increments. Typical data for the 60 mole% PMW composition is given in Fig. 3, where the shifting of ε'_w maximum to higher temperatures with increasing measuring frequency is clearly evident. To summarize the dispersion data, Fig. 4 is a plot of the values of T_{max}, the temperature of ε'_{max}. Taken at frequencies of 1, 10, 100 and 1,000 kHz for compositions across the solid solution range Fig. 4b plots the "dispersion range" (T_{max} at 1MHz - T_{max} 1kHz) as a function of composition. It is interesting to note that up to 60 mole% PMW, the dispersion range increases, then for higher PMW content decreases rapidly to abrupt transition behavior at the 80 mole% PMW content.

An indication of the decreasing ferroelectric characteristics in the lower temperature region (below the T_{max} range) was obtained from measurements of dielectric hysteresis under very low frequency drive (0.1 Hz). Maximum remanent polarization levels as a function of temperature and composition are shown in Fig. 5, from which the peak value of the P_r vs composition (Fig. 5b) can be derived. The fact that the hysteretic dielectric behavior is more complex in these relaxor compositions than in conventional ferroelectric ceramics is clearly demonstrated by an examination of the weak field permittivity as a

function of cyclic bias fields. For pure PMN these data are shown in Fig. 6. At higher temperatures (above the relaxation range. Fig. 6a) there is conventional dielectric saturation. For temperature in the relaxation range there is a peculiar inverse hysteresis, giving maxima both in the positive and negative field regions when the applied field is decaying (Fig. 6b). On further cooling the sample again displays almost anhysteretic behavior (Fig. 6c), before finally reverting at even lower temperature to the more conventional "butterfly" loop expected for normal ferroelectrics (Fig. 6d).

Discussion

The continuous change of lattice parameter with composition, and the absence of any detectable second phase except in the PMW composition clearly indicates complete solid solution between PMN and PMW as would be expected for these lead-containing perovskites. The early appearance of superlattice reflections, when just over 20% of the PMN is substituted by PMW gives a clear indication of the very strong tendency for the Mg^{2+} and W^{6+} ions to dictate an ordered cation arrangement; however the dielectric data clearly show that relaxor character and diffuse transition behavior is preserved up to more than 70 mole% PMW substitution.

Phenomenologically, the rapid reduction of the general levels of ε_w in the paraelectric phase may be due either to a rapid reduction of the Curie Weiss temperature θ, or a lowering of the Curie constant C with PMW substitution. Plots of the reciprocal susceptibilities (dielectric stiffness) as a function of temperature (Fig. 7) suggest that both play some role, but that the dominant influence is a rapid reduction of the Curie constant C with PMW content (Fig.7b).

Evidence from the high field polarization behavior at low temperatures indicates that some weak ferroelectric behavior, and a finite level of remanent polarization persists even up to 80 mole% PMW in the solid solution. It is clear, however, from the bias behavior that even in pure PMN, the ferroelectric

response is quite abnormal with a true remanent polarization very much smaller than the total polarization level which can be included under field, and a most unusual "inverse" hysteresis at temperatures in the relaxation range.

On the model which has been proposed by Smolenskii et al.[1] and others[2,3] diffusion of the phase transition is attributed to spatial fluctuations in the distribution of the disordered B site cations in the PMN giving rise to a spatial distribution of "local" transition temperatures, and a complex admixing of both intrinsic and extrinsic polarization mechanisms. The slow components of the polarizability are suggested to arise primarily through extrinsic phenomena such as domain wall motion in the ferroelectric regions or phase boundary motion at the edges of the polar ferroelectric regions, and to give rise to the observed low frequency dispersion in ε'.

Recent studies on the "aging" phenomena in relaxor ferroelectrics in the PLZT family[7] and in PMN[8] give further support to this model by demonstrating an aging of the dispersive component similar to that observed in conventional ferroelectric ceramics in the ferroelectric phase.

We believe that the present study gives further rather conclusive evidence for local spatial heterogeneity in the cation distribution for this solid solution system. Obviously, Nb^{5+} and Mg^{2+} cannot order in a simple alternate fashion without massive change or chemical imbalance developing, yet even at a 40 mole% PMW addition there is clear evidence of an ordered arrangement giving quite strong superlattice reflections. It is natural to suggest that these must arise primarily from local regions which are richer in tungsten, and that the order would break down in the local regions which are richer in niobium. In this manner, locally disordered regions with fluctuations in the Nb^{5+} Mg^{2+} ratios and associated distributed Curie temperatures should persist across most of the phase diagram and it would not be surprising to find dispersive behavior up to compositions with more than 70 mole% PMW.

Similarly, however, it would be expected that ordered regions rich in tungsten, which have a tendency to favor antipolar cation displacements would not provide paths of easy flux linkage for the dielectric displacement at high fields and would strongly reinforce the role of the "low Curie temperature" regions in the pure PMN, and thus rapidly reduce any true ferroelectric remanence in the lower temperature phase as is observed.

Summary

These studies have shown that PMN:PMW form a complete range of solid solutions with, at higher temperatures, a cubic perovskite structure. Relaxor character in the weak field dielectric response is presented in compositions up to 60 mole% PMW, but decreases rapidly at higher concentrations, whereas superlattice reflections corresponding to an ordered cation arrangement begin to appear in compositions with more than 20 mole% PMW. High field response at low temperatures indicate a rapid diminution in remanent polarization with PMW concentration, but weak ferroelectricity has been traced up to 80 mole% PMW compositions. All samples with relaxor character exhibit an unusual "inverse" hysteresis in ε_w under bias when measured at temperatures close to the Curie range. The behavior is qualitatively explained on the basis of the Smolenskii model for the ferroelectric with a diffuse phase transition.

References

1. G.A. Smolenskii, A.I. Agranovskaya. Soviet Phys.-Solid State 1, 1429 (1959).
2. V.H. Bokov, I.E. Mylnikova. Soviet Phys.-Solid State 3, 613 (1961).
3. Ferroelectric and Antiferroelectric Substances. Landolt Bornstein (New Series) Vol. 3. Editor in Chief K. Hellwege. Springer, 1969.
4. Ferroelectric and Antiferroelectric Substances. Landolt Bornstein (New Series) Vol. 9. Editor in Chief K. Hellwege. Springer, 1975.
5. A.I. Zaslavskii, M.F. Bryzhina. Kristallografiya 1, 709 (1962).
6. E.G. Steward, H.P. Rooksby. Acta Cryst. 4, 503 (1951).
7. W.A. Schulze, J.V. Biggers, L.E. Cross. J. Am. Ceram. Soc. 61, 46 (1978).
8. W.A. Schulze. Private Communication.

Figure Captions

Fig. 1 Lattice constant and superstructure line intensity as a function of composition in PMN:PMW solid solutions.

Fig. 2 Dielectric permittivity as a function of temperature in PMN:PMW solid solid solutions at a fixed frequency of 100 KHz.

Fig. 3 Dielectric dispersion in a 0.6PMN:0.4PMW solid solution.

Fig. 4 (a) Dispersion of the temperature of maximum permittivity in PMN:PMW solid solutions.

(b) Dispersion range as a function of composition in PMN:PMW solid solutions.

Fig. 5 (a) Maximum remanent polarization P_r vs temperature.

(b) Maximum remanence as a function of composition.

Fig. 6 Dielectric saturation as a function of DC biasing field in PMN.

(a) 39°C (b) -17°C (c) -94°C (d) -136°C

Fig. 7 (a) Inverse dielectric susceptibility (dielectric stiffness) as a function of temperature in PMN:PMW solid solutions.

(b) Curie constant C as a function of composition in PMN:PMW solid solutions.

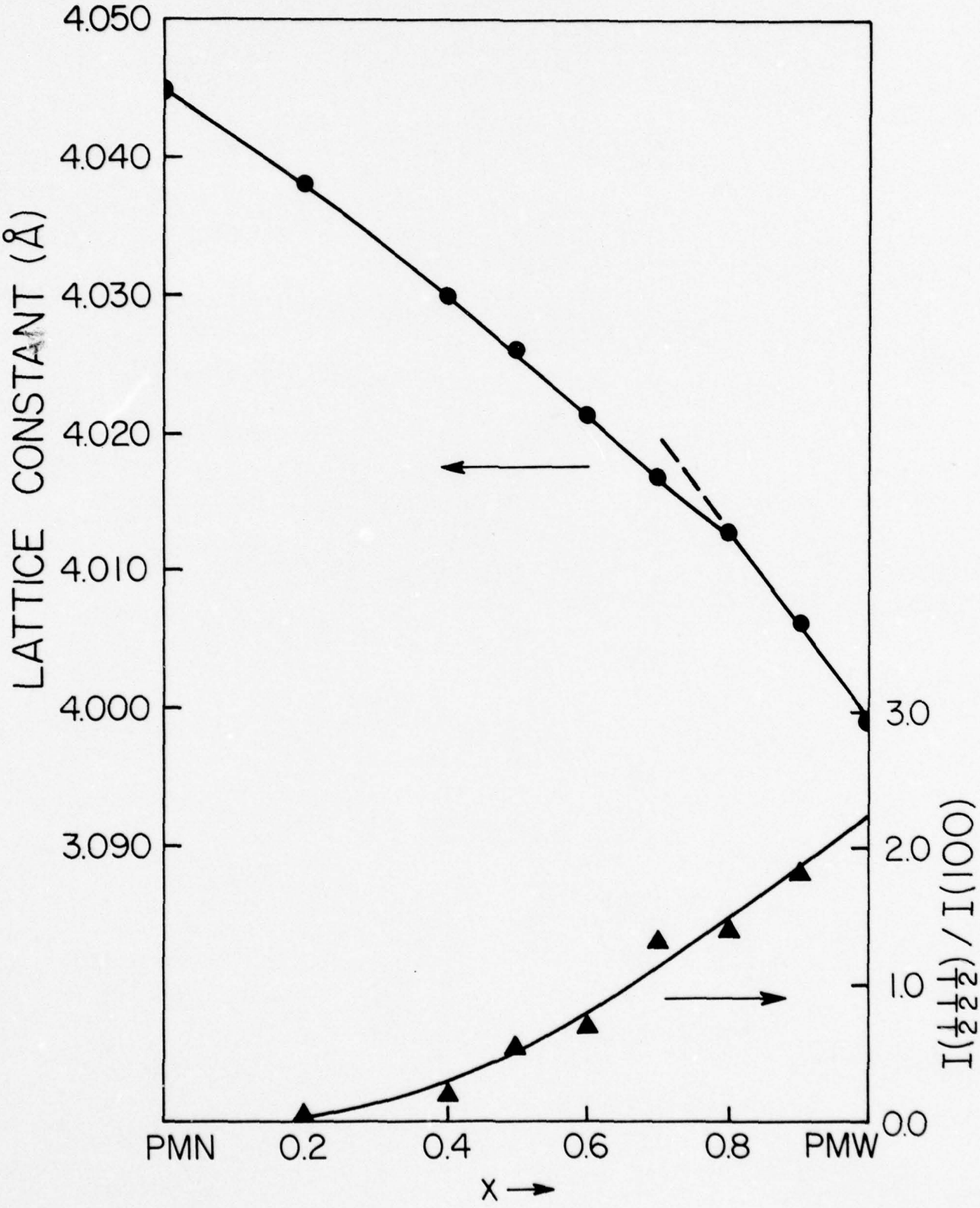
4.050
4.040
4.030
4.020
4.010
4.000
3.090
LATTICE CONSTANT (Å)
3.0
2.0
1.0
0.0
I(111) / I(100)
PMN
0.2
0.4
0.6
0.8
PMW
X →

Fig. 1

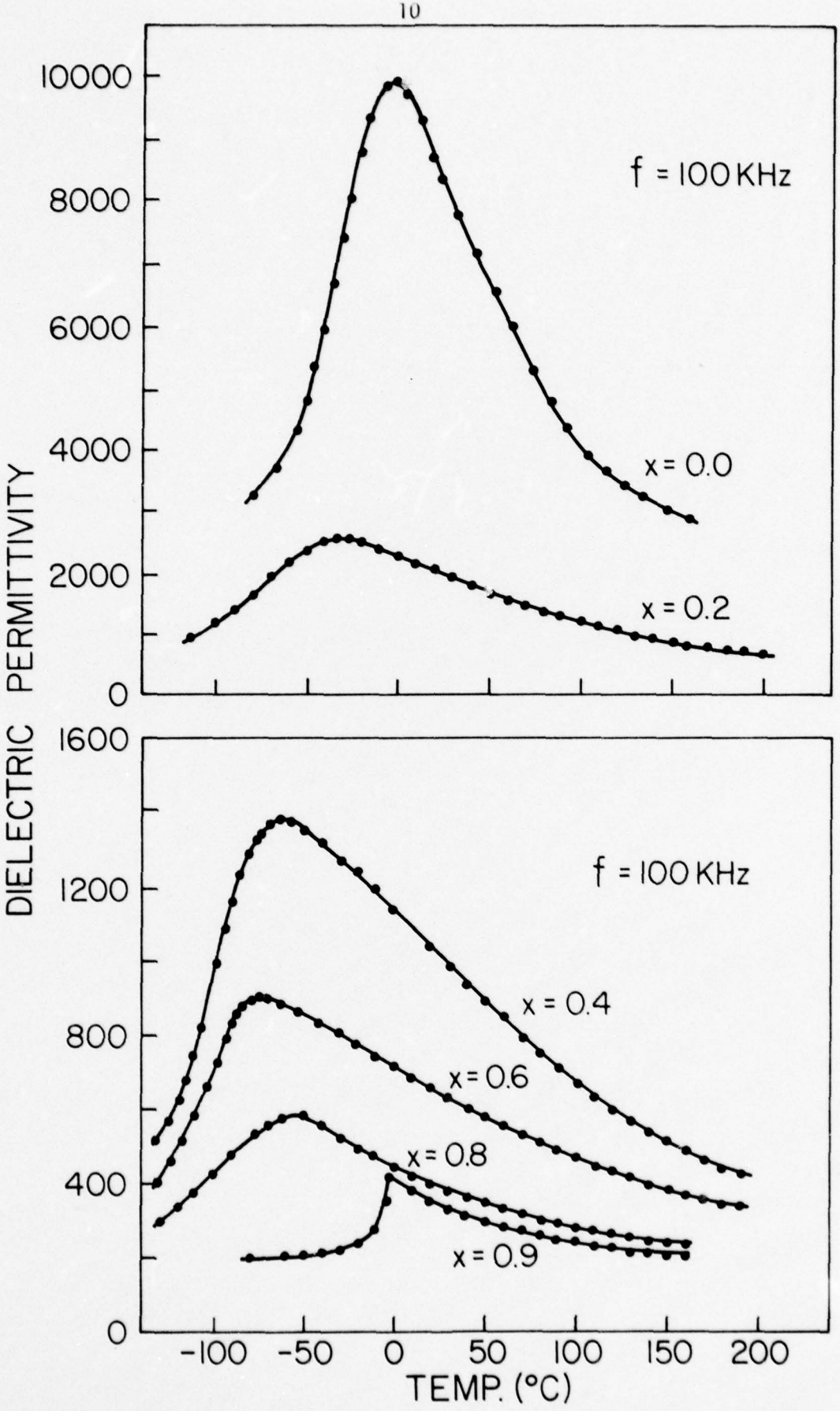
10000
8000
6000
4000
2000
0
f = 100 KHz
x = 0.0
x = 0.2
DIELECTRIC PERMITTIVITY
1600
1200
800
400
0
f = 100 KHz
x = 0.4
x = 0.6
x = 0.8
x = 0.9
-100
-50
0
50
100
150
200
TEMP. (°C)

Fig. 2

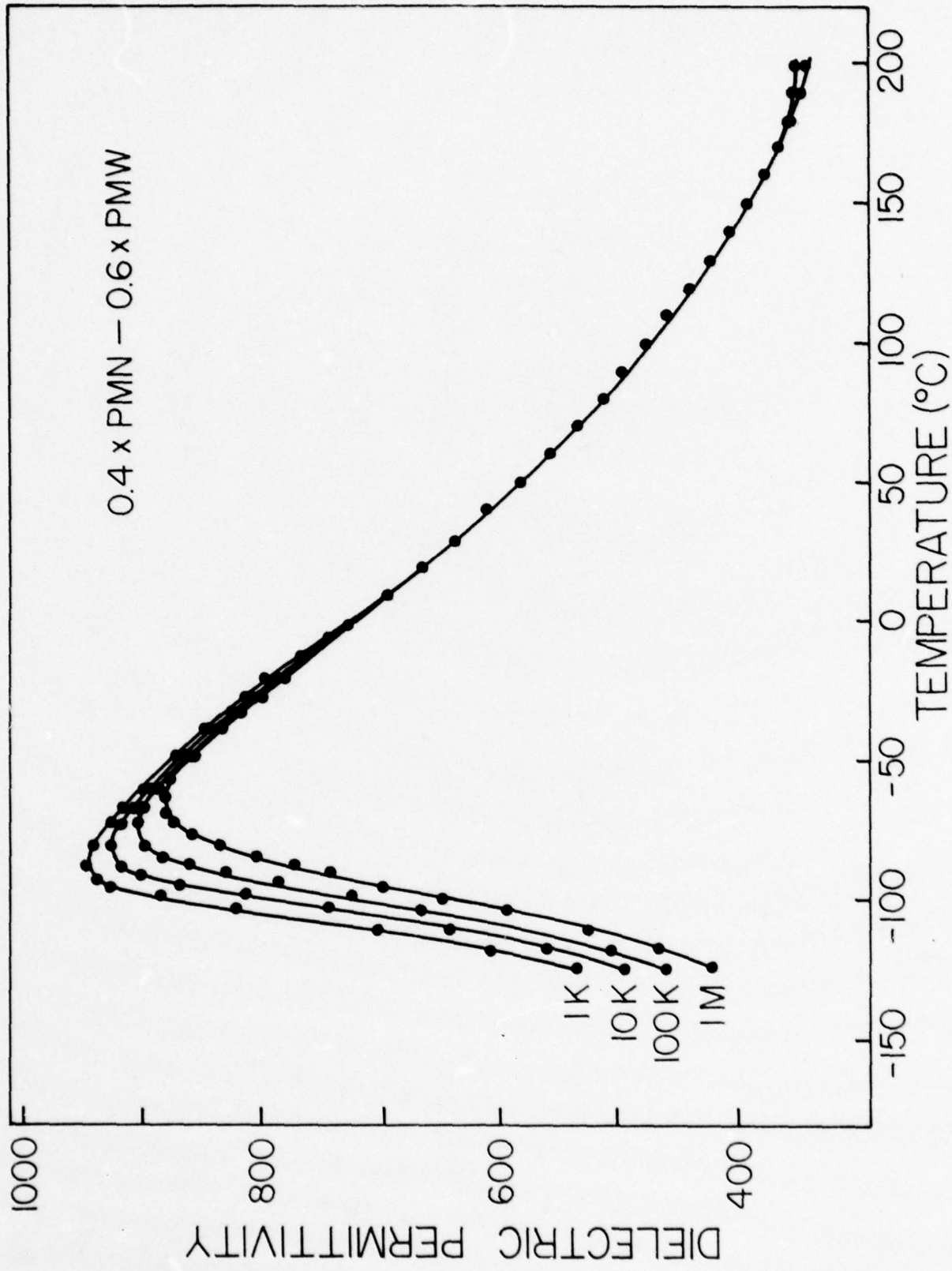
0.4 x PMN — 0.6 x PMW
1K
10K
100K
1M
DIELECTRIC PERMITTIVITY
1000
800
600
400
-150
-100
-50
0
50
100
150
200
TEMPERATURE (°C)

Fig. 3

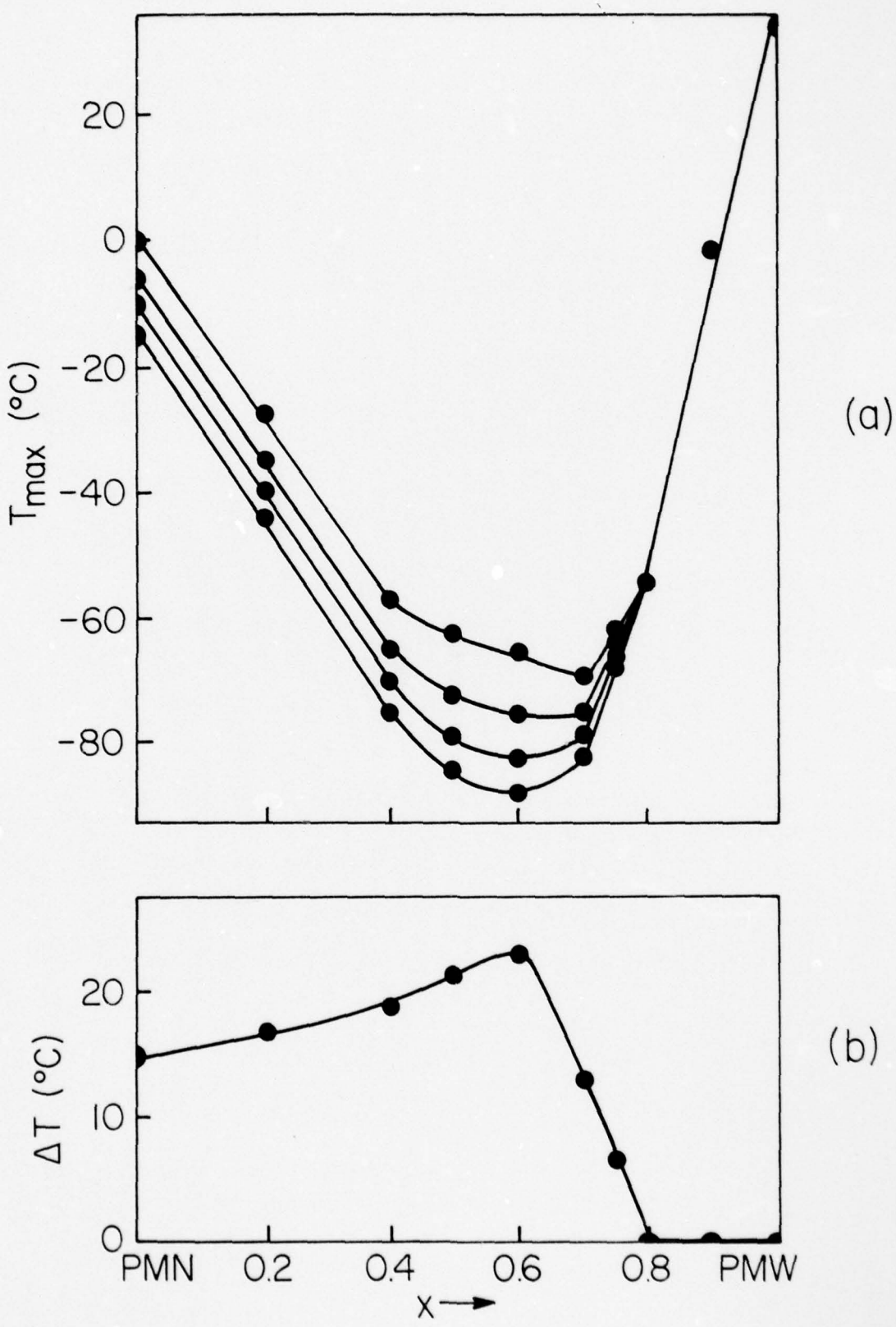

Fig. 4

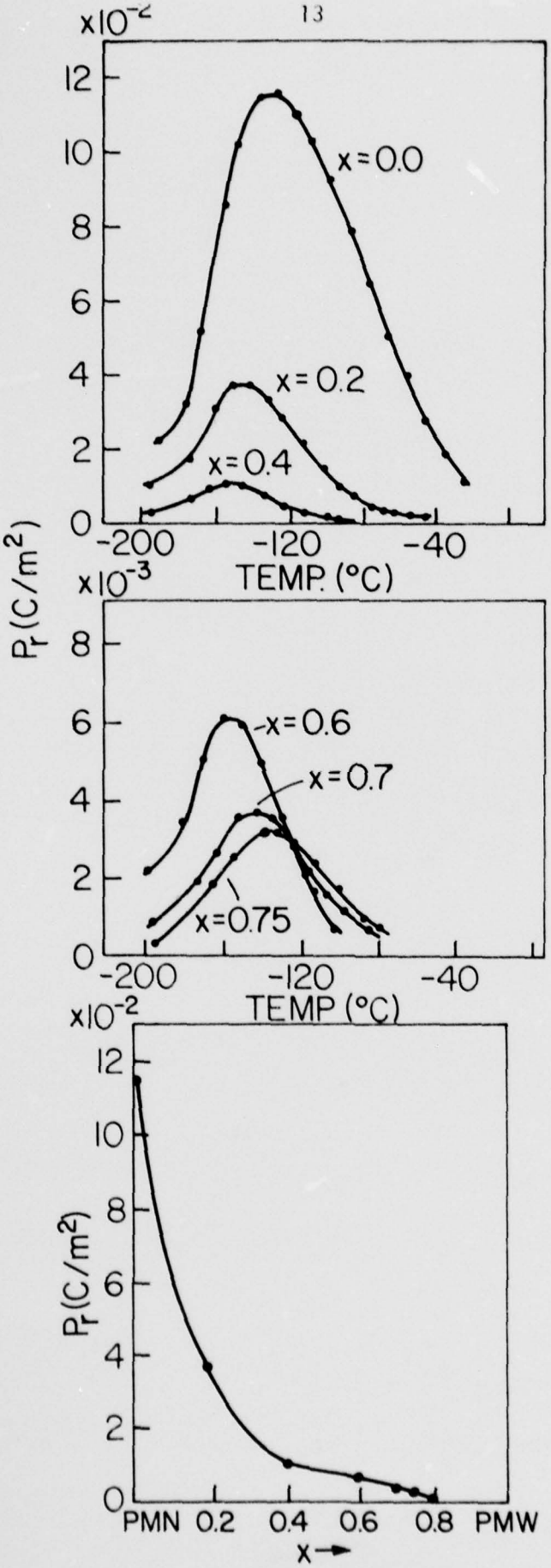
x10⁻²
12
10
8
6
4
2
0
x=0.0
x=0.2
x=0.4
-200
-120
-40
TEMP. (°C)
Pr(C/m²)
x10⁻³
8
6
4
2
0
x=0.6
x=0.7
x=0.75
-200
-120
-40
TEMP (°C)
x10⁻²
12
10
8
6
4
2
0
Pr(C/m²)
PMN 0.2 0.4 0.6 0.8 PMW
x→

(a)

(b)

Fig. 5

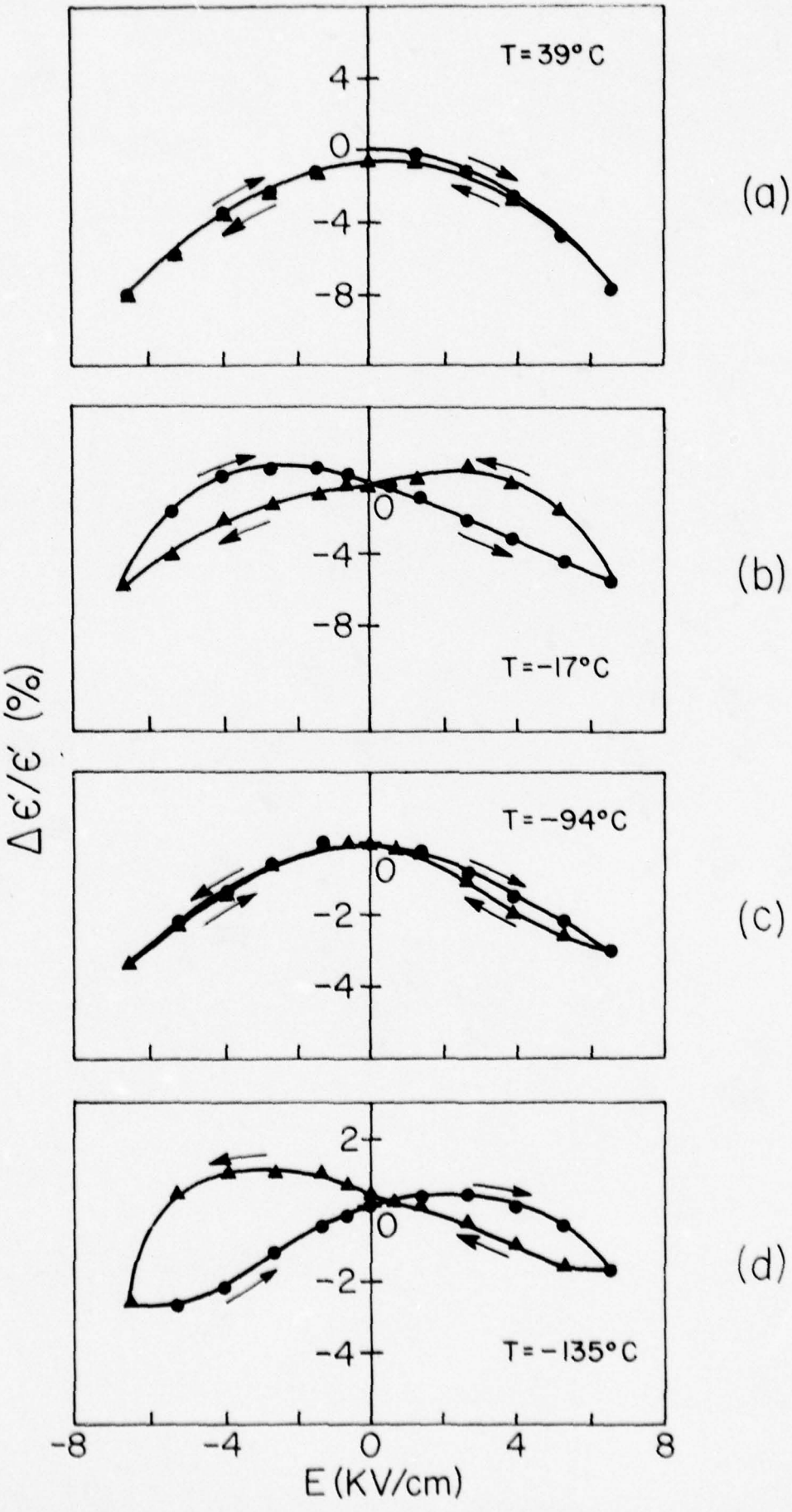

Fig. 6

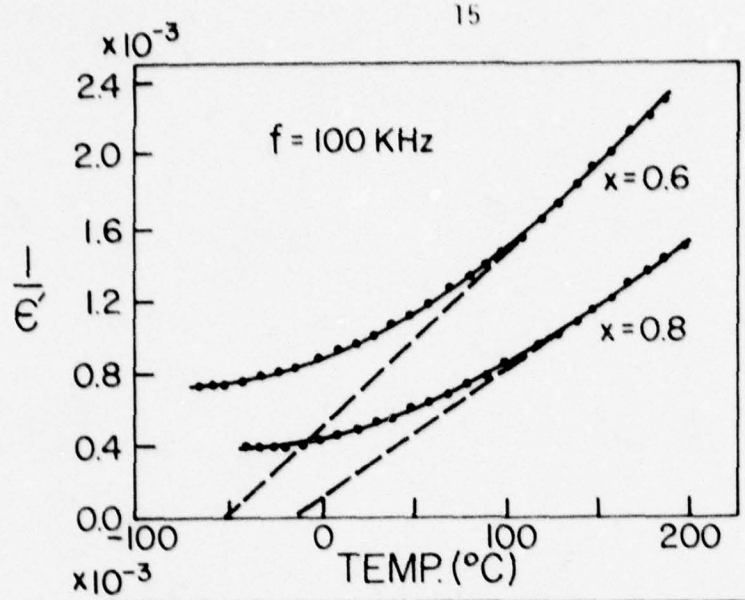
x10⁻³
2.4
2.0
1.6
1.2
0.8
0.4
0.0
f = 100 KHz
x = 0.6
x = 0.8
1/ε'
-100
0
100
200
TEMP. (°C)

(a)

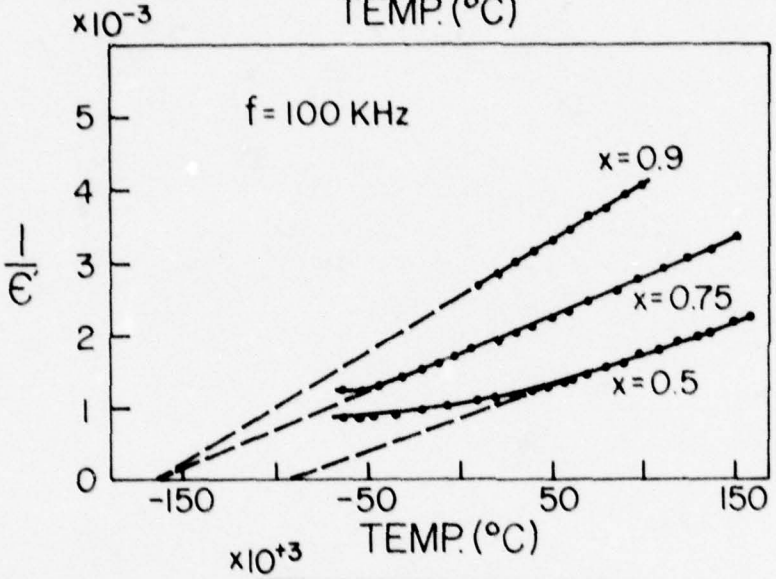
x10⁻³
5
4
3
2
1
0
f = 100 KHz
x = 0.9
x = 0.75
x = 0.5
1/ε'
-150
-50
50
150
TEMP. (°C)

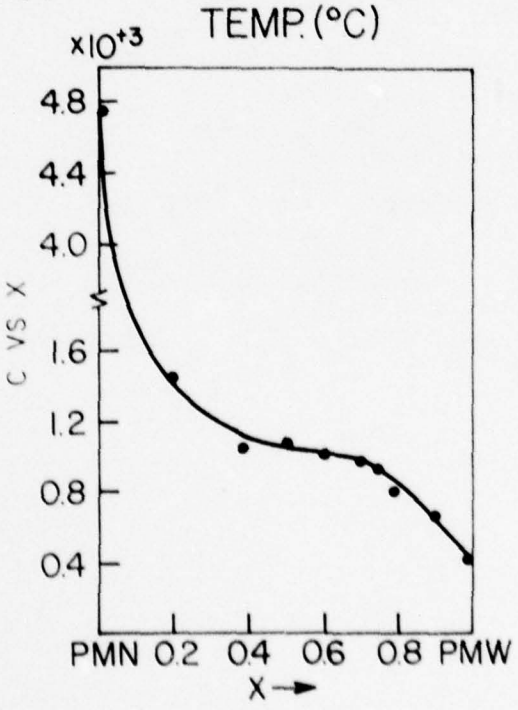
x10⁺³
4.8
4.4
4.0
1.6
1.2
0.8
0.4
C VS X
PMN 0.2 0.4 0.6 0.8 PMW
X →

(b)

Fig. 7

APPENDIX II

CONNECTIVITY AND PIEZOELECTRIC-PYROELECTRIC COMPOSITES

R.E. Newnham, D.P. Skinner and L.E. Cross
Materials Research Laboratory
The Pennsylvania State University
University Park, Pennsylvania 16802

ABSTRACT

Connectivity is a critical parameter in composites designed for use as piezoelectric transducers or as pyroelectric detectors. There are ten important connectivity patterns in diphasic solids, ranging from a 0-0 unconnected checkerboard pattern to a 3-3 pattern in which both phases are three dimensionally self-connected. Processing methods for manufacturing some of these patterns are described. Series and parallel models for composite piezoelectrics and pyroelectrics lead to several interesting results, such as a diphasic pyroelectric in which neither phase is pyroelectric. The models are also helpful in interpreting the structure-property relations in single-phase materials where the crystal structures mimic certain connectivity patterns.

Introduction

Led by the semiconductor industry, materials science has entered a new era, the age of carefully patterned inhomogeneous solids designed to perform specific functions. No longer as much concerned with the properties of the best single-phase materials, many scientists now search for the best combination of materials and ways to process them. In a very real sense, the field has matured from science to engineering just as electrical science changed to electrical engineering years ago.

In most electronic devices there are several phases involved and a number of material parameters to be optimized. An electromechanical transducer, for example, may require a combination of properties such as large piezoelectric coefficient (d or g), low density, and mechanical flexibility. A pyroelectric detector might require large pyroelectric coefficient, low thermal capacity, and low dielectric constant. In general, the task of materials design may be considerably simplified if it is possible to devise a figure of merit which combines the most sensitive parameters in a form allowing simple intercomparison of the possible "trade offs" in property coefficients. In certain pyroelectric systems, for example, a useful figure of merit is p/ε where p is the pyroelectric coefficient and ε the electric permittivity.

Unfortunately, the figure of merit often involves property coefficients which are conflicting in nature. To make a flexible electromechanical transducer it would be desirable to use the large piezoelectric effects in a poled ceramic piezoelectric, but ceramics are brittle and stiff lacking the required flexibility, while polymers having the desired mechanical properties are at best very weak piezoelectrics. Thus, for such an application a composite material combining the desirable properties of two different phases might be vastly superior. The main problem is to effect the combination in such a manner as to exploit the desirable features of both components and thereby maximize the figure of merit.

Combining materials means not only choosing component phases with the right properties, but also coupling them in the best manner. Connectivity of the individual phases is of utmost importance, because this controls the electric flux pattern as well as the mechanical properties. Symmetry is a second important consideration, since symmetry and properties are interrelated through tensor coefficients. In this regard there are several levels of symmetry to be considered: the crystallographic symmetry of each phase, the symmetry after processing, the combined symmetry of the composite, and the environmental influence on the total symmetry including electrodes and clamps.

The points of interest are schematically formalized in Fig. 1 for a simple two-phase system. It is interesting to note that in some composites, not only are the properties of the separate phases modified (sum properties), but the composite may exhibit completely new couplings (product properties) not found in the separate phases.

A physical property relates an input physical quantity X to an output physcial quantity Y. The X-Y effect may be a linear relationship specified by a property coefficient $C = \partial Y/\partial X$, or it may be a more complicated effect. As pointed out by van Suchtelen (1), two classes of X-Y effects can be distinguished in composites.

Sum properties are those in which the X-Y effect of the composite is determined by the X-Y effects in phases 1 and 2. As an example, consider the stiffening of a matrix by strong parallel fibers. Young's modulus of the composite ($\bar{E}$) depends on the moduli of the matrix phase (^1E) and the embedded fiber phase (^2E). In the direction of the fibers, $\bar{E}$ is given by $^1Ex + {}^2E(1-x)$, where x is the volume fraction (2). When measured in various directions, such properties often vary between the geometric and arithmetic mean of the properties associated with the constituent phases.

Product properties are less expected and somewhat more complicated: An X-Y effect in the composite results from an X-Z effect in phase 1 and a Z-Y effect in phase 2. In other words, applying X to the composite causes Z to change in phase 1; the change in Z in phase 1 causes Z to change in phase 2, which then results in a change in Y in phase 2. The transfer of the quantity Z from 1 to 2 can be accomplished by several different kinds of coupling.

As an example of a product property, consider a magnetoelectric composite made from a ferroelectric (phase 1) and a ferromagnetic (phase 2). Crystallites of the two phases are assumed to be in good mechanical contact. The ferroelectric grains are poled near the ferroelectric Curie temperature in a strong electric field to make the composite piezoelectric. Magnetic poling of the ferromagnetic phase is accomplished in a similar way, by annealing the composite in a magnetic field.

When an electric field is applied to a magnetoelectric composite of this type the ferroelectric grains elongate parallel to the electric field. The change in shape of the ferroelectric grains causes the ferromagnetic grains to deform, resulting in a change in magnetization.

To illustrate, consider a composite of barium titanate and cobalt ferrite. The single crystal monodomain point symmetries are 4mm1' for $BaTiO_3$ and $\frac{4}{m}$ m'm' for $CoFe_2O_4$. When prepared as polycrystals, the symmetries revert to spherical $\infty\infty$m1'. If poled, however, the ferroelectric ceramic becomes ∞m1' and the ferrimagnetic ceramic $\frac{\infty}{m}$m'. If the electric and magnetic poling fields are applied in the same direction, the net symmetry of the composite is magnetic point group ∞m'. This point symmetry exhibits the magnetoelectric effect, even though neither $BaTiO_3$ nor $CoFe_2O_4$ alone is magnetoelectric! Measurements on $BaTiO_3$–$CoFe_2O_4$ composites prepared by unidirectional solidification at the eutectic composition show magnetoelectric coefficients two orders of magnitude larger than the best single phase material (3,4). Another interesting product property is described in a later section: a pyroelectric composite made from two non-pyroelectric phases.

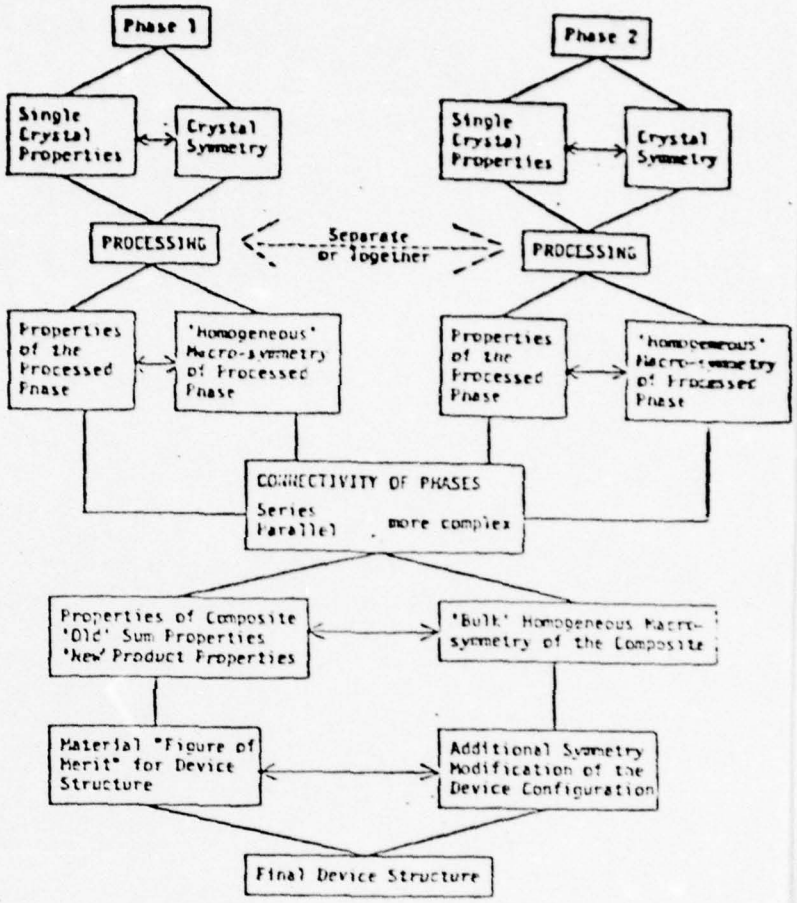

FIG. 1
Flow chart illustrating design considerations for optimizing the performance of solid state devices. The task of the materials engineer is to find the materials, processing methods, and connectivity patterns which maximize the figure of merit.

Connectivity

Connectivity is a key feature in property development in multiphase solids since physical properties can change by many orders of magnitude depending on the manner in which connections are made. Imagine, for instance, an electric wire in which the metallic conductor and its rubber insulation were connected in series rather than in parallel.

Each phase in a composite may be self-connected in zero, one, two, or three dimensions. It is natural to confine attention to three perpendicular axes because all property tensors are referred to such systems (5). If we limit the discussion to diphasic composites, there are ten connectivities: 0-0, 1-0, 2-0, 3-0, 1-1, 2-1, 3-1, 2-2, 3-2, and 3-3. The ten different connectivities are illustrated in Fig. 2, using a cube as the basic building block. A 2-1 connectivity pattern, for example, has one phase self-connected in two-dimensional layers, the other self-connected in one-dimensional chains or fibers. The

connectivity patterns are not geometrically unique. In the case of a 2-1 pattern the fibers of the second phase might be perpendicular to the layers of the first phase, as in Fig. 2, or they might be parallel to the layers.

In passing we note that connectivity patterns for more than two phases are basically similar to the diphasic patterns, but far more numerous. There are 20 three-phase patterns and 35 four-phase patterns compared to the 10 two-phase patterns in Fig. 2. For n phases the number of connectivity patterns is $(n+3)!/3!n!$. Triphasic connectivity patterns are important when electrode patterns are incorporated in the diphasic ceramic structures discussed later.

During the past few years we have been developing processing techniques for making diphasic ceramic composites with different connectivities. Extrusion, tape-casting and replamine methods have been especially successful. The 3-1 connectivity pattern in Fig. 2 is ideally suited to extrusion processing. A ceramic slip is extruded through a die giving a three-dimensionally connected pattern with one-dimensional holes, which can later be filled with a second phase.

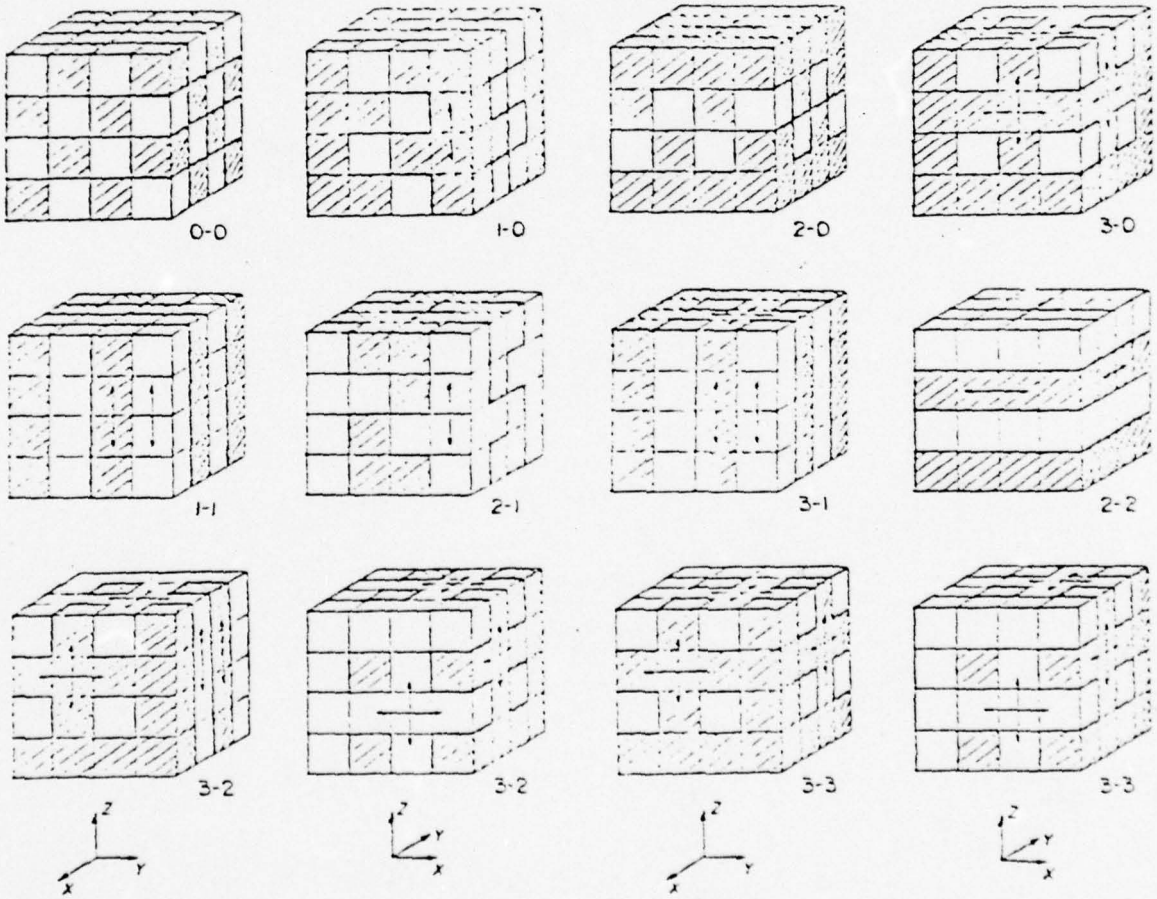

FIG. 2

Ten connectivity patterns for a diphasic solid. Each phase has zero-, one-, two- or three-dimensional connectivity to itself. In the 3-1 composite, for instance, the shaded phase is three-dimensionally connected and the unshaded phase is one-dimensionally connected. Arrows are used to indicate the connected directions. Two views of the 3-3 and 3-2 patterns are given because the two interpenetrating networks are difficult to visualize on paper. The views are related by 90° counterclockwise rotation about Z.

Another type of connectivity well suited to processing is the 2-2 pattern made up of alternating layers of the two phases. The tape-casting of multilayer capacitors with alternating layers of metal and ceramic is a way of producing 2-2 connectivity. In this arrangement both phases are self-connected in the lateral X and Y directions but not connected perpendicular to the layers along Z.

In 3-2 connectivity, one phase is three-dimensionally connected, the other in two. This pattern can be considered a modified multilayer pattern with 2-2 connectivity. If holes are left in the layers of one phase, layers of the second phase can connect through the holes giving three-dimensional connectivity.

The most complicated and in many ways the most interesting pattern is 3-3 connectivity (Fig. 2) in which the two phases form interpenetrating three-dimensional networks. Patterns of this type often occur in living systems such as coral where organic tissue and an inorganic skeleton interpenetrate one another. These structures can be replicated in other materials using the lost-wax method (6). The replamine process, as it is called, can also be used to duplicate the connectivity patterns found in foam, wood, and other porous materials.

Four examples of electroceramics with different connectivity patterns are shown in Fig. 3. Diphasic ceramic capacitors have been made of $BaTiO_3$ grains separated by thin layers of $NaNbO_3$ in the grain boundary regions. The sodium niobate is three-dimensionally connected while the barium titanate grains are not in contact, making it a 3-0 connectivity pattern. The ceramic is manufactured by liquid phase sintering at temperatures above the melting point of $NaNbO_3$ but below that of $BaTiO_3$. At these temperatures, sodium niobate melts and coats the $BaTiO_3$ grains but rapid cooling prevents reaction between the two phases. High dielectric constant capacitors made with these microstructures show excellent high-voltage characteristics. Normally, the polarization of barium titanate capacitors saturates at high voltages, with the dielectric constant decreasing by as much as a factor of two; but separating the grains of ferroelectric $BaTiO_3$ with a thin layer of antiferroelectric $NaNbO_3$ compensates the saturation effect to give a flat voltage response (7).

Connectivity patterns can be synthesized as macrostructures, as microstructures, or even as crystal structures. The $BaTiO_3$-$NaNbO_3$ composite just considered had a 3-0 microstructure. The next three examples involve macrostructures with 3-1, 2-2, and 3-3 connectivities. Figure 3b shows an extruded $BaTiO_3$ honeycomb ceramic made by Dr. Irwin Lachman of the Corning Research Center. The ceramic is three-dimensionally connected with empty channels in one direction to provide the desired 3-1 connectivity. When the channels are filled with metal electrodes, sizable electric fields can be applied across the thin ceramic walls. The device is intended for use as an electrostrictive micropositioner for adaptive optic systems.

Two composite piezoelectric transducers are illustrated in Figs. 3c and 3d. The multilayer composite of "hard" and "soft" PZT has 2-2 connectivity and properties superior to a single-phase piezoelectric. The soft PZT has a large piezoelectric response and is kept in a poled state by the hard PZT. Figure 3d shows a silicone rubber-PZT composite made by the replamine process (6). The 3-3 connectivity provides mechanical strength and flexibility from the high polymer, and electric continuity and a large piezoelectric effect from PZT. These materials will be discussed in more detail in later articles.

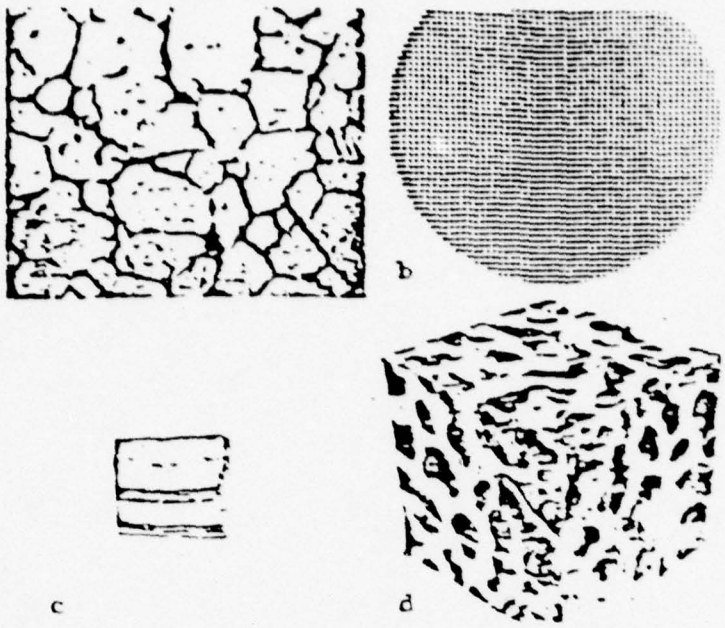

FIG. 3
(a) $BaTiO_3$-$NaNbO_3$ ceramic microstructure with 3-0 connectivity.
(b) Extruded $BaTiO_3$ ceramic with 3-1 connectivity.
(c) Hard and soft PZT multilayers having 2-2 connectivity.
(d) Replamine PZT cast on a coral pattern with 3-3 connectivity.

Piezoelectric Composites

To illustrate the major modifications in ensemble properties which can be effected even in simple linear systems, one-dimensional solutions are presented for the piezoelectric and pyroelectric properties of heterogeneous two-phase structures.

Series Connection: Consider first the piezoelectric properties of lamellar diphasic composites. Longitudinal piezoelectric coefficient $\bar{d}_{33}$ has been derived for a diphasic piezoelectric with the constituent phases arranged in alternating layers normal to the x_3 direction (Fig. 4a). Designating phase 1 with a superscript 1, and phase 2 with superscript 2, phase 1 has volume fraction ^1v, piezoelectric coefficient $^1d_{33}$ and permittivity $^1\varepsilon_{33}$, and phase 2 has ^2v, $^2d_{33}$, and $^2\varepsilon_{33}$, respectively. Solving for the piezoelectric coefficient of the composite gives

$$\bar{d}_{33} = \frac{^1v\,^1d_{33}\,^2\varepsilon_{33} + {}^2v\,^2d_{33}\,^1\varepsilon_{33}}{^1v\,^2\varepsilon_{33} + {}^2v\,^1\varepsilon_{33}} \tag{1}$$

Using the relation $\bar{g}_{33} = \bar{d}_{33}/\bar{\varepsilon}_{33}$ yields the piezoelectric voltage coefficient

$$\bar{g}_{33} = \frac{^1v\,^1d_{33}}{^1\varepsilon_{33}} + \frac{^2v\,^2d_{33}}{^2\varepsilon_{33}} = {}^1v\,^1g_{33} + {}^2v\,^2g_{33} \tag{2}$$

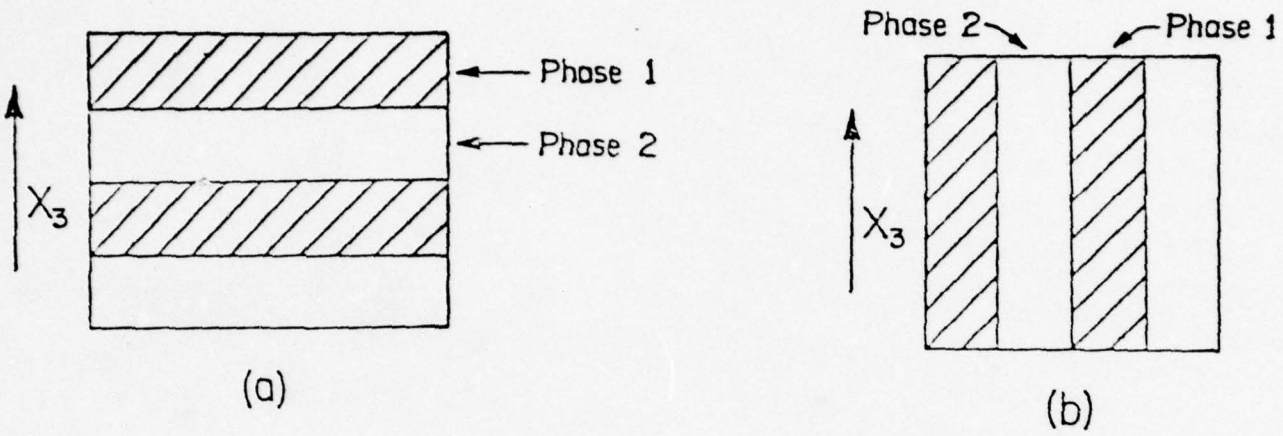

FIG. 4
The series (a) and parallel (b) models used in estimating the piezoelectric and pyroelectric effects of diphasic solids.

It is interesting to note that for series connection even a very thin low-permittivity layer rapidly lowers the d-coefficient but has little effect on the corresponding g-coefficient.

Parallel Connection: If the two phases lie in layers perpendicular to the electrode (Fig. 4b), again for the one-dimensional case and neglecting transverse coupling, the composite piezoelectric coefficient is

$$\bar{d}_{33} = \frac{{}^1v\,{}^1d_{33}\,{}^2s_{33} + {}^2v\,{}^2d_{33}\,{}^1s_{33}}{{}^1v\,{}^2s_{33} + {}^2v\,{}^1s_{33}} \tag{3}$$

where ${}^1s_{33}$ and ${}^2s_{33}$ are the elastic compliances for stresses normal to the electrodes. For the voltage coefficient,

$$\bar{g}_{33} = \frac{{}^1v_1\,{}^1d_{33}\,{}^2s_{33} + {}^2v\,{}^2d_{33}\,{}^1s_{33}}{({}^1v\,{}^2s_{33} + {}^2v\,{}^1s_{33})({}^1v\,{}^1\varepsilon_{33} + {}^2v\,{}^2\varepsilon_{33})} \tag{4}$$

A composite of interest here is that of an elastically compliant nonpiezoelec-

tric in parallel with a stiff piezoelectric. In this case ${}^1d_{33} >> {}^2d_{33} = 0$, ${}^1s_{33} << {}^2s_{33}$, ${}^1v = {}^2v = 1/2$ then $\bar{d}_{33} = {}^1d_{33}$, and if ${}^1\varepsilon_{33} >> {}^2\varepsilon_{33}$, then $\bar{g}_{33} = {}^2{}^1g_{33}$, and for smaller volume fractions of the piezoelectric phase, the g-coefficient is correspondingly amplified. It is this case which accounts for the highly successful performance of the replamineform transducer structure described in a later paper. The structure also has considerable hydrostatic sensitivity.

Pyroelectric Composites

The corresponding series and parallel connected diphasic systems have also been studied for pyroelectric response. It is well known that all pyroelectric crystals are also piezoelectric and that the thermal expansion generated on heating gives rise to a strain which operates through the piezoelectric coefficients to give an additional secondary pyroelectric effect. If the crystal is free to expand, what is normally measured is the sum of primary and secondary effects, and in some materials both components are of the same order of magnitude. It must be remembered, however, that in many materials (poled PZT is a good example) the hydrostatic piezoelectric effect is small, due to cancellation between coefficients with opposite sign. Clearly, if the negative part of the piezoelectric response could be removed by suitable clamping, the secondary contribution to the pyroelectric effect could be strongly enhanced.

Simple Series Connection: Consider the response of a multilayer diphasic pyroelectric (Fig. 4a) made up from a volume fraction ${}^1v$ of phase with permittivity ${}^1\varepsilon_{33}$ and pyroelectric coefficient ${}^1p_3$, interleaved along the x_3-direction with a phase of volume fraction ${}^2v$, permittivity ${}^2\varepsilon_{33}$, and pyroelectric coefficient ${}^2p_3$. Piezoelectric and thermal expansion coefficients are represented by d_{ij} and α_i, respectively. To simplify the calculation we assume that both phases are poled ceramics with conical symmetry and with the polar axis (x_3) perpendicular to the plane of the interleaving layers.

With close transverse connection of thin sheets, and assuming no surface tractions, the total pyroelectric effect is calculated for a uniform temperature change ΔT. There are two terms corresponding to the primary and secondary effects:

$$\bar{p}_3 = \frac{{}^1v\,{}^1p_3\,{}^2\varepsilon_{33} + {}^2v\,{}^2p_3\,{}^1\varepsilon_{33}}{{}^1v\,{}^2\varepsilon_{33} + {}^2v\,{}^1\varepsilon_{33}} +$$

$$\frac{{}^1v\,{}^2v({}^2\varepsilon_{33}\,{}^1d_{31} - {}^1\varepsilon_{33}\,{}^2d_{31})({}^2\alpha_1 - {}^1\alpha_1)}{({}^1v\,{}^2\varepsilon_{33} + {}^2v\,{}^1\varepsilon_{33})[{}^1v({}^2s_{11} + {}^2s_{12}) + {}^2v({}^1s_{11} + {}^1s_{12})]}$$

and for the figure of merit:

$$\frac{\bar{p}_3}{\varepsilon_{33}} = \frac{{}^1v\,{}^1p_3}{{}^1\varepsilon_{33}} + \frac{{}^2v\,{}^2p_3}{{}^2\varepsilon_{33}} + \frac{{}^1v\,{}^2v({}^2\alpha_1 - {}^1\alpha_1)}{[{}^1v({}^2d_{11} + {}^2s_{12}) + {}^2v({}^1s_{11} + {}^1s_{12})]}\left(\frac{{}^1d_{31}}{{}^1\varepsilon_{33}} - \frac{{}^2d_{31}}{{}^2\varepsilon_{33}}\right)$$

The secondary pyroelectric effect makes a major contribution for sizable thermal expansion mismatch ($^2\alpha_1 - {}^1\alpha_1$). This is a good example of a product property since neither phase is required to exhibit primary pyroelectricity. Devices based on these principles are under construction, both here and elsewhere.

Secondary pyroelectric effects also appear in composite with parallel connectivity. In this case, the composite pyroelectric coefficient is

$$\bar{p}_3 = {}^1v\,{}^1p_3 + {}^2v\,{}^2p_3 + \frac{{}^1v\,{}^2v({}^2\alpha_3 - {}^1\alpha_3)({}^1d_{33} - {}^2d_{33})}{{}^1v\,{}^2s_{33} + {}^2v\,{}^1s_{22}}$$

We are experimenting with SbSI - plastic composites based on this geometry.

Structure-Property Relationships

Many of the ideas developed for composite materials are relevant to single-phase materials as well. The concepts of parallel and series connectivity, for instance, can be used to explain the anisotropy in properties of single crystals. As an example, it is instructive to examine the structure-property relationships for the hydrostatic piezoelectric effect, and to compare the relationships with the composite models derived in the earlier sections.

Hydrostatic pressure coefficients for a number of piezoelectric crystals and ceramics are given in Table 1. Since the symmetry requirements for pyroelectricity and hydrostatic piezoelectricity are identical, all the materials are also pyroelectric. For purposes of discussion, they can be divided into ferroelectric pyroelectrics and ordinary (non-ferroelectric) pyroelectrics. As shown in Table 1, the ferroelectrics have substantial d_h coefficients but the g_h values are not very big because of their large permittivities.

Ordinary pyroelectrics can be further subdivided into water-soluble pyroelectrics and oxide pyroelectrics. Oxides and sulfides with the wurtzite structure (Fig. 5a) have very small hydrostatic piezoelectric effects. The wurtzite crystal structure is based on a hexagonal close-packed anion lattice with cations in tetrahedral interstices. Compared to the other pyroelectrics, the atomic bonding in the wurtzites is very isotropic. It is not surprising, therefore, that under hydrostatic pressure they deform isotropically, leading to very small piezoelectric effects.

Silicate pyroelectrics have somewhat larger hydrostatic coefficients than the wurtzite group. Tourmaline is a complex borosilicate mineral containing tetrahedral SiO_4 groups. The silica tetrahedra are arranged in Si_6O_{18} rings oriented perpendicular to the pyroelectric axis. This imparts an anisotropy to the structure not found in the wurtzite group. But the silicate and borate groups are linked together by Al^{3+} and Mg^{2+} ions which also form fairly strong chemical bonds and hence tourmaline is not as anisotropic as some other crystals.

More anisotropic structures are found among the water-soluble pyroelectrics. Lithium sulfate monohydrate ($Li_2SO_4.H_2O$) is an important example with an extremely large g_h coefficient, so large that the crystals have been used as hydrostatic pressure sensors. The crystal structure of lithium sulfate contains Li^+ cations, tetrahedral SO_4^{2-} anions, and water molecules. Ionic

TABLE 1

Hydrostatic piezoelectric coefficients for a number of materials. For a given pressure, d_h measures the electric polarization, and g_h the open-circuit electric field. d_h is expressed in units of 10^{-12} C/N and g_h in $10^{-3} m^2/C$.

	d_h	g_h
Water-Soluble Pyroelectrics		
Ethylene diamine tartrate (EDT) $C_2H_4(NH_3)_2\ C_4H_4O_6$	1.0	15
Lithium sulphate monohydrate (LH) $Li_2SO_4.H_2O$	16.4	180
Others	<4	<100
Pyroelectric Silicate Minerals		
Tourmaline $(Na,Ca)(Mg,Fe)_3B_3Al_6Si_6(O,OH,F)_{31}$	2.5	38
Others	<3	<30
Wurtzite-Family Pyroelectrics		
BeO,ZnO,CdS,CdSe	<0.2	<3
Ferroelectric Single Crystals		
Barium titanate $BaTiO_3$	16.6	11
Triglycine sulfate (TGS) $(NH_2CH_2COOH)_3.H_2SO_4$	8.0	30
Antimony sulfur iodide (10°C) SbSI	1100	14
Lithium niobate $LiNbO_3$	14.5	57
Poled Ferroelectric Ceramics		
Barium titanate $BaTiO_3$	34	2
Lead niobate $PbNb_2O_6$	67	34
Lead zirconate titanate (PZT) $Pb(Ti,Zn)O_3$	20-50	2-9
Sodium potassium niobate $(Na,K)NbO_3$	40	10

bonds between cations and anions extend in all directions in the crystals but the hydrogen bonding between water molecules extends only along b, the unique polar axis (Fig. 5b). Tension in this direction produces a large electric polarization. Short hydrogen bonds like those in lithium sulfate make an important contribution to the piezoelectric effect because the proton position changes as the oxygen-oxygen is stretched. In short hydrogen bonds the proton is midway between the oxygens, whereas the proton is unsymmetrically positioned in long H bonds. Mechanical stress, therefore, directly affects the dipole moments of the water molecules, producing electric polarization along the b axis and producing an unusually large d_{22} coefficient in lithium sulfate. The large piezoelectric effect together with a small dielectric constant gives it the largest hydrostatic voltage coefficient (g_h) of any materials, including ferroelectrics.

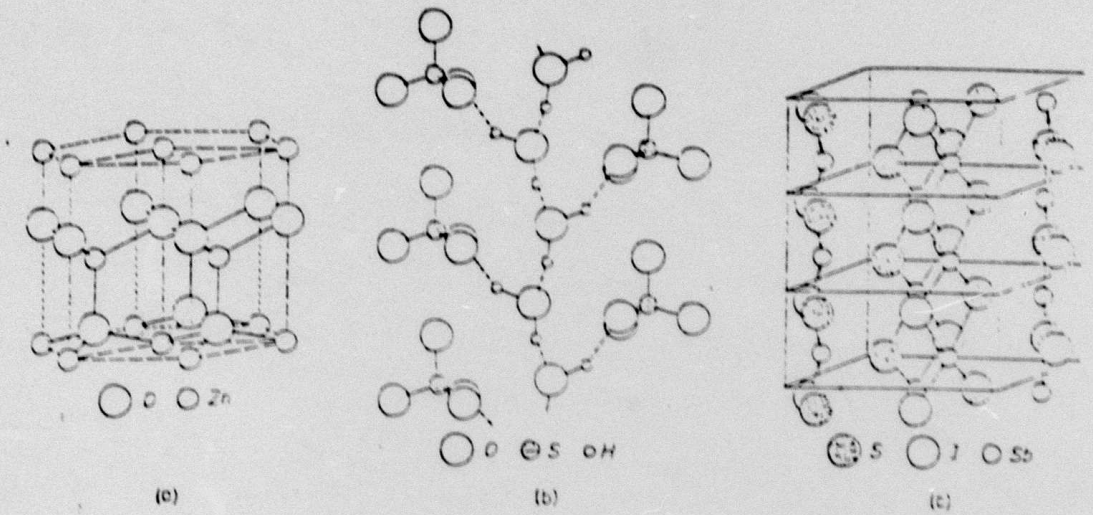

FIG. 5
(a) The wurtzite structure in which ZnO and several other pyroelectrics crystallize. Hydrostatic piezoelectric effects develop along the c axis, but the coefficients are small; (b) In lithium sulfate monohydrate the water molecules form a chain of hydrogen bonds along the polar axis, but are not linked laterally; (c) Ferroelectric SbSI also has a chain structure and great hydrostatic sensitivity. Both materials mimic the parallel connectivity required for large d_{33} coefficients and small d_{31} values.

Because of their large polarizabilities, ferroelectrics also have large piezoelectric constants but the hydrostatic coefficients are not large for those with symmetric crystal structures. $BaTiO_3$, $(Na,K)NbO_3$ and $Pb(Zr,Ti)O_3$ have the perovskite structure which has a close-packed array of oxygens and large cations. The $LiNbO_3$ structure also has close-packed oxygens. The hydrostatic piezoelectric coefficients for these materials are small compared to antimony sulfur iodide (SbSI) which has the largest d_h coefficient in Table 1.

The structure of SbSI (Fig. 5c) is very anisotropic with covalently-bonded chains parallel to the polar axis. Neighboring chains are only weakly bonded by ionic or van der Waals forces. Crystals of SbSI cleave readily parallel to the polar c axis. Under tensile force parallel to c, the crystals develop a large piezoelectric polarization similar in origin to thatin lithium sulfate. The antimony cations displace relative to the anions causing the polarization. Piezoelectric effects in the perpendicular directions are much smaller because of the loose packing of chains.

In summary, we see that the best piezoelectrics for hydrostatic sensors are those with anisotropic structures and a molecular mechanism for piezoelectricity. The analogy with the composite piezoelectrics discussed earlier is rather striking. A particularly useful composite for hydrostatic applications is one with the parallel arrangement composed of a stiff piezoelectric in a compliant matrix. The structures of $LiSO_4.H_2O$ and SbSI resemble this composite on an atomic scale, leading to the conclusion that one can use the composite models in interpreting the properties of a single phase materials as well as composites.

Acknowledgments

This work was sponsored by the Office of Naval Research and by Advanced Research Projects Agency through Contract NOOO14-76-C-0515. We also wish to thank our colleagues at the Materials Research Laboratory for their advice and assistance.

References

1. J. van Suchtelen, Philips Res. Rpts. 27, 28 (1972).

2. J.L. Broutman and R.H. Krock, Modern Composite Materials, Addison-Wesley Publ. Co., Reading, Mass. (1967).

3. J. van den Boomgaard, D.R. Terrell, R.A.J. Born and H.F.J.I. Giller, J. Mat. Sci. 9, 1705 (1974).

4. A.M.J.G. van Run, D.R. Terrell and J.H. Scholing, J. Mat. Sci. 9, 1710 (1974).

5. J.F. Nye, Physical Properties of Crystals, Oxford University Press, London (1957).

6. R.A. White, J.N. Weber and E.W. White, Science 176, 922 (1972).

7. D.A. Payne, "The Role of Internal Boundaries Upon the Dielectric Properties of Polycrystalline Ferroelectric Materials." Ph.D. Dissertation in Solid State Science, The Pennsylvania State University, March 1973.

8. Landolt-Bornstein Tables on Elastic, Piezoelectric, Piezooptic and Electrooptic Constants of Crystals. VOls. II, I (1966) and II,2 (1969). Springer Verlag, Berlin.

APPENDIX IV

APPENDIX III

FLEXIBLE COMPOSITE TRANSDUCERS

D.P. Skinner, R.E. Newnham and L.E. Cross
Materials Research Laboratory
The Pennsylvania State University
University Park, Pennsylvania 16802

ABSTRACT

Flexible PZT/polymer composite transducers have been fabricated with a novel microstructural configuration. The concept of connectivity has been applied in the evaluation of the type of structure needed to optimize the properties of the composite. Properties of several kinds of piezoelectric transducers are compared.

Introduction

Twenty-five years of research have failed to uncover a better piezoelectric than the $Pb(Zr,Ti)O_3$ or PZT family of compositions now in use as ceramic transducers. Similar situations prevail in semiconductors, superconductors, magnetics, and other fields of solid state science. To effect further improvements, many materials engineers are turning to composites--combinations of phases selected for the best individual properties and put together in a manner designed to make maximum use of these properties. Traditionally composites have been formulated with basic properties such as mechanical strength in mind. There exists, however, a number of "coupled properties" which have received considerable attention in single phase materials, but have been relatively neglected in composites. An example of a coupled property is piezoelectricity. In the direct piezoelectric effect an applied mechanical force is coupled to an electrical response in an acentric material. It is through these coupled properties that composite materials are expected to play a vital role in future device design.

In selecting a material to be used in a device, a useful guideline is the "figure of merit"--a combination of parameters pertaining to a particular application which allows one to easily compare the properties of a number of materials and evaluate their potential usefulness. In the case of piezoelectrics used as passive detectors (such as hydrophones) a figure of merit is the piezoelectric voltage coefficient, referred to as the g coefficient. This quantity is arrived at by dividing the piezoelectric strain coefficient, d_{ijk}, by the appropriate permittivity coefficient, ε_{ij}.

One of our recent interests has been in developing low-density, compliant, flexible piezoelectric transducers. A low-density piezoelectric should have better acoustic coupling to water and more easily adjusted buoyancy than the high-density PZT ceramics now used for hydrophones. A compliant material would have better resistance to mechanical shock than a conventional ceramic transducer and a large compliance would also mean high damping, which is desirable in a passive device. A flexible material could be used as a conformal detector. The development of a piezoelectric material which exhibits this combination of seemingly conflicting properties may be carried out in basically two different ways. The traditional approach is to look for a single homogeneous material possessing all the required properties. A material of current interest in this category is poly(vinylidene fluoride), PVF_2.

Piezoelectricity was first reported in this material in 1969 by Kawai (1). In order to make PVF_2 piezoelectrically active, a film of the material usually about 25 to 75 μm thick is electroded and polarized under application of very large electric fields (about 10^7 to 10^8 V/m) at elevated temperatures (>100°C) for times up to several hours. The films are then cooled to room temperature before the field is turned off (2). PVF_2 has a dielectric constant of 15 which is high for normal organic materials but two orders of magnitude lower than a typical PZT ceramic. The longitudinal piezoelectric strain coefficients (d_{33}) of "poled" PVF_2 are quite high for polymers--on the order of 10×10^{-12} C/N, but this is also significantly lower than the d_{33} values for PZT ceramics which range from about 100 to 600×10^{-12} C/N. Although PVF_2 has a relatively small d_{33}, the permittivity of this material is low enough that a large figure of merit is obtained (140×10^{-3} Vm/N compared to about 20×10^{-3} Vm/N for a typical PZT ceramic) (3). The compliance and flexibility of PVF_2 is high and the density is low compared to conventional ceramic piezoelectrics. Overall this combination of properties appears quite attractive and, in fact, PVF_2 has gained the attention of a number of investigators whose efforts have been directed toward developing devices based on piezoelectricity in PVF_2 (3,4). There are, however, problems associated with the use of PVF_2. The low piezoelectric strain coefficient indicates that the material would not be of interest as an active device, and although its high voltage sensitivity means it should be good as a passive device, a problem arises here, too. When used as a hydrophone, the material must be fixed to a curved surface which can flex in response to pressure changes. The difficulty lies in designing a sealed flexible mount for the polymer which will function when exposed to the high pressures which exist deep in the ocean and still retain sensitivity near the surface. So we see, then, that the figure of merit d_{ijk}/ε_{ij} is not the sole criterion, but that other aspects of the problem must be examined.

A second approach involves the design and use of a composite material. The composite should be designed to take maximal advantage of the useful properties of each phase. A logical choice is a composite made of a polymer and a PZT ceramic. The polymer phase would lower the density and permittivity and increase the elastic compliance. If an elastomer is used, the composite would be compliant and flexible. If an epoxy is used, the transducer could possibly be used as a resonator. The properties of piezoelectric PZT are well known to electromechanical transducer designers, and these materials could impart large piezoelectric strain coefficients to the composite. A few attempts have been made at creating an elastomer/PZT composite for use as a flexible low-density transducer (5). The approach used in these attempts was to load a polymer film with particles of a piezoelectric material. The degree of flexibility and the magnitude of the d and g coefficients are primarily controlled by the size of the piezoelectric particles in the heavily loaded elastomer film.

The Gould flexible composite was fabricated using 5 to 10 μm particles bound in a polyurethane matrix. A similar material (T-flex) was developed at Honeywell using 120 μm particles in a silicone rubber matrix. The longitudinal d values obtained in both cases were comparable to the piezoelectric PVF_2 material but the voltage sensitivities were lower because of the higher permittivities in the composites. The difficulty with this type of composite where the piezoelectric particles are smaller in diameter than the thickness of the polymer sheet (Fig. 1a) is that low permittivity polymer layers interleave the piezoelectric particles preventing saturation poling after the composite is formed. After some poling has been achieved, the interleaved compliant polymer attenuates the piezoelectric response of the composite.

Composites were also made at Honeywell which contained much larger particles (up to 2.4 mm in diameter). A material of this type is shown schematically in Fig. 1b. Here the particle size approaches the thickness of the composite. Since the piezoelectric particles run from electrode to electrode, near saturation poling can be achieved. The large rigid piezoelectric particles can transmit an applied stress well leading to high d values if d is measured across the particles. Permittivities in these materials are low compared to homogeneous PZT, resulting in high g values. The problem here is that properties of the composite are extremely position sensitive.

To make an effective composite transducer, it can be seen that one cannot merely mix two materials together--some other consideration is necessary. Designing a composite entails not only choosing component phases with the right properties but also coupling the materials in the optimal manner. The connectivity of each phase is of major importance since this controls the electric flux pattern and the mechanical stress distribution.

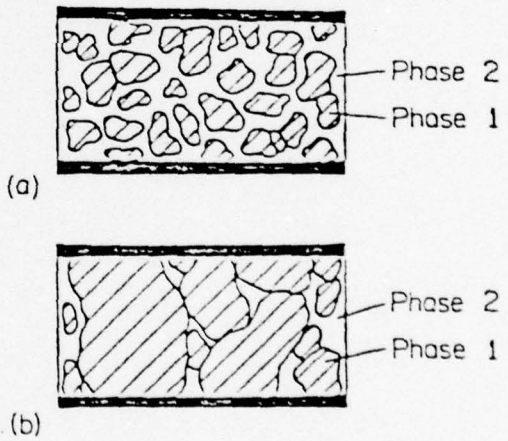

FIG. 1
Two types of piezoelectric/polymer composites: (a) represents small piezoelectric particles suspended in a polymer film; (b) represents bound piezoelectric particles of a size comparable to the thickness of the polymer sheet.

Connectivity

The importance of connectivity was illustrated in reference 6 by considering the piezoelectric properties of lamellar diphasic composites and calculating the one dimensional solutions for $\bar{d}_{33}$ (the average longitudinal piezoelectric voltage coefficient) for various connectivity types. Considering simple one-dimensional solutions (neglecting transverse coupling) for a two phase composite we have two possible cases: series connection and parallel connection.

The series connection case (Fig. 2a) corresponds to that in which small piezoelectric particles are suspended in a polymer film (Fig. 1a). The applicable equations for the piezoelectric coefficients are

$$\bar{d}_{33} = \frac{{}^1v\,{}^1d_{33}\,{}^2\varepsilon_{33} + {}^2v\,{}^2d_{33}\,{}^1\varepsilon_{33}}{{}^1v\,{}^2\varepsilon_{33} + {}^2v\,{}^1\varepsilon_{33}}$$

$$\bar{g}_{33} = {}^1v\,{}^1g_{33} + {}^2v\,{}^2g_{33}$$

where the v's represent the volume fractions of phase 1 and phase 2, the d_{33}'s represent the piezoelectric strain coefficients, the ε_{33}'s represent the permittivities, and the g_{33}'s($=d_{33}/\varepsilon_{33}$) are the piezoelectric voltage coefficients.

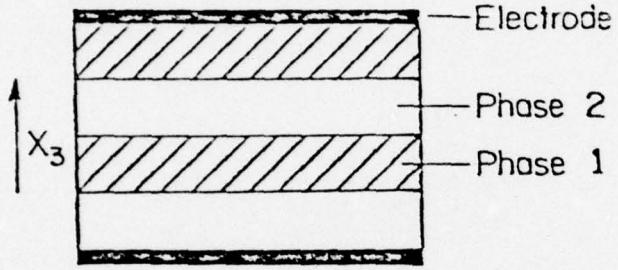

(a) SERIES CONNECTION

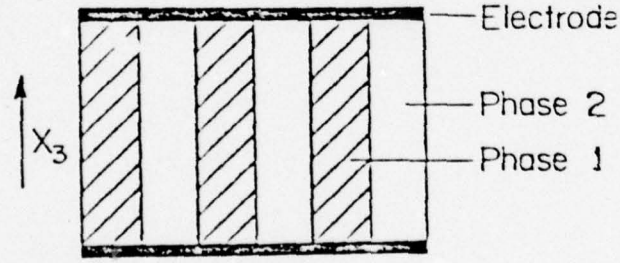

(b) PARALLEL CONNECTION

FIG. 2
Simple lamellar diphasic composites: (a) series connection, alternating layers of piezoelectric ceramic and nonpiezoelectric polymer; (b) parallel connection, alternating stripes of piezoelectric ceramic and nonpiezoelectric polymer connected continuously between the electrodes.

Substitution of numerical values into these equations shows that a mere 1% volume fraction addition of low permittivity nonpiezoelectric polymer drastically lowers the d coefficient, while the g value is essentially unchanged. This result is in qualitative agreement with the values obtained in the Gould material and the Honeywell T-flex material (5).

The parallel connection case (Fig. 2b) corresponds to the composite in which the particle size equals the film thickness (Fig. 1b). The resulting equations are:

$$\bar{d}_{33} = \frac{{}^1v\,{}^1d_{33}\,{}^2s_{33} + {}^2v\,{}^2d_{33}\,{}^1s_{33}}{{}^1v\,{}^2s_{33} + {}^2v\,{}^1s_{33}}$$

$$\bar{g}_{33} = \frac{{}^1v\,{}^1d_{33}\,{}^2s_{33} + {}^2v\,{}^2d_{33}\,{}^1s_{33}}{({}^1v\,{}^2s_{33} + {}^2v\,{}^1d_{33})({}^1v\,{}^1\varepsilon_{33} + {}^2v\,{}^2\varepsilon_{33})}$$

where the variables are defined as in the series case and the s_{33}'s are the elastic compliances of the two phases. Substitution of appropriate values and equal volume fractions for a compliant, nonpiezo-

electric, low permittivity polymer and a rigid, high permittivity, piezoelectric ceramic indicates that $\bar{d}_{33}$ is approximately equal to the d_{33} of the ceramic and that there is actually an amplification of the g coefficient. For smaller volume fractions of the piezoelectric phase, the g value is amplified even further.

From these simple calculations one can see that a composite piezoelectric transducer material should have a parallel connection in which the piezoelectric phase is continuous from one electrode to the other to provide the continuity of electric flux required for saturation poling. The ceramic phase should also be oriented normal to the electroded surfaces for the transmission of mechanical stress and high piezoelectric response. Clearly, the type of structure desired for effective mixing is one of closely spaced, colinear, one-dimensional piezoelectric rods held in a three-dimensional polymer matrix (Fig. 3). A composite of this type is said to have 3-1 connectivity (6).

Hydrostatic Sensitivity

A problem arises when one attempts to use PZT as a single-phase hydrostatic sensor because d_{33} is approximately equal to $-2d_{31}$ resulting in a low piezoelectric response to pressure change. Since sizable $\bar{g}_{33}$ coefficients can be obtained for composites with parallel connection, it is interesting to inquire into the hydrostatic sensitivity of this type of connectivity.

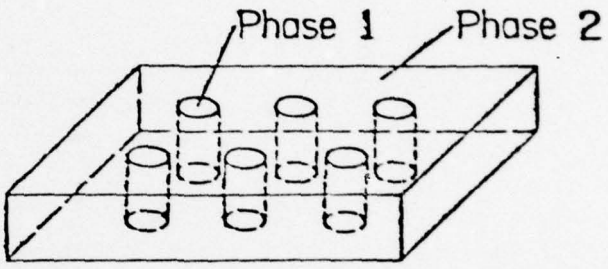

FIG. 3
A 3-1 structure. Ceramic rods one-dimensionally connected between electrodes and held in a three-dimensionally connected polymer matrix.

To evaluate the effective hydrostatic sensitivity for parallel connection, it is necessary to evaluate the transverse piezoelectric coefficient $\bar{d}_{31}$ since $P_3 = -(\bar{d}_{33} + 2\bar{d}_{31})\,\sigma$ where σ is the applied hydrostatic pressure. It can be shown that $\bar{d}_{31} \cong {}^1v\,{}^1d_{31} + {}^2v\,{}^2d_{31}$, so that

$$\bar{d}_h = \bar{d}_{33} + 2\bar{d}_{31} \cong \frac{{}^1v\,{}^1d_{33}\,{}^2s_{33} + {}^2v\,{}^2d_{33}\,{}^1s_{11}}{{}^1v\,{}^2s_{33} + {}^2v\,{}^1s_{33}} + 2({}^1v\,{}^1d_{31} + {}^2v\,{}^2d_{31})$$

Suppose for the composite we choose equal volumes of piezoelectric PZT (phase 1) and a soft elastomer (phase 2) such that: ${}^1v = {}^2v = 1/2$, ${}^1s_{33} \ll {}^2s_{33}$, ${}^1d_{33} \gg {}^2d_{33}$, and ${}^1d_{33} \simeq -2\,{}^1d_{31}$. For the composite $\bar{d}_{31} \simeq 1/2\ {}^1d_{31}$ and $\bar{d}_{33} \simeq {}^1d_{33}$, giving $\bar{d}_h \simeq 1/2\ {}^1d_{33}$.

This is a considerable improvement over single phase performance. Since the hydrophones used under hydrostatic conditions are normally voltage generators, the further favorable enhancement of the voltage coefficient $\bar{g}_h$ can also be exploited.

Composite Fabrication

We have seen that the simple calculations indicate a composite with 3-1 connectivity is needed to make an effective composite transducer. Since, however, in firing the ceramic fibers one must maintain their orientation, interconnections between the rods are needed and therefore in practice partial 3-3 character is required. In a 3-3 template, both phases are continuously connected in all three dimensions. This type of structure is exhibited by certain polymer foams, some diphasic glasses, three-dimensionally woven materials, and by biological substances such as wood and coral.

Coral skeletons are characterized by a structure with the following features: (i) a narrow pore size distribution; (ii) a pore volume approximately equal to the solid phase volume, and (iii) complete pore interconnectivity making every pore accessible from all other pores. The dimensions of the pores vary from species to species, but within one species the size range is quite narrow. Different species of coral have various degrees of anisotropy in their structure ranging from a 3-1 connectivity of nearly parallel tubes to highly isotropic 3-3 structures. Figure 4 shows a micrograph cube of the calcium carbonate skeleton of the coral species goniopora which we have used as a structural template for making composite transducers. The replicating technique, known as the replamineform process, was developed at the Materials Research Laboratory at Penn State for producing prosthetic materials (7). We chose the replamineform process for reproducing the 3-3 connectivity type because of past experience with this procedure, but are investigating other templates which are not subject to the vagaries of coral growth.

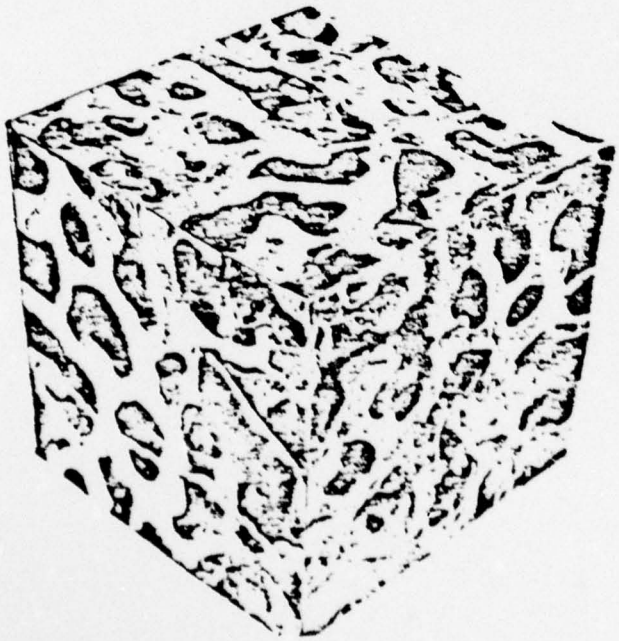

FIG. 4
Micrograph cube of the calcium carbonate skeleton of goniopora coral. The largest pore diameters are about 600 μm.

Replamineform Process

The first step of the replamine process is to shape the coral, which is quite easily machinable, to the desired geometry. The coral template is then vacuum-impregnated with Kerr Inlay casting wax and the wax allowed to harden, after which the calcium carbonate coral skeleton is leached away in hydrochloric acid leaving a wax negative of the original coral template. The negative is reinvested with a PZT slip containing by volume 43% PZT, 53% H_2O, and 4% poly(vinyl alcohol). The PZT used in making the coral replicas was Ultrasonics PZT-501A with an average grain size of 1.66 μm (σ = 1.0). Investment is carried out by vacuum impregnation with vibratory action to render the thixotropic PZT slip fluid. The wax negative is burned off at 300°C leaving a coral-type structure of PZT which is then sintered at 1280°C for one hour. About 13% linear shrinkage is observed in the replicas and the solid surface area of the sintered body is 35% of

the total area (the original coral template is 57% solid). The PZT replica is then backfilled with a suitable polymer such as Dow Corning MDX-4-4210 Elastomer which is a high purity silicone rubber. After the surface has been cleaned, a silver-loaded silicone rubber electrode is applied. The composite is then poled at a field strength of 14 Kv/cm for 5 minutes at 100°C. The relative permittivity of the unbroken composite as determined on a HP 4270A automatic capacitance bridge is about 100. The longitudinal piezoelectric coefficient was evaluated on a Channel Products Berlincourt d_{33} meter. The d_{33} values obtained for the unbroken composite are relatively area insensitive and agree well with the simple parallel model prediction of about 160×10^{-12} C/N. As poled, the replamine replica is still a rigid structure because of the three-dimensional connectivity of the ceramic phase. If, however, the body is now crushed to break the ceramic connectivity an extremely flexible piezoelectric composite results (Fig. 5). Crushing is carried out by reducing the sample height to 80% of its original value and simultaneously shearing the sample 20% of the sample height about an axis perpendicular to the crushing force direction.

By breaking the poled ceramic, the easy electric flux path through the poled piezoelectric is interrupted, thus lowering the permittivity. The pieces of poled piezoelectric are still held in position by the polymer matrix and will therefore still transmit stress. As a result, the d coefficient remains high while the permittivity is reduced and thus the longitudinal piezoelectric voltage coefficient, $\bar{g}_{33}(= \bar{d}_{33}/\bar{\epsilon}_{33})$, is greatly enhanced with respect to the g value of a homogeneous ceramic piezoelectric.

After disrupting the connectivity of the PZT phase by crushing the sample, the relative permittivity is reduced to about 40, while d_{33} is only reduced to about 100×10^{-12} C/N. The g values of these flexible composites are approximately 300×10^{-3} Vm/N which is fifteen times better than a homogeneous PZT transducer. Table 1 contains a comparison of transducer characteristics, from which it is obvious that the replamine composite of PZT-501A and silicone rubber compares very favorably with homogeneous transducer materials for passive device applications. The density of the 3-3 composite is low compared to homogeneous PZT, so the acoustic coupling to water should be better. The compliance of the composite and PVF_2 are large compared to solid PZT, imparting mechanical shock resistance.

The d_{33} value of the 3-3 composite is reasonably good, so that if the connectivity is not broken and a rigid polymer is used in place of silicone rubber, it may be possible to fabricate a low density, high coupling resonator.

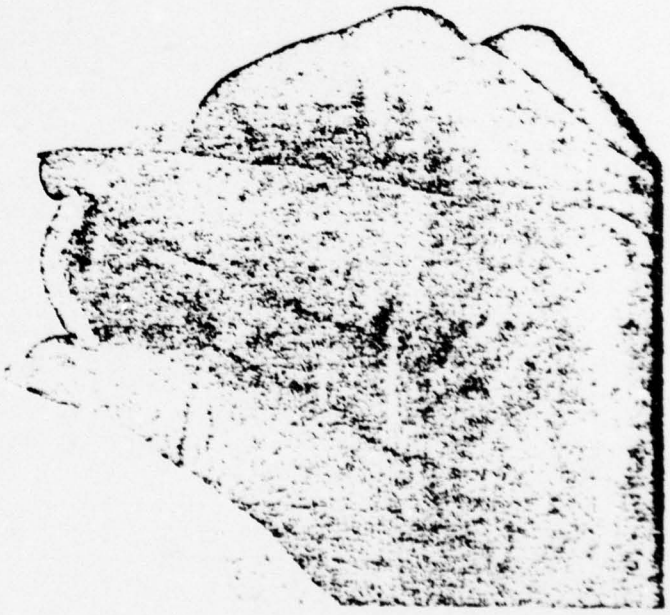

FIG. 5
Flexible PZT/silicone rubber piezoelectric composite produced by the replamineform process. The sample is approximately 25 x 25 x 4 mm.

TABLE 1

Comparison of several transducer materials

Property	PVF_2 (Ref. 3)	Homogeneous PZT-501A*	Flexible 3-3 composite
Density $\times 10^3$ Kg/m^3	1.8	7.9	3.3
Compliance	High	Low	High
d_{33} $\times 10^{-12}$ C/N	14	400	100
ε_R	10	2000	40
g_{33} $\times 10^{-3}$ V·m/N	140	20	300

*Ultrasonic Powder, Inc. "Piezosonic Powders" data sheet.

The g_{33} of PVF_2 is high compared to conventional PZT but, as noted previously, the use of this material as a hydrophone is limited by mechanical problems. The hydrostatic voltage sensitivity of the replamine composite is quite large, about 200 times the sensitivity of an equal-sized homogeneous PZT-501A slug and about twice that of PVF_2.

Hydrophone designers have improved the response of homogeneous PZT by using a thin-walled hollow cylinder with capped ends poled in a manner which greatly enhances the hydrostatic response of the device, but these rigid devices are susceptible to failure from low-level mechanical shocks. Also, the necessity of sealing the ends of the device (as in the case of the PVF_2 device) limits the lifetime and the range of depths for which the hydrophone can be used. This is not the case with the solid replamine composite. The 3-3 composite is highly shock resistant. Its designed inhomogeneous structure attenuates the lateral components of the hydrostatic pressure and enhances the longitudinal response without a complicated sealed device configuration, so it could be used to any depth.

Further evaluation of this new type of transducer material is in progress and will be the subject of later papers.

Acknowledgments

This work was sponsored by the Office of Naval Research and by Advanced Research Projects Agency through Contract N00014-76-C-0515. We also wish to thank our colleagues at the Materials Research Laboratory for their advice and assistance.

References

1. H. Kawai, Japan. J. Appl. Phys. 8, 975 (1969).

2. H. Burkard and G. Pfister, J. Appl. Phys. 45, 3360 (1974).

3. S. Edelman, Proceedings of the Workshop on Sonar Transducer Materials, Naval Research Laboratory (Feb. 1976).

4. Y. Wada and R. Hayakawa, Japan. J. Appl. Phys. 15, 2041 (1976).

5. W.B. Harrison, Proceedings of the Workshop on Sonar Transducer Materials, Naval Research Laboratory (Feb. 1976).

6. R.E. Newnham, D.P. Skinner and L.E. Cross, Mat. Res. Bull (submitted).

7. R.A. White, J.N. Weber and E.W. White, Science 176, 922 (1972).

APPENDIX IV

Reactivity of Zirconia in Calcining of Lead Zirconate-Lead Titanate Compositions Prepared from Mixed Oxides

J.V. Biggers and S. Venkataramani

Materials Research Laboratory
The Pennsylvania State University
University Park, Pennsylvania 16802

Abstract

The reactivity of zirconia is an important factor in calcining PZT compositions. In this study we have compared the reactivity using several different techniques of a commercial zirconia and high purity chemically prepared powder produced by hydrolysis of a butoxide. The results of the work show that there is a considerable difference in the calcining behavior of mixed oxide composition prepared with the two different zirconia sources.

1. INTRODUCTION

Zirconia is presumably the least reactive of the constituent oxides used to produce ceramics in the PbO-ZrO_2-TiO_2 system. In the formation of PZT ($PbZrO_3$-$PbTiO_3$) solid solutions from mixed oxides, the solid state reactions during calcining of the oxide mixtures usually begins with the formation of a $PbTiO_3$ phase around 700°C. The remaining PbO, ZrO_2 and TiO_2 react at a higher temperature (~800°C) to form the $Pb(Zr_\lambda Ti_{1-\lambda})O_3$. The more specific sequence of reaction is reported[1,2] to be the formation of $PbTiO_3$ followed by an intermediate $Pb(ZrTi)O_3$ and finally both reacting to form the required PZT. However, exceptions have been noted in which the reaction sequence was opposite, a $PbZrO_3$ phase formed first with PbO, and TiO_2 reacting later as $PbTiO_3$ or forming the solid solution PZT[3].

In the present work we have determined the reaction sequence on calcining of four PZT compositions covering a wide range of ZrO_2 content. Two sets of compositions were prepared, one using commercial oxides and one in which a high purity, submicron chemically prepared ZrO_2 was substituted for the commercial powder.

2. EXPERIMENTAL

2.1 Preparation of the Zirconia Powder

The zirconia for this study was prepared by the hydrolysis of the zirconium-tetra-(n)-butoxide (ZBT). Figure 1 gives the flow sheet of the process. The method is similar to the one used by Mazdiyasni et al.[4].

Two hundred ml of ZBT were added in a slow stream to 500 ml of deionized water agitated in a high speed blender. The butoxide was hydrolyzed with an exothermal reaction to form the hydroxide

$$Zr(OBu)_4 + 4H_2O \xrightarrow{nH_2O} Zr(OH)_4 + BuOH + nH_2O$$

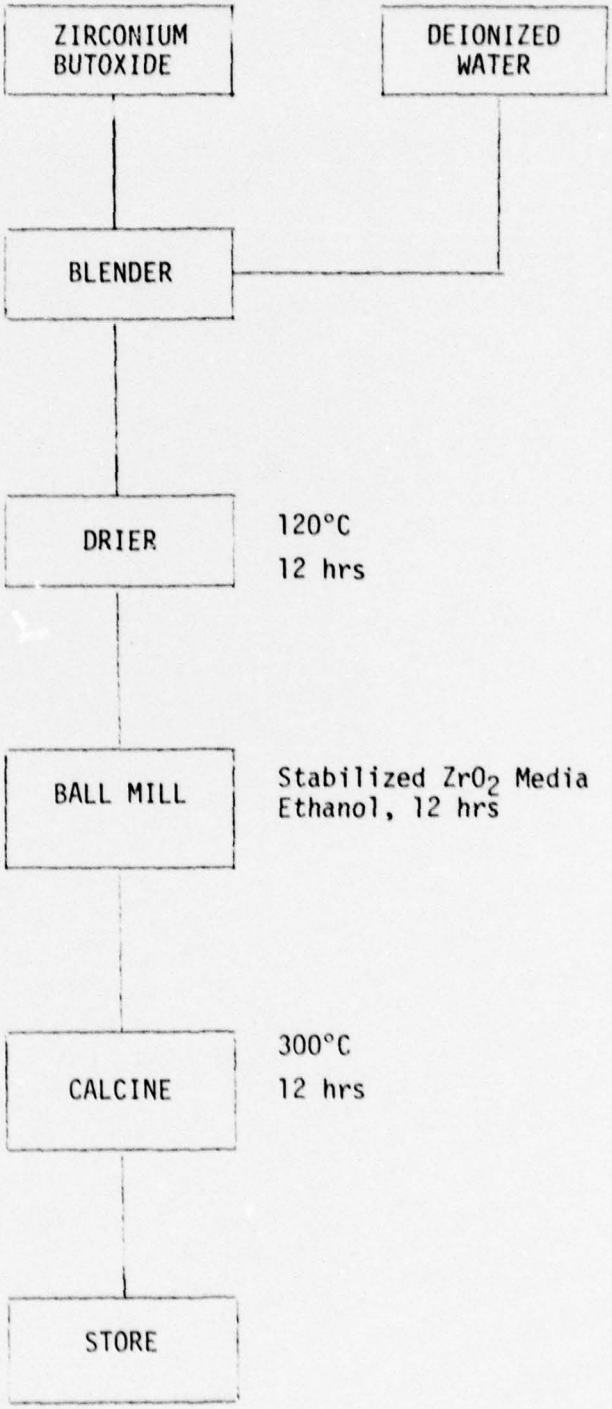

Fig. 1. Flow Sheet - Preparation of Alkoxy Derived Zirconia

The resulting slurry was pan dried at ~120°C and ball milled for 8 hours in a polyethylene jar using stabilized ZrO_2 balls and an ethanol medium. The slurry was then dried and the powder was calcined at 500°C for 12 hours.

2.2 PZT Preparation

Four compositions with ZrO_2/TiO_2 mole ratios varying as 40/60, 52/48, 60/40, and 90/10 were prepared using "Analar" PbO, Tizon TiO_2, and Harshaw Lot 6/76 ZrO_2 for the standard compositions (designated as H series). The chemically prepared ZrO_2 was used instead of the Harshaw Lot 6/76 for the experimental compositions (designated as P series).

The oxides were weighed and ball milled for 12 hours in polyethylene jars using stabilized ZrO_2 cylinders in an ethanol medium. The slurry was then dried and the powders were used in the calcining studies. Table I gives the details of the PZT compositions.

2.3 Calcining (Reactivity) Studies

The calcining studies were done in a resistance heated muffle furnace. The temperatures were 500, 600, and 800°C with holding periods of 3, 6, and 9 hours. The PZTs were weighed into alumina crucibles, covered with alumina lids and calcined at the temperatures and periods mentioned above.

Weight losses on calcining were recorded. The calcined samples were also analyzed using x-ray diffraction for the detection of the major phases.

Unreacted or "free" PbO was volumetrically determined by treatment with 1:3 acetic acid and titrating the solution with a standard EDTA using xylenol orange as indicator. In some samples unreacted (ZrO_2 + TiO_2) were also estimated by a gravimetric method described by Robinson and Joyce[2].

Table I. PZT Compositions

No.	Composition	Weight %		
		PbO	ZrO_2	TiO_2
1	$PbZr_{0.5}Ti_{0.5}O_3$	69.66	15.38	14.96
2	$PbZr_{0.52}Ti_{0.48}O_3$	68.54	19.68	11.78
3	$PbZr_{0.6}Ti_{0.4}O_3$	67.82	22.47	9.71
4	$PbZr_{0.9}Ti_{0.1}O_3$	65.26	32.42	2.34

3. RESULTS AND DISCUSSION

3.1 Chemical Preparation of ZrO_2

Results of surface area measurements as determined by a BET technique on typical chemically prepared and commercial powders are shown in Table II.

A computer assisted scanning electron microscope (SEM) and a technique described by Lebiedzik et al.[5] were used to determine the particle size and shape distribution of the commercial ZrO_2. The process uses computer control of the SEM raster which generates both particle size and shape data based on a set of eight orthogonal axes imposed on each particulate in a large sample population.

The min/max ratio listed is the ratio of the minimum and maximum diameter of the particles and is indicative of particle shape. A spherical particle would have a min/max ratio of 1. The results of the analysis are shown in Fig. 2.

A quantitative particle size and shape measurement of the chemically prepared powders could not be made because of their fineness. Transmission electron microscopy showed that the particle size distribution was narrow and that the average particle was about 300Å in diameter with an irregular shape. These particle size and surface area data for the chemically prepared ZrO_2 are in good agreement with the values reported by Mazdiyasni et al.[4] for powders obtained by a vapor phase hydrolysis of the alkoxide.

The powders as precipitated were amorphous to x-rays, and the peaks gradually sharpened up when heated at 500°C. The TGA and DATA data (Fig. 3) indicate that the precipitate is a complex gel (probably $Zr(OH)_4 \cdot xH_2O$) which becomes a well crystallized ZrO_2 on heating.

Table II. Surface Area of the Oxides Used in the PZT Preparation

Material	Surface Area [M^2/gm]
Lead oxide (National Lead)	0.42
Titanium oxide (Tizon)	9.28
Zirconium oxide (Harshaw lot 6/76)	15.00
Zirconium oxide (Chemically prepared)	154.00

Average Diameter Distribution (# Percent)
Harshaw ZrO_2 6/76

Class Limit	0 1 2 3 4 5 6 7 8 9 10	Class %	No.
0.16	[	0.00	0
0.25	[	0.56	23
0.40	[****	7.11	292
0.63	[**********	20.06	824
1.00	[**********	32.41	1331
1.60	[**********	27.71	1138
2.50	[*****	10.57	434
4.00	[*	1.39	57
6.30	[	0.15	6
10.00	[	0.05	2

For All Types

Class Limit	0 1 2 3 4 5 6 7 8 9 10	Class %	No.
0.050	[*	1.14	47
0.100	[**	3.26	134
0.150	[**	4.65	191
0.200	[***	5.55	228
0.250	[***	6.84	281
0.300	[****	7.43	305
0.350	[****	8.04	330
0.400	[****	8.16	335
0.450	[*****	9.62	395
0.500	[****	7.91	325
0.550	[*****	9.93	408
0.600	[****	8.11	333
0.650	[****	8.13	334
0.700	[**	4.72	194
0.750	[**	4.07	167
0.800	[*	1.66	68
0.850	[	0.66	27
0.900	[	0.12	5

Fig. 2. Particle size distribution of the ZrO_2 powders.

Average Diameter Distribution (# Percent)

For all types

Class Limit	0 1 2 3 4 5 6 7 8 9 10	Class %	No.
0.16	[	0.00	0
0.25	[	0.07	2
0.40	[****	8.62	261
0.63	[******************	34.78	1053
1.00	[****************	30.12	912
1.60	[*********	17.40	527
2.50	[***	6.04	183
4.00	[*	2.38	72
6.30	[	0.36	11
10.00	[	0.13	4
16.00	[	0.10	3

Min/Max Diameter Distribution

For all types

Class Limit	0 1 2 3 4 5 6 7 8 9 10	Class %	No.
0.050	[*	1.29	39
0.100	[**	3.20	97
0.150	[***	5.05	153
0.200	[***	5.75	174
0.250	[***	6.24	189
0.300	[***	6.57	199
0.350	[****	7.79	236
0.400	[***	6.87	208
0.450	[*****	10.73	325
0.500	[***	6.27	190
0.550	[*****	10.70	324
0.600	[****	7.56	229
0.650	[*****	9.78	296
0.700	[***	5.35	162
0.750	[**	3.34	101
0.800	[*	2.31	70
0.850	[	0.96	29
0.900	[	0.17	5
0.950	[	0.07	2

Fig. 2. Particle size distribution of the ZrO_2 powders (Cont'd).

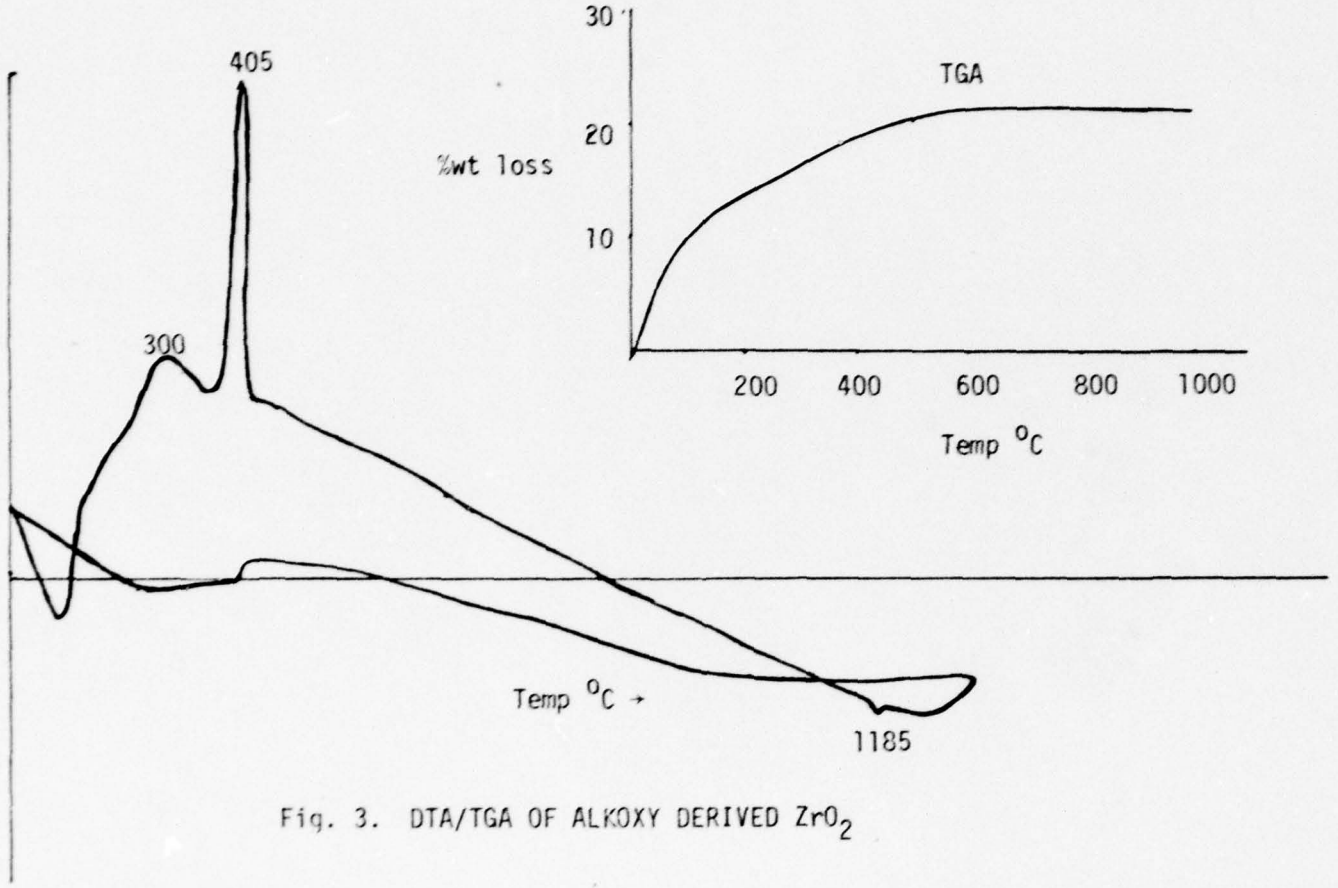

Fig. 3. DTA/TGA OF ALKOXY DERIVED ZrO_2

3.2 Reactivity Studies of PZT Compositions

Table III gives qualitatively the major phases detected in the various PZT compositions as a function of temperature and period of calcination. The sequence of reactions in the compositions P1 to P4 containing the chemically prepared ZrO_2 is distinctly different from those containing the commercial ZrO_2. In these powders a PZ and PT phase are found along with a PZT phase and finally a stoichiometric PZT phase. Depending on the amount of ZrO_2 in the PZT the formation and the relative amount of the PZ phase formed varies (P1 to P3 has less PZ formed than P4).

3.3 Chemical Analysis of PZT

Figure 4 shows the amount of unreacted PbO as a function of the calcining time and temperature for the 90/10 PZT composition ($PbZr_{0.9}Ti_{0.1}O_3$). The amount of PbO decreases as the calcining temperature and/or time increase. Further the "free" PbO content in the P4 sample containing the chemically prepared ZrO_2 is consistently lower than that in the samples containing the Harshaw ZrO_2. It is interesting to note that the free PbO in the P4 sample at the 500°C calcine is even lower than that in the H4 sample at the 600°C calcine. The reversal of these results for the 800°C calcine is probably due to the higher loss of the uncombined PbO from the H4 samples which lost 2-3 w/o at 800°C and 0.5-1 w/o at 500 and 600°C. The P4 lost consistently 2-3 w/o for the whole range of the calcining sequences; the higher loss was probably due to adsorbed species on the ultrafine ZrO_2.

Table IV shows the amount of the unreacted (ZrO_2 + TiO_2) for 2 calcines. It is obvious that the reaction is more complete in the P4 sample and also that there is a $PbZrO_3$ (PZ) formation occurring as evident from the x-ray data. Though the values agree with the calculations, a more complex reaction sequence involving an intermediate PZT, PZ and PT could not be ruled out.

Table III. Phase Analysis by X-Ray Diffraction

Sample Number	MAJOR PHASES FROM X-RAY DIFFRACTION DATA								
	500°C			600°C			800°C		
	3 hr	6 hr	9 hr	3 hr	6 hr	9 hr	3 hr	6 hr	9 hr
H 1	P,Z,T, PT	P,PT, T,Z	P,PT, T, Z	PT,P, T,Z	PT,P, T,Z	PT,P, T,Z	PZT, PT	PZT, PT	PZT, PT
H 2									
H 3									
H 4									
P 1	P,Z, T,PZ	PZ,P T,Z PZT	(P,PZ), T,Z, PZT	(P,PZ), T,PT, PZT	PZ,P, PT,T, PZT	PZ,PT P,PZT	PZT, PT	PZT, PT	PZT
P 2									
P 3									
P 4	P,Z,T, PZ,PZT	P,PZ,Z T,PZT	P,Z,T, PZ,PZT	P,PZ,Z, T,PZT	PZ,P,Z PZT	PZT,PT PZ	PZT	PZT	PZT

H1-H4 = Harshaw ZrO_2

P1-P4 - Alkoxy derived ZrO_2

P = Lead oxide

Z = Zirconium oxide

T = Titanium oxide

PT = Lead titanate

PZ = Lead zirconate

PZT = Lead zirconate titanate solid solution

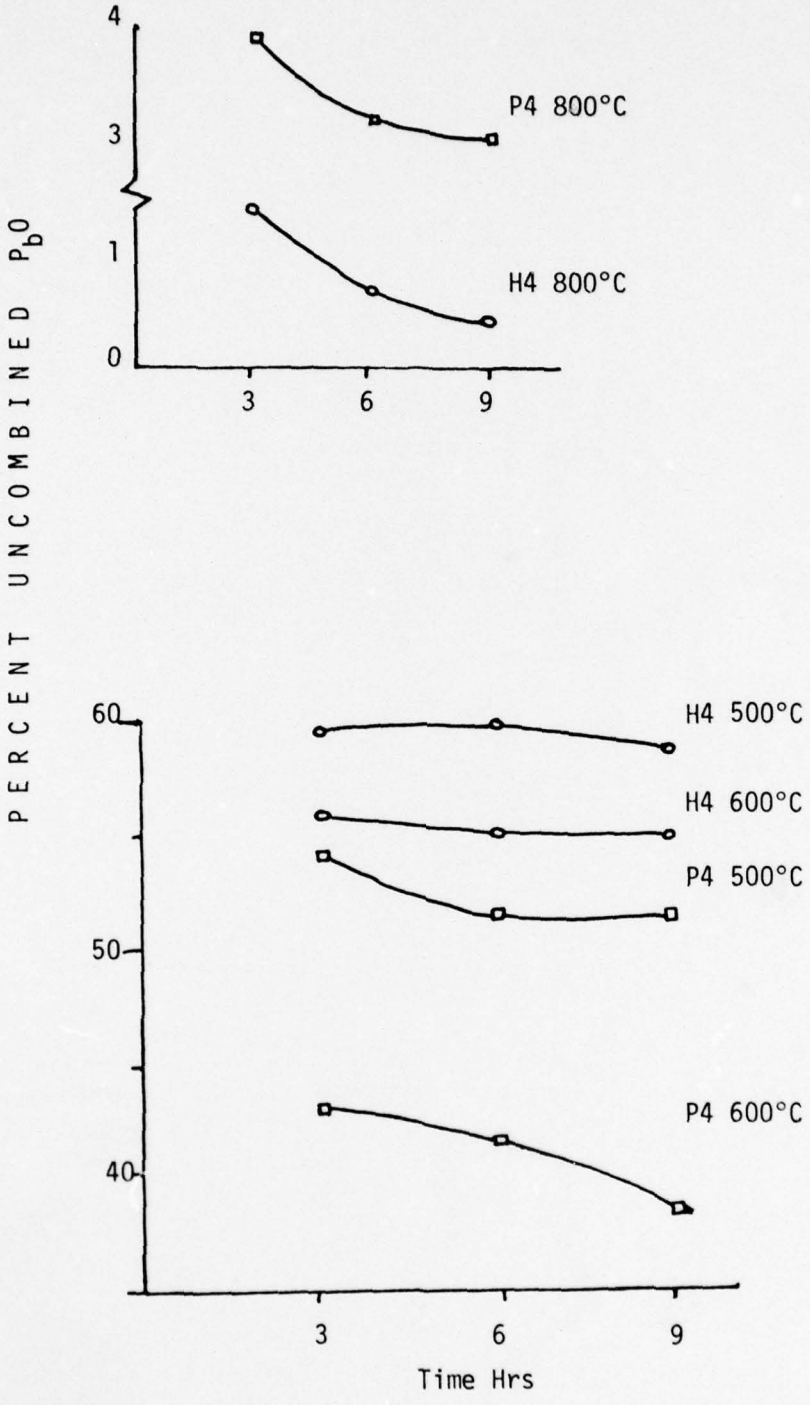

Fig. 4. Uncombined PbO vs Period of Calcining for Various Temperatures.

Table IV.

Temp/Time °C hr	Free PbO		Unreacted (ZrO_2+TiO_2)	
	H4	P4	H4	P4
500/9	58.8	51.7	32.50	28.25
600/9	54.9	38.4	30.26	18.65

Formulation: $Pb(Zr_{.9}Ti_{.1})O_3$ { PbO - 65.25 wt%; ZrO_2 - 32.42 wt%; TiO_2 - 2.34 wt% }

$0.9\ PbO + 0.9\ ZrO_2 = 0.9\ PbZrO_3$ - (a)

$0.1\ PbO + 0.1\ TiO_2 = 0.1\ PbTiO_3$ - (b)

(e.g.) P4 in serial number 1

If all the reacted PbO follows reaction (a)

Amount of ZrO_2 combined

$$= (65.25-51.7) \times \frac{123.22}{223.19} = 7.48$$

Percent unreacted (ZrO_2 + TiO_2) $= \frac{(34.76-7.48)}{10}$

$= 27.28$

If (b) is complete and the rest of the reacted PbO takes part in reaction (a)

Percent unreacted (ZrO_2 + TiO_2) 28.55

4. CONCLUSIONS

We have shown that the use of chemically prepared ZrO_2 significantly alters the calcining reaction sequence for mixed oxide PZT compositions. The first compound formed with the commercial ZrO_2 compositions is lead titanate and lead zirconate is formed first when using the chemically prepared zirconia. A PZT phase is formed at 500°C using chemically prepared zirconia, while the commercial ZrO_2 composition shows PZT as a phase only for the 800°C calcines.

The increased reactivity of the chemically prepared ZrO_2 might be used to great advantage in the processing of commercial PZT compositions. It is possible that the separate calcining step normally employed to produce ceramics from mixed oxide powders could be eliminated and a single firing schedule could be devised with suitable time at low temperatures to promote formation of the right combination of phases to produce high density ceramics. The introduction of such a process could lead to lower production costs and more reproducible properties. However, in order to develop a one step firing sequence, considerably more must be known about sintering mechanisms and kinetics for PZT compositions. Specifically, we must better understand the role of unreacted and intermediate phases on the sintering behavior.

At present work is in progress that will generate more detailed reaction sequence maps for the mixed oxides using chemically prepared zirconia. In parallel studies the sintering behavior of discs with different combinations of unreacted and intermediate phase will be determined.

References

1. Yoshihiro Matsuo and Hiromu Sasaki. Formation of Lead Zirconate-Lead Titanate Solid Solutions. J. Am. Cer. Soc. 48, 289-91 (1965).

2. A.E. Robinson and T.A. Joyce. Preparation of Lead Zirconate-Titanate Compositions. I. Determination of Unreacted Constituents. Trans. Brit. Cer. Soc. 61(2) 85-93 (1962).

3. B. Jaffe, W.H. Cook, Jr. and H. Jaffe. Piezoelectric Ceramics, pp. 137-38, Academic Press, London and New York.

4. K.S. Mazdiyasni, C.T. Lynch and J.S. Smith. Preparation of Ultra High Purity Submicron Refractor Oxides. J. Am. Cer. Soc. 48, 372-75 (1965).

5. J. Lebiedzik, R.G. Burke, S. Troutman, G.G. Johnson and E.W. White. New Methods for Quantitative Characterization of Multiphase Particulate Materials Including Thickness Measurement. Scanning Electron Microscopy, Part 1, 26-33 (1973).

APPENDIX V

Preparation and Reactivity of Lead Zirconate-Titanate Solid Solutions Produced by Precipitation from Aqueous Solutions

S. Venkataramani and J. V. Biggers

Materials Research Laboratory
The Pennsylvania State University
University Park, Pennsylvania 16802

Abstract

A process for preparation of PZT by precipitation from butoxide precursors is described. The reactivity of the powders during low temperature firing (calcining) has been determined using weight loss, x-ray diffraction, and DTA-TGA techniques.

1. INTRODUCTION

Solid solutions of lead zirconate - lead titanate (PZT) ceramics are widely used in piezoelectric devices. The most useful PZT compositions are of those in the vicinity of the morphotropic boundary $Pb(Zr_xTi_{1-x})O_3$ with x between 0.50 and 0.55. Most commercial ceramics are prepared from calcined mixed oxide powders. Difficulties in mixing and variations in composition and physical characteristics of the individual powders lead to inhomogeneities in both composition and microstructure which in turn affect the mechanical and piezoelectric properties.

Alternate methods of preparing fine, homogeneous powder have been developed. The ceramic oxide powders thus obtained are generally termed "chemically prepared" oxides. In short, the process involves the physico-chemical reaction of the precursor compounds of the required oxides. The widely used precursors are organic and inorganic compounds, especially alkoxides, oxalates, citrates, nitrates, sulfates, etc. The usual physico-chemical reactions are evaporation, pyrolysis, hydrolysis, co-precipitation, sol-gel formation and freeze drying.

Haertling and Land[1] synthesized PZT with lanthanum additions (PLZT) by the hydrolysis of alkoxides, by adding a lanthanum acetate solution to a mixture of lead oxide, zirconium and titanium butoxides kept agitated in a high speed blender. The butoxides were hydrolyzed by the water of the acetate solution and the resulting slip was a complex oxide, hydroxide mixture of the PLZT composition. On drying and calcining the PLZT oxide was obtained. The oxide was of very high purity and submicron in size and the ceramics made from it had superior electro-optic properties. Brown and Mazdiyasni[2] also have reported the preparation of

PLZT from the constituent alkoxide hydrolysis.

Preparations of PZT and PLZT composition from nitrates has been reported by McNamara[3], Murata[4] and Thompson[5]. The oxides were obtained by either spray drying, evaporation, freeze drying, or more commonly, coprecipitation of the nitrate solution of the constituent oxide in the right proportion. The problem of stabilizing the titanium nitrate solution was overcome by either adding titanium oxide as the alkoxide or adding H_2O_2 to the nitrate solution. PZT compositions have also been obtained by the coprecipitation of citrates and formates of the constituent oxides in alcohol.

In this work the PZT were prepared from mixtures of alkoxides and lead acetate. The sequence of reactions for calcining at various temperatures and times has been investigated.

2. EXPERIMENTAL

The starting materials for the preparation of PZT were lead acetate solution (25 wt %). Zirconium tetra-n-butoxide (28 - 66 wt % ZrO_2) and titanium tetra-n-butoxide (23.71 wt % TiO_2). The zirconium and titanium butoxides were weighed into a high speed blender and mixed for about 3 - 5 minutes. The lead acetate solution was slowly added to this alkoxide mixture as agitation was continued. The water of the acetate solution hydrolyzed the alkoxides exothermically, and the resulting precipitate was a complex PZT hydroxide acetate. The total mixing time was about 20 minutes. The resulting viscous slip was dried overnight in an oven at ~120°C. The dried "cake" was then ball milled for 8 hours in a polyethylene jar using stabilized ZrO_2 cylinders and an ethanol medium. The ball milled powder was dried in the oven at ~120°C.

The compositions had varying ZrO_2/TiO_2 mole ratios of 52/48, 60/40, 70/30, 80/20, and 40/60. Some of these compositions were also prepared by adding deionized water to an agitated mixture of PbO, zirconium, and titanium butoxides. The general process flow sheet is shown in Fig. 1.

The compositions were calcined in sintered alumina crucibles at 500°, 600°, 800°, and 1000°C for periods ranging from 2 - 16 hours. The weight losses during calcining were determined and x-ray diffraction data were obtained in order to detect the major phases present. DTA and TGA were done on the 52/48 composition.

3. RESULTS AND DISCUSSION

The as-precipitated, dried samples were "amorphous" to x-ray. The BET surface area of the PZT was ~28 M^2/gm. Scanning electorn microscopic analysis of the powder revealed an average particle size of ~0.5 μm.

The weight losses on calcining shown in Table I indicate that the co-precipitated material from lead acetate and the alkoxides is a mixture of acetate and oxyhydroxide rather than a single phase PZT oxyhydroxide complex. The weight loss of $PbZr_{0.52}Tr_{0.48}O_3$ is around 22% which is in good agreement with the figure obtained from the TGA (Fig. 2). Assuming that the precipitate is a mixture of lead acetate and the hydroxides of zirconium and titanium the weight loss on calcining would be ~29.0%. On the other hand if all the constituents are hydrolyzed to the respective hydroxides the loss would be ~14%. A complex mixture of acetate and oxyhydroxides would have weight loss within the range of 14 - 29%. Hence the weight loss figures of the samples (~ 22%) show that the precipitate as dried is a complex acetate oxyhydroxide. The precipitate obtained by the hydrolysis of PbO, and the alkoxides, lost ~5.5 ± 1.1 in weight on

calcining. If the dried precipitate is a totally hydrolysed PZT hydroxide, the weight loss would be ~10%, and if it is a PZT oxide the loss would be zero %. Moreover, it can be calculated that if the PbO is converted to $Pb(OH)_2$ and the zirconium and titanium butoxides to the respective oxyhydroxides the loss would be ~7.0%. Hence the hydrolysis of a mixture of PbO, and the alkoxides apparently result in a complex oxyhydroxide of the PZT.

The DTA (Fig. 2) of the $Pb(Zr_{0.52}Ti_{0.48})O_3$ precipitate obtained by the hydrolysis of the lead acetate and the butoxides of zirconium and titanium shows an endothermic peak at ~290°C and broad exotherm around 350°-400°C corresponding to the melting and conversion of lead acetate to lead oxide. Apart from these there is another exothermic peak around 580°C. There are no exothermic peaks seen at 600°C; no broad regions around 700 and no endothermic peaks around 780°C as reported[7] for the reaction among a mixture of PbO, ZrO_2 and TiO_2 to form PZT.

The TGA (Fig. 2) as mentioned before indicates that the major weight losses occur till 500°C and further loss due to the PbO evaporation around 900-1000°C.

X-ray diffraction analysis (Table 2) reveals the sequence of the reactions occurring at various calcining cycles.

(i) In the 500°C calcines the only prominent observation is the reduction of the amount of unreacted PbO. The samples were still poorly crystalline to x-rays. However, the sharpness of the peaks increases as the period of calcine increases. The other major phase is probably an intermediate PZT phase. There is no obvious evidence of either $PbTiO_3$ or $PbZrO_3$ occurring as a major phase as detected by x-rays.

(ii) The only major phase detectable in the 600°C/8 hrs; 800°C/2 hrs

and 1000°C/2 hr calcines is a PZT phase. There is no detectable peak of the unreacted PbO.

The precipitate obtained by the hydrolysis of PbO and the zirconium and titanium butoxides has qualitatively (from peak intensities) lower amounts of unreacted PbO after the 600°C/2 hrs calcine than the one obtained by the hydrolysis of a mixture of lead acetate and the butoxides. The former precipitate is chemically more homogeneous in that it is a complex PZT oxyhydroxide.

On calcining, with a simultaneous loss of the hydroxyl PZT formation starts.

The lead acetate in the latter precipitate decomposes giving PbO which then reacts to form the PZT.

Many workers[7,8,9] have shown that PZT forms only at temperatures greater than 700°C from mixed oxides whereas the alkoxy derived precipitates seem to react at 500°C to form PZTs and the reaction is almost complete on calcining for 8 hrs at 600°C. The PZTs thus obtained are stoichiometric, extreme-y fine and very pure. Haertling and Land[1] and Mazdiyasni[2] showed that the lanthanum added PZTs from alkoxides reacted at 500°C to form a single phase PLZT. Mazdiyasni found that the PLZT after drying in vacuum at 60°C was a single phase material, "amorphous" to x-rays and slowly "crystallized" on heating.

4. CONCLUSIONS

In this initial study we have shown that it is possible to produce a single phase, high purity, ultrafine PZT powder by calcining at low temperatures a complex lead zirconium titanium hydroxide produced by precipitation from an aqeous solution.

With the improved reactivity of these powders it is possible that they could be used to produce ceramics without a separate calcining step.

At present the reaction kinetics of the conversion of the hydroxide to PZT and the sintering kinetics of the resultant solid solutions are under investigation.

Once these processes are better understood, a series of PZT ceramics with a wide range of compositions will be produced using the chemically prepared powders. Electrical and mechanical property comparisons will be made with conventionally produced ceramics of the same compositions.

REFERENCES

1. G. H. Haertling and C. E. Land. Hot Pressed PLZT Ferroelectric Ceramics for Electro-optic Applications. J. Am. Cer. Soc. 54 (1), 1-11 (1971).

2. L. M. Brown and K. S. Mazdiyasni. Cold Pressing and Low Temperature Sintering of Alkoxy Derived PLZTs. J. Am. Cer. Soc. 55 (11), 541-544 (1972).

3. V. M. McNamara. A Wet Chemical Method for the Preparation of Oxide Chemicals Applicable to Electronic Ceramics. Mines Branch Investigation Report - IR 63-39, April (1963).

4. M. Murata, K. Wakino, K. Tanaka and Y. Hamakawa. Chemical Preparation of PLZT Powder from Aqueous Solutions. Mat. Res. Bull. 11, 323-328 (1976).

5. John Thompson, Jr. Chemical Preparation of PLZT Powders from Aqueous Nitrate Solutions. J. Am. Cer. Soc. Bull. 53 (5), 421-444 (1974).

6. B. J. Mulder. Preparation of $BaTiO_3$ and Other Ceramic Powders by Coprecipitation of Nitrates in an Alcohol. J. Am. Cer. Soc. Bull. 49 (11), 990-993 (1970).

7. V. A. Russell and C. H. Spink. The DTA Behavior of Lead Zirconate

Titanate Materials. Thermochimica Acta 19, 45-54 (1974).

8. Y. Matsuo and H. Sasaki. Formation of Lead Zirconate-Lead Titanate Solid Solutions. J. Am. Cer. Soc. 48, 289-291 (1965).

9. A. E. Robinson and T. A. Joyce. Preparation of Lead Zirconate Titanate Compositions. I. Determination of Unreacted Constituents. Trans. Brit. Cer. Soc. 61 (2), 85-93 (1962).

FIGURE CAPTIONS

Fig. 1. Flow Sheet for Alkoxy Derived PZT.

Fig. 2. TGA and DTA of $PbZr_{0.52}Ti_{0.48}O_3$.

TABLE I

Weight Loss Data

Composition	Calcination Temp/Time	Percent wt loss
$PbZr_{0.6}Ti_{0.48}O_3$	500/2 hr	20.44
	500/4 hr	20.61
	500/6 hr	21.33
	500/8 hr	22.02
	500/10 hr	---
	500/12 hr	21.81
	500/16 hr	21.85
	600/2 hr	22.73
	600/3 hr	22.74
	800/2 hr	22.62
	1000/2 hr	22.47
$PbZr_{0.52}Ti_{0.48}O_3$*	800/2 hr	6.68
$PbZr_{0.6}Ti_{0.4}O_3$	600/2 hr	19.35
	1000/2 hr	17.53
$PbZr_{0.-}Ti_{0.4}O_3$*	600/2 hr	4.43
$PbZr_{0.7}Ti_{0.3}O_3$	1000/2 hr	17.62
$PbZr_{0.8}Ti_{0.2}O_3$	1000/2 hr	13.18

*By the hydrolysis of PbO, zirconium-tetra-n-butoxide and titanium-tetra-n-butoxide.

TABLE 2

X-ray Diffraction Data

Composition	Calcining Temp(°C)/Time(hr)	Major Phases	Remarks
$PbZr_{0.52}Ti_{0.48}O_3$	500/2	PbO,PZT?	Broad peaks
	500/4	PbO,PZT	Poorly
	500/6	PbO,PZT	crystallized
	500/8	PbO/PZT	
	500/10	PZT;PbO	PbO peaks are of lower intensity than the PZT peaks better crystallized
	500/12	PZT;PbO	
	500/16	PZT/PbO	
	600/2	PZT,PbO	
	600/8	PZT,PbO?	
	800/2	PZT	well crystallized
	1000/2	PZT	
$PbZr_{0.52}Ti_{0.48}O_3$*	800/2	PZT	
$PbZr_{0.6}Ti_{0.4}O_3$	600/2	PZT/PbO	
	1000/2	PZT	
$PbZr_{0.6}Ti_{0.4}O_3$*	600/2	PZT,PbO	well crystallized
$PbZr_{0.7}Ti_{0.3}O_3$	1000/2	PZT	
$PbZr_{0.8}Ti_{0.2}O_3$	1000/2	PZT	

*By the hydrolysis of PbO + zirconium tetra-n-butoxide + titanium tetra-n-butoxide.

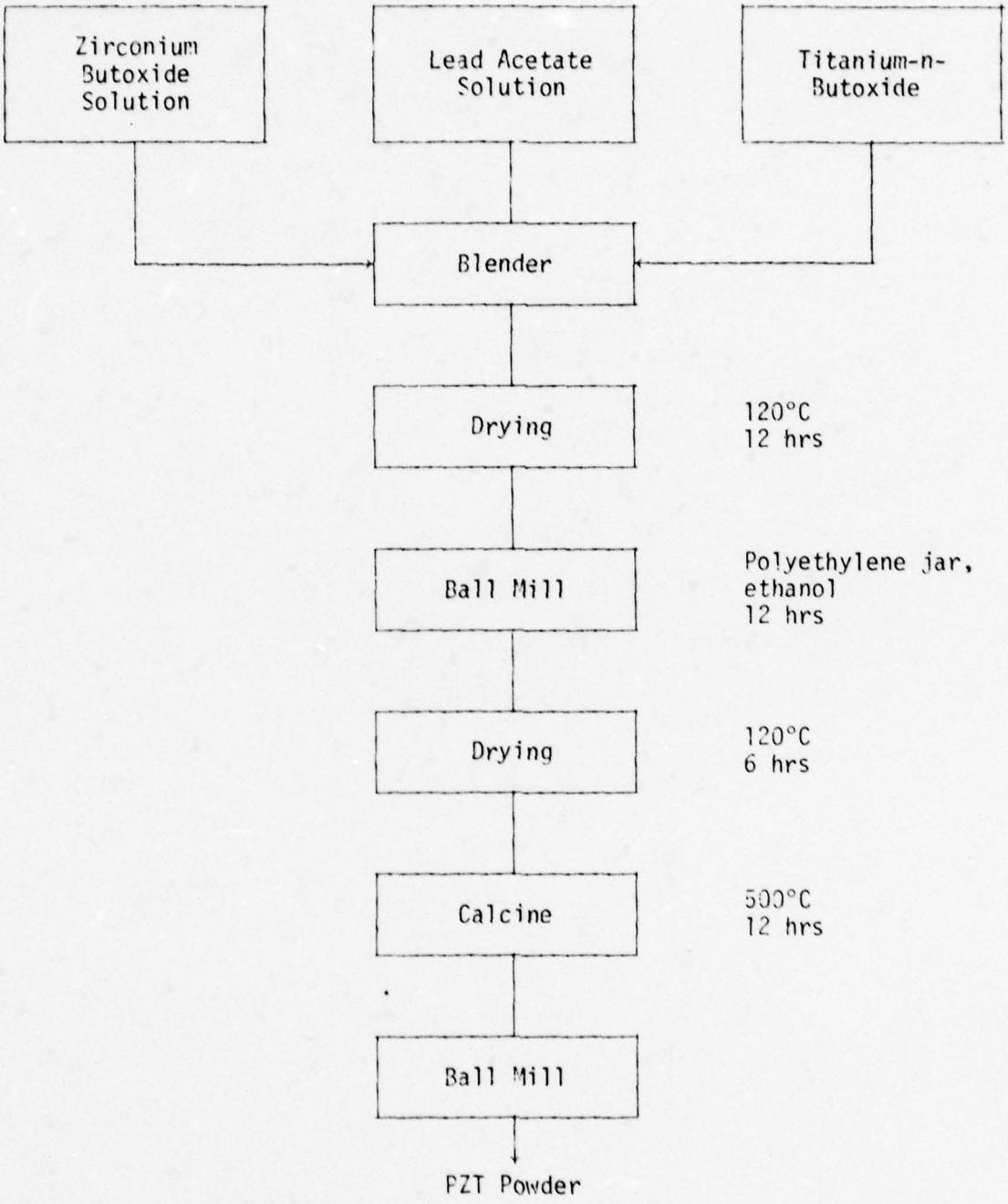

FIG. 1. Flow Sheet for Alkoxy Derived PZT.

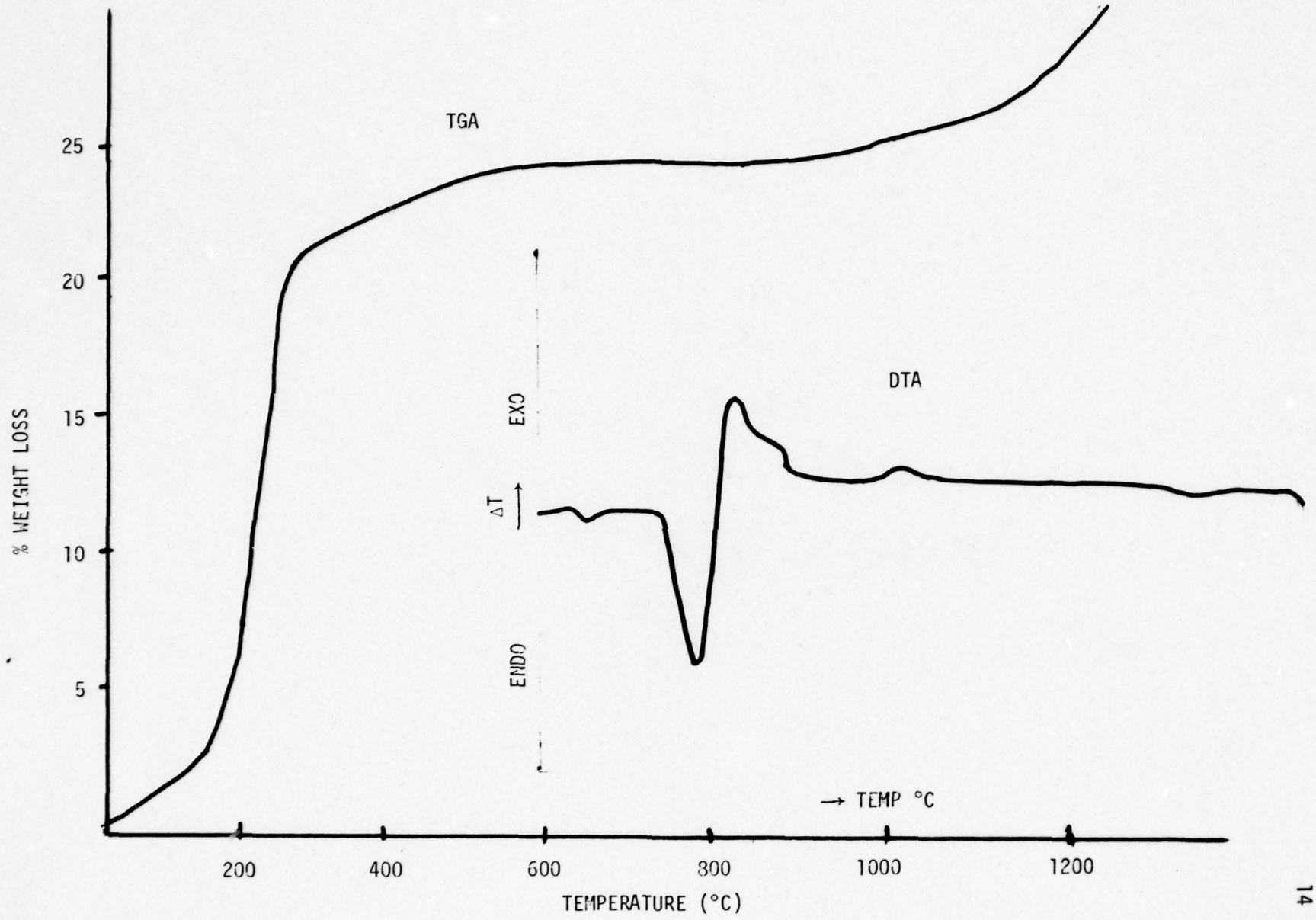

FIG. 2. TGA and DTA of $PbZr_{0.52}Ti_{0.48}O_3$.

APPENDIX VI

THE ROLE OF ZrO_2 POWDERS IN MICROSTRUCTURAL DEVELOPMENT OF PZT CERAMICS

J.V. Biggers, D.L. Hankey, L. Tarhay

Materials Research Laboratory
The Pennsylvania State University
University Park, Pennsylvania 16802

Processing electrical ceramics to obtain reproducible properties is not an easy task. Seemingly inconsequential changes in raw materials or processing steps can produce ceramics with quite different properties.

The lead zirconate-lead titanate solid solutions used in manufacture of piezoelectric devices are a good example of processing sensitive materials. The major precessing variables are generally considered to be: powder characteristics (composition and particle size distribution and morphology), material mixing, calcining and control of furnace atmosphere during firing.

The calcining step is usually limited to temperatures of about 900°C. A recent paper by Buckner and Wilcox[1] shows the strong influence of calcining temperature on the properties of the fired ceramics. These differences are certainly in large part related to the reactivities of the powders which in turn depend to a large extent on particle composition and morphology. Studies of reactions occurring during calcining[2,3] have shown that commercial ZrO_2 is the least reactive of the powders. Matsuo and Sasaki[2] suggest that the reaction sequence of the mixed oxide powders used to make PZT ceramics involves first the formation of $PbTiO_3$ and then reaction of this with ZrO_2 to form PZT. There is usually a mixture of several phases present after precessing, e.g. PZT, $PbTiO_3$ and ZrO_2. Rosolowski et al.[4] have determined that commercial calcines contain several weight percent of unreacted ZrO_2. They note also that the ceramics after final firing can contain 1-2 w/o ZrO_2.

While there is ample evidence to suggest that reactivity of the ZrO_2 is an important factor, it is extremely difficult to relate

observed differences in powder composition and morphology to the reactivity. Recent work in this laboratory has shown that the only noticeable difference in lots of powders judged good or bad (according to the ceramic produced) was the state of agglomeration[5].

Quantitative measurements of the agglomeration in powders are very difficult. In order to test the hypothesis that the state of agglomeration affects reactivity, a series of experiments was undertaken which compared ceramics produced under identical conditions but with different ZrO_2 starting powders.

The ZrO_2 lots chosen were judged from a qualitative basis to have differing agglomerate character. In addition, portions of each lot were subjected to different high energy milling pretreatments in an attempt to change the particle and agglomerate size distribution.

The different ZrO_2 powders were used to produce ceramics with the composition $PbZr_{0.55}T_{0.45}O_3$. This composition was chosen as being representative of many commercial PZT ceramics and it was far enough from the morphotropic boundary to preclude anomalies associated with the phase transition[6].

EXPERIMENTAL

Three different lots of commercial ZrO_2 powders were selected for this work--Tizon lot 367m and Harshaw lots 5-76 and 1-75. The initial characterization of these lots using optical emission spectroscopy for impurities and wet chemical analysis for major elements has been reported earlier[5].

Particle size and shape were measured using a beam controlled SEM technique[7] and surface area was determined by a BET method.

The as-received ZrO_2 powders were then milled using two types of equipment--a fluid energy mill and an attrition mill. Construction details and operation of both types of mills are described by Wang[8].

The fluid energy mill (Fluid Energy Products, Hatfield, Pa.) uses high-pressure air which accelerates the individual particles and impacts them in a rubber-lined chamber. Operating air pressures were 600 K Pa and the residence time for particulates in the mill was about 10 minutes.

The attrition mill, built at this laboratory, used a polyurethane lined jar mill, a stainless steel impellor covered with tygon tubing and a charge of 0.011 m diameter zirconia balls. The milling was done for 20 minutes at 200 rpm impellor speed with equal volumes

of powder, ethyl alcohol and ball charge.

Figure 1 shows a processing flow chart used to produce ceramic discs. The powder mixing steps were carried out in rubber-lined jar mills. Pan drying was done at 100°C for 24 hours. The dried cake was broken up in an alumina mortar. This powder was calcined in closed 99.9 w/o Al_2O_3 crucibles for 2 hours at 900°C in an electrical resistance furnace.

The calcined powders were pressed into about 0.015 m diameter discs using a Stokes rotary press. Green densities were carefully controlled at 65 ± 1.0% of theoretical for all pellets. The green thickness of the pellets was about 0.0012 m. Firing of the pellets was carried out in closed alumina crucibles using a technique described by Klicker and Biggers[5].

Samples of the different pellets were distributed randomly on the setters inside the closed alumina crucibles to minimize effects of thermal and PbO atmosphere gradients.

RESULTS AND DISCUSSION

Table 1 shows the particle size distribution and surface area data for the as-received and milled powders. Table 2 shows in more detail the particle size distribution of the Harshaw lot 1-75 powders. The particle size changes after milling were not significant. Jet milling increased slightly the surface area of the three lots used while attritor milling appeared to slightly decrease the surface areas for the Harshaw lots and increase the area for the Tizon material.

As can be seen from Table 2, the milling did tend to remove large particles and shift the distribution slightly toward a lower mean diameter. The results were the same for the other lots.

The shape of the particles given by the min/max particle diameter ratios in Table 1 remains essentially constant.

Emission spectroscopy was used to check for impurity pick-up during milling and no contamination was detected. After calcining the phases present were checked using x-ray diffraction and a wet chemical method for PbO[9]. With all as-received lots the x-ray diffraction showed PZT and $PbTiO_3$. In all milled powders only PZT was detected. The results of the PbO analyses are shown in Table 3.

There was a significant difference in unreacted PbO between the Tizon and Harshaw as-received lots. Milling of the ZrO_2 powders did not, however, alter the amount of PbO in the calcine.

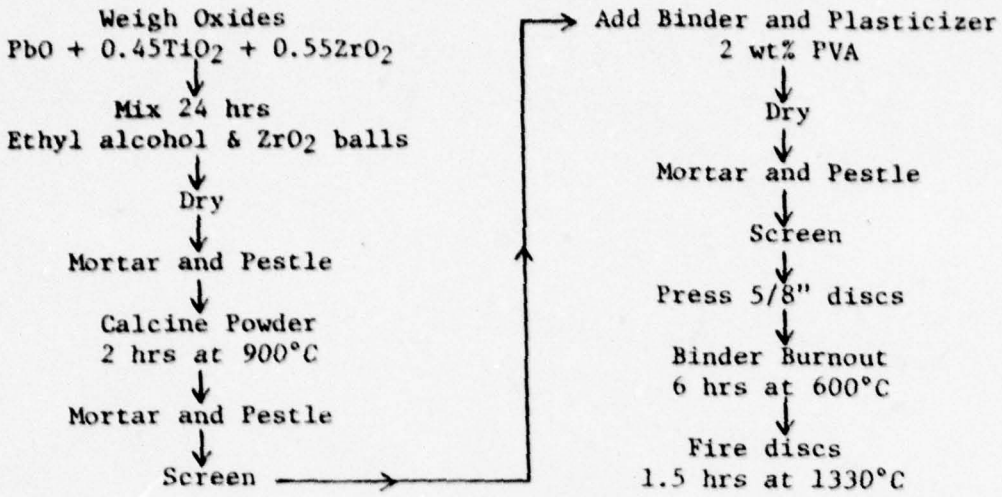

Figure 1. Processing Flow Chart for ZrO_2 Study.

Table 1. Data on ZrO_2 Powders from Automated SEM Image Analysis and Surface Area Analysis.

ZrO_2 Sample	Average Diameter Mean(m)	σ	Min/Max Diameter Mean(m)	σ	Surface Area (BET) $m^2/kg(x10^{-3})$
Tizon Lot 367m					
As received	0.69	0.5	0.47	0.17	18.4
3 jet mills	0.59	0.5	0.50	0.18	18.7
Attritor milled	0.68	0.5	0.50	0.18	19.4
Harshaw Lot 1-75					
As received	0.72	0.5	0.53	0.17	13.5
3 jet mills	0.62	0.3	0.49	0.17	14.6
Attritor milled	--	--	--	--	12.5
Harshaw Lot 5-76					
As received	0.89	0.5	0.44	0.18	14.6
3 jet mills	0.69	0.4	0.51	0.17	15.5
Attritor milled	0.68	0.4	0.50	0.17	12.8

Table 2. Average Diameter Distribution for Harshaw Lot 1-75

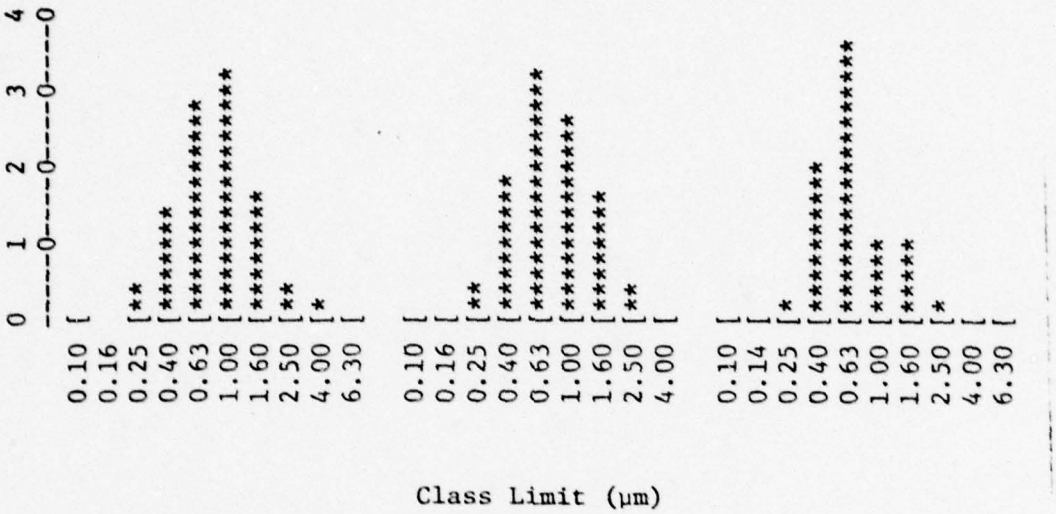

Table 3. Wet Chemical Analysis to Determine "Free" PbO

Specimen (ZrO_2 Specifications)	Weight % "Free" PbO After Calcining at 900°C For 2 Hours (σ=±0.1%)
Tizon-Lot 367m	
As received	1.1
3 jet mills	1.0
Harshaw-Lot 1-75	
As received	0.6
3 jet mills	0.4
Attritor milled	0.3
Harshaw-Lot 5-76	
As received	0.6
3 jet mills	0.4
Attritor milled	0.5

Table 4. Grain Size Data for Fired PZTs

Fired PZT Spec.	Ave. Grain Size μm
Tizon 367m	
As received	8.9
Jet milled	4.2
Harshaw 1-75	
As received	8.26
Jet milled	3.90
Attritor milled	3.10
Harshaw 5-76	
As received	8.14
Jet milled	4.08
Attritor milled	3.25

Microstructures of the ceramics produced from the as-received and attrition milled powders from Harshaw Lot 5-76 are shown in Fig. 2.

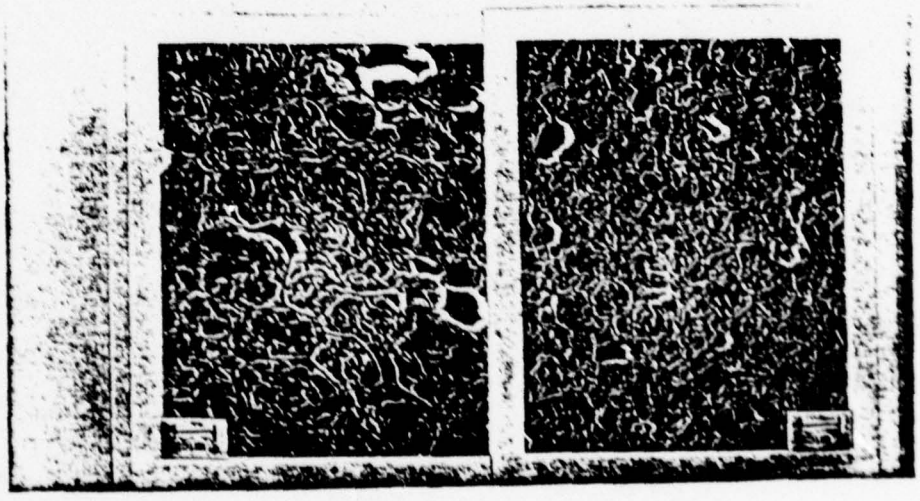

Fig. 2. Harshaw 5-76 as-received; Harshaw 5-76 attritor milled.

Table 4 lists the average grain sizes determined by a linear intercept technique for the different ceramics. As can be seen, there is the same result in all cases--the as-received ceramics had a significantly larger grain size than those produced from milled powders. In each lot the attrition milled powders had the finest grain size. While it is only speculation at this point, it seems likely that the differences in grain size between the as-received and milled powders must be due to reactivity differences during calcining. It is presumed that the absence of the low melting $PbTiO_3$ phase and the presence of a PZT phase with higher ZrO_2 content would lead to a situation where less liquid phase was present during final sintering. This could result in a finer grained product.

Table 5 shows the fired density and dielectric properties of the different ceramics. The densities are essentially the same for all specimens. The weak field K and tan δ values measured using unpoled specimens are in general agreement with those for ceramics of the same composition reported by Berlincourt et al.[10]. There were, however, significant differences in K between as-received lots and as a function of milling. Some of the differences can be attributed to grain size effects, but different phase combinations present as a result of reactivity differences must account for some of the variations.

Table 5. Density and Electrical Data for $PbZr_{0.55}Ti_{0.45}O_3$

Specimen (ZrO_2 Spec.)	Ave. Density* of Fired Discs $kg/m^3(x10^{-3})$	Ave. Dielectric† Constant (K)	Ave. Dielectric Loss (Tan δ)
Tizon Lot 367m			
As received	7.63	534 ± 16	.0026
3 jet mills	7.62	501 ± 8	.0036
Harshaw Lot 1-75			
As received	7.69	641 ± 16	.0033
3 jet mills	7.64	523 ± 13	.0040
Attritor mill	7.64	549 ± 13	.0043
Harshaw Lot 5-76			
As received	7.66	568 ± 13	.0031
3 jet mills	7.62	496 ± 15	.0041
Attritor mill	7.60	547 ± 11	.0048

*All density measurements are geometrical and were randomly checked using a mercury porosimeter.

†All electrical measurements were made at 22°C and 1 MHz.

CONCLUSIONS

We have shown that high-energy milling of different ZrO_2 powders used to produce PZT ceramics can have a significant effect on the ceramics' microstructure and electrical properties. Characterization of the powders showed that there was little difference in composition and particle morphology before and after milling. Qualitatively the milled powder appeared to contain fewer agglomerates.

The reactivity of the ZrO_2 powders with the other oxides during calcining was increased by milling. In all the calcines produced from milled powders, only PZT was detected.

The results of this work strongly suggest that the variability of the piezoelectric properties of commercial PZT ceramics is related to the reactivity of the ZrO_2 used in the process. More work is needed to determine the relation between the reactivity of the powders, the phases produced during calcining, and the resultant ceramic properties.

Acknowledgments

This work was carried out under Contract N0014-76-C-0515 under the joint sponsorship of the Office of Naval Research and the Defense Advanced Research Projects Agency.

References

1. D.A. Buckner and P.D. Wilcox. Am. Ceram. Soc. Bull. 51[3]218-222 (1977).
2. Y. Matsuo and H. Sasaki, J. Am. Ceram. Soc. 48[6]289-291 (1965).
3. V.M. McNamara, J. Can. Ceram. Soc. 33, 102-119 (1964).
4. J.H. Rosolowski, R.H. Arendt and J.W. Szymanszek, Annual Report, G.E. Schenectady, NY, Contract No. N0014-76-C-0659, Office of Naval Research (1977).
5. L.E. Cross, J.V. Biggers and R.E. Newnham, Semi-Annual Report, Contract No. N00014-76-C0515, Office of Naval Research (1977).
6. B. Jaffe, W.R. Cook and H. Jaffe, Piezoelectric Ceramics, Academic Press, NY (1971).
7. J. Lebiedzik, R.G. Burke, S. Troutman, G.G. Johnson and E.W. White. Scanning Electron Microscopy, Part 1, 26-33 (1973).
8. F.Y. Wang. Treatise on Materials Science and Technology, vol.9, Academic Press, NY (1976).
9. A.E. Robinson and T.A. Joyce. Trans. Brit. Ceram. Soc. 61[2] 85-93 (1962).

10. D. Berlincourt, C. Canolik and H. Jaffe. Proc. IRE, 48, 220-229 (1960).

The Effect of Post Casting Pressing On the Density of Tape Cast PZT

J.V. Biggers, T.R. Shrout and W.A. Schulze

Materials Research Laboratory
The Pennsylvania State University
University Park, Pennsylvania 16802

Abstract

The fabrication of piezoelectric devices using ceramic tape requires careful control of green density. The feasibility of using a post casting pressing process to increase the green density has been investigated. Results of increasing tape green density on fired density, ceramic microstructure and some electrical properties of a commercial PZT formulation are described.

1. INTRODUCTION

Tape casting is widely used in the manufacture of ceramic capacitors[1] and substrates for microelectronic circuits[2]. In this process a suspension of ceramic powders in a liquid is cast on a smooth surface such as glass, stainless steel, or plastic. Evaporation of the liquid produces a thin, flexible ceramic loaded plastic sheet that can be cut into the desired shape and fired to produce the finished ceramic parts. The microstructure and properties of the cast parts are usually indistinguishable from parts fabricated in other ways such as cold pressing or extrusion.

At present little use is made of tape casting in the fabrication of piezoelectric devices. From a conceptual standpoint, however, assembly of piezoelectric devices from tape cast ceramics seems to offer some definite advantages. Lamellar heterogeneous structures consisting of either layers of ceramic of the same composition with internal electrodes, alternating layers of ceramics of different composition and external electrodes, or alternating layers of ceramic of different composition with internal electrodes could be expected to have interesting piezoelectric properties; for instance by proper choice of internal electrode configurations and (or) ceramic layer compositions it should be possible to produce devices with one or more of the following characteristics: easier poling, better resistance to depoling, improved temperature stability, and better piezoelectric response.

To produce these device configurations, it will undoubtedly be necessary to carefully control the particle size and shape distribution of the powders and the green density of the tape. This is necessary to obtain acceptable fired densities consistent with firing schedules that are suitable for cofiring of internal metal electrodes or ceramic layers of different composition.

To effect this control of the sintering kinetics would normally require painstaking characterization and communition of the ceramic powders and considerable manipulation of the solvents, binders, plasticizers and deflocculants of the liquid suspension system plus changes in milling and casting procedures.

If the green density of the tape is the controlling factor in determining the sintering behavior a simpler and possibly more effective alternative process is suggested--post casting pressing. If this technique can be used to increase the green density and if the green density determines shrinkage and final density, then it is possible that a "standard" casting procedure can be used to produce tapes with lower than desired green densities which can then be raised to the desired value by pressing.

In the work described here we have investigated the effect of post casting pressing on properties of tapes produced from a commercial lead zirconate-lead titanate (PZT) formulation.

2. EXPERIMENTAL

A commercial organic liquid suspension system* (binder) and PZT powder† were used to produce the tape for these experiments.

To determine the effect of powder size distribution on the pressing behavior a portion of the PZT powder was passed through a high energy mill††.

The particle size and shape distribution of the powders was determined using a computer assisted scanning electron microscope and a technique described by Lebiedzik et al.[3]. The process involves computer control of the SEM raster which generates both a particle size distribution and a shape distribution based on a set of eight orthogonal diameters imposed on each particulate in a large sample.

*Claydon Binder B-62, Lot 117, Cladar Inc., 11404 Sorrento Valley, San Diego, Ca. 92121.
†Ultrasonic powder PZT-401, Ultrasonic Powders, Inc., 2383 S. Clinton Ave., South Plainsfield, N.J. 07080.
††Fluid Energy Mill, Fluid Energy Products, Hatfield, Pa.

Figure 1 shows the size and shape distribution of the as received powder. The average diameter is about 4 μm and the grain shapes are somewhat elongated.

Figure 2 shows the size and shape distribution of the as received powders after jet milling. The average particle size has been shifted to about 2.5 μm with a much sharper distribution. The shapes are more nearly spherical, which suggests that much of the size change was due to agglomerate breakup.

Suspensions of four different powder/organic binder ratios were produced by mixing the powders and liquid in small polyurethane jars for 48 hours. The normal mill charge consisted of Borundum cylinders, 0.5" dia, amounting to about 25 v/o of the jar.

Typical viscosities of the slips are listed in Table 1.

Tapes were cast on a laboratory casting machine which utilizes a moving glass plate as the casting surface. The fixed doctor blade assembly is based on design by Runk and Andrejco[4] which utilizes two blades and double slip hoppers to minimize the effects of hydrostatic head variation and surface tension.

Casting was done at the rate of 0.4"/sec with blade heights of 0.025". Tape thickness after drying was greater than 0.01".

The dried tapes were cut into 1" squares and pressed at pressures ranging from 850 to 38000 psi (5.87×10^6 - 2.62×10^8 n/m^2) using a small hydraulic press. Green density of the tapes before and after pressing was calculated from thicknesses measured using a dial micrometer gauge.

Sintering was done in closed high purity alumina crucibles. The tapes were placed on fired setters of the same composition and a small amount of lead zirconate was added as a source of PbO. A silicon carbide resistance furnace with a programable controller was used for all firings. The heating rate was 200°C/hr and the samples were cooled with power off.

Average Diameter Distribution (# Percent)

Class Limit (μm)	0 1 2 3 4	Class %
	-----0----0----0----0	
0.40	[	0.00
0.63	[	0.21
1.00	[**	3.10
1.60	[******	12.27
2.50	[**************	27.36
4.00	[******************	35.05
6.30	[**********	19.53
10.00	[*	2.33
16.00	[	0.07
25.00	[	0.07

Min/Max Diameter Distribution

Class Limit	0 1 2 3 4	Class %
	-----0----0----0----0	
0.050	[	0.14
0.100	[	0.35
0.150	[	0.28
0.200	[	0.49
0.250	[*	1.48
0.300	[*	2.96
0.350	[**	3.39
0.400	[**	3.88
0.450	[***	6.14
0.500	[***	6.56
0.550	[******	11.92
0.600	[******	11.21
0.650	[*******	14.17
0.700	[******	11.42
0.750	[******	11.99
0.800	[****	8.25
0.850	[**	4.23
0.900	[	0.99
0.950	[	0.14

Fig. 1. Particle Size Analysis for PZT-401.

Average Diameter Distribution (# Percent)

Class Limit (μm)	0 1 2 3 4 5	Class %
	-----0---- 0----0----0----0	
0.40	[	0.00
0.63	[	0.46
1.00	[****	7.82
1.60	[**********	24.92
2.50	[**************************	49.66
4.00	[*********	16.95
6.30	[	0.11
10.00	[	0.00
16.00	[	0.06

Min/Max Diameter Distribution

Class Limit	0 1 2 3 4 5	Class %
	-----0---- 0----0----0----0	
0.050	[	0.00
0.100	[	0.11
0.150	[	0.57
0.200	[*	1.14
0.250	[	0.80
0.300	[*	1.31
0.350	[*	1.60
0.400	[*	2.23
0.450	[**	3.31
0.500	[**	3.20
0.550	[****	7.59
0.600	[****	7.99
0.650	[*******	13.13
0.700	[******	11.70
0.750	[********	16.38
0.800	[*******	14.10
0.850	[******	11.30
0.900	[**	3.31
0.950	[	0.23

Fig. 2. Particle Size Analysis for Jet-Milled PZT-401.

Table I. Viscosity for Different Powder/Organic Binder Slip Systems

Powder/Organic	Viscosity (cps)*
74/26 wt%	2250
65/35 wt%	330
50/50 wt%	170
34/66 wt%	110
†74/26 wt%	1000

*Viscosities measured using a Brookfield viscometer at 22°C ± 1°C, with spindle #6 at 100 rpm.

†Jet milled powder used.

3. RESULTS AND DISCUSSION

Figure 3 shows the results of the pressing experiments. Each point on the curve is an average of at least 6 separate pressings.

For all powder/organic ratios studied the pressing behavior was essentially the same--the initial densification rate was high and then leveled off. The pressure at which the densities reached a maximum was inversely related to the amount of organic in the tape.

Table II shows the initial and maximum green densities of the tapes as a function of the powder/organic ratios. For the as received powders the maximum increase in density decreased with increasing organic content. The jet milled powder with the smaller particle size and more nearly spherical shapes showed the largest increase in density.

DTA studies of the Cladan binder system showed that about 10 w/o of the binder--a high molecular weight polymer--would be retained after normal drying of the tapes. This means that increasingly large amounts of organic are retained in the tape as the powder/organic ratios decreased.

The compaction behavior suggests that the polymer influences the compaction mechanism(s). At high polymer contents the samples quickly reached their maximum density and further pressure caused only elastic deformation. With decreasing amounts of polymer, powder particle breakdown and rearrangement was probable and compaction continued to higher pressures resulting in higher green densities.

The importance of the powder particle size and shape distribution on compaction behavior is seen by comparing the data for tapes made with the as received and jet milled powders. The jet milled powders had a smaller average particle size, a narrower size distribution, and were more nearly spherical. Tapes made with these powders had a larger percentage increase in density, and the compaction process continued to higher pressures.

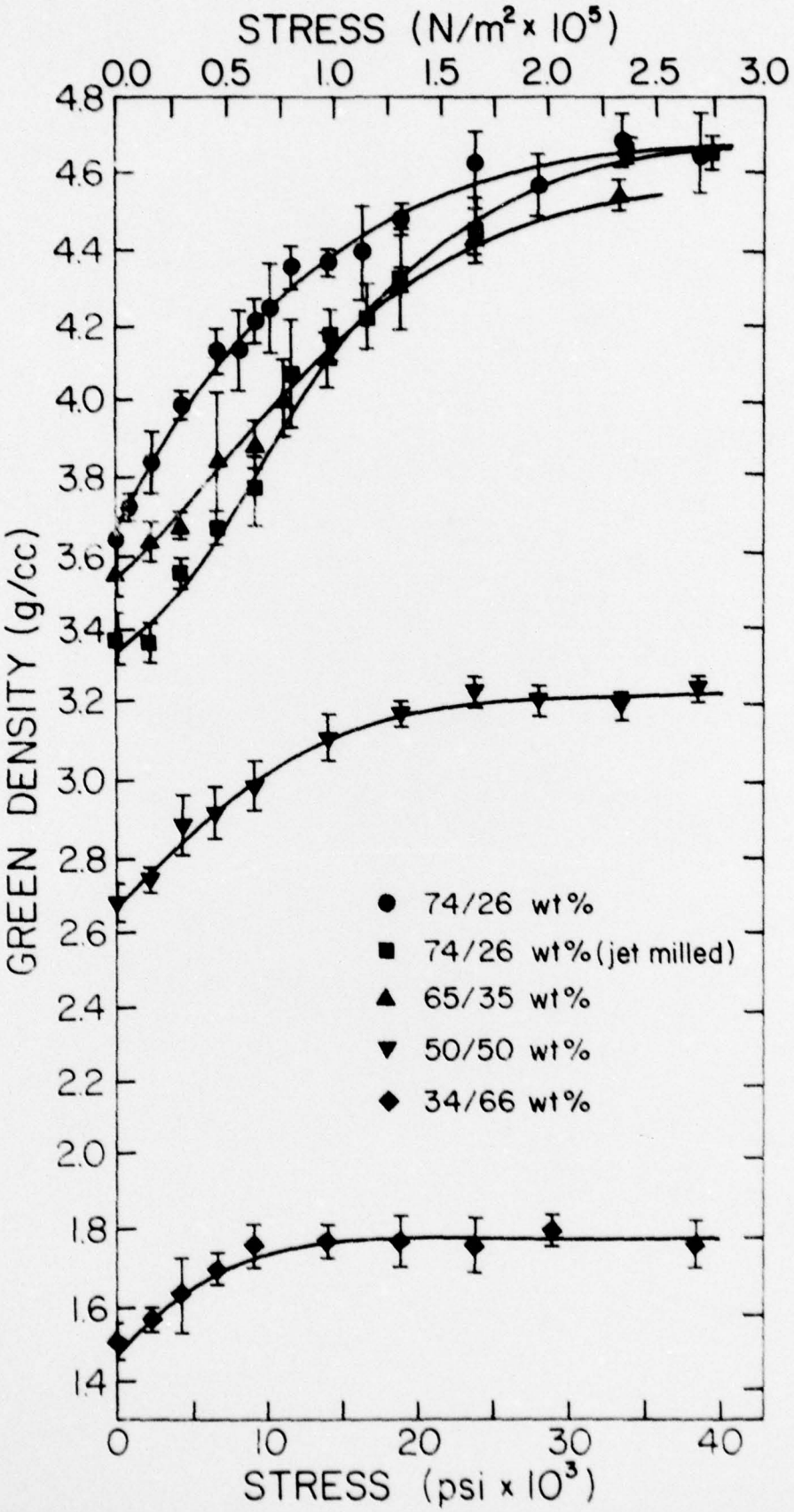

Fig. 3 Green density as a function of stress for different powder/organic tape ratios.

Table II. Initial and Maximum Green Densities of Tapes as a Function of the Powder/Organic Ratios.

Powder/Organic	Initial Density (g/cc)	Maximum Pressed Density (g/cc)	% Increase
74/26 wt%	3.63	4.65	28.1%
65/35 wt%	3.54	4.54	28.2
50/50 wt%	2.68	3.24	20.9
34/66 wt%	1.56	1.80	15.4
74/26 wt%*	3.36	4.66	38.7

*Jet milled powders used.

Typical SEM micrographs of a tape before and after pressing are shown in Fig. 4. The closing of porosity during pressing is evident.

Initial firing studies have been limited to the tapes with the highest as cast densities--those with a powder/organic ratio of 74/26 w/o. Four firing temperatures, 1220, 1240, 1270, and 1325°C with hold times of 1.5 hours were used.

For the range of green densities investigated (3.6 and 4.7 gm/cc) the relation between green and fired densities is essentially linear for each of the firing temperatures, as shown in Fig. 5. The slope of the lines decreases with firing temperature and then apparently converge to values of green density and fired density of ~4.8 and 7.7 gm/cc.

Aside from the amount of porosity the microstructures of the tapes pressed to the different green densities and fired at the same temperature were essentially the same. Firing of higher temperatures led to an increase in grain size. Typical microstructures for the 1220° and 1335°C firings are shown in Fig. 6. The average grain size determined using a linear intercept technique was 2.2 μm for 1220°C, 2.8 μm for 1240°C, 5.6 μm for 1270°C, and 7.8 μm for the 1325°C firings.

Dielectric and piezoelectric properties varied little with pressing pressure. Typical values of weakfield K and tan δ measured at 1KHz and d_{33}[†] determined 24 hours after poling of 3000 v/cm, 100°C for 2 min are shown in Table III for ceramics pressed to the highest green densities.

While there is an apparent grain size dependence of the permittivity and d_{33}, the values are all within the manufacturer's specifications.

[†]Piezoelectric coefficient.

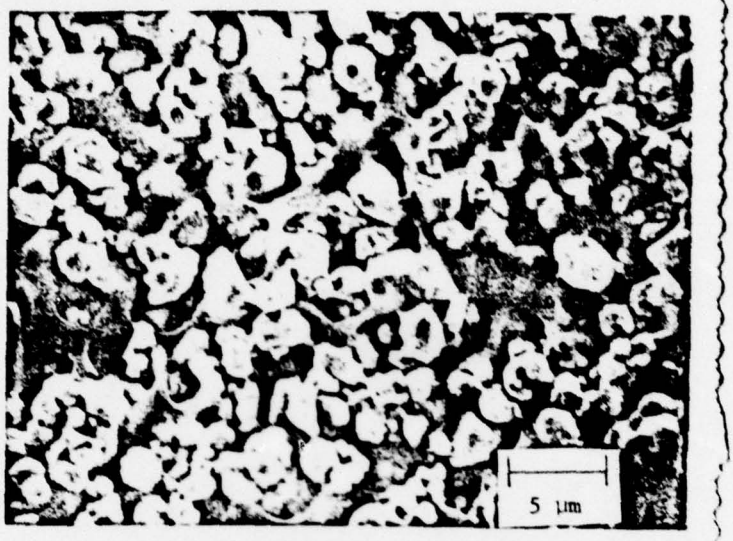

Fig. 4a. Micrograph of PZT-401, 74 wt% dried green tape unpressed.

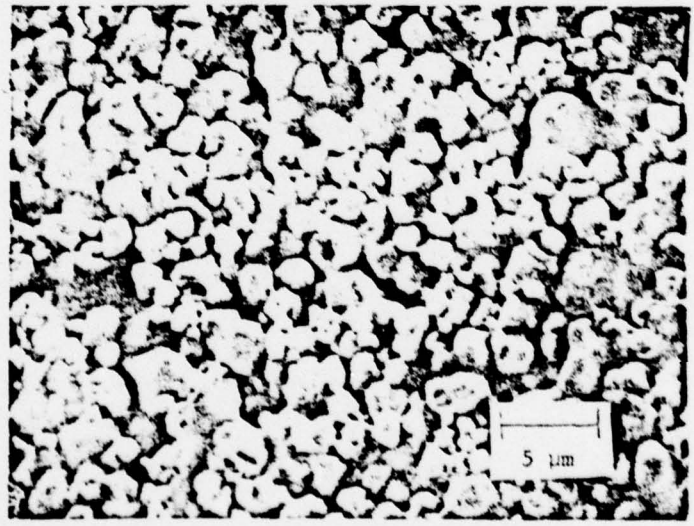

Fig. 4b. Micrograph of PZT-401, 74 wt% dried green tape pressed at ~16,500 psi.

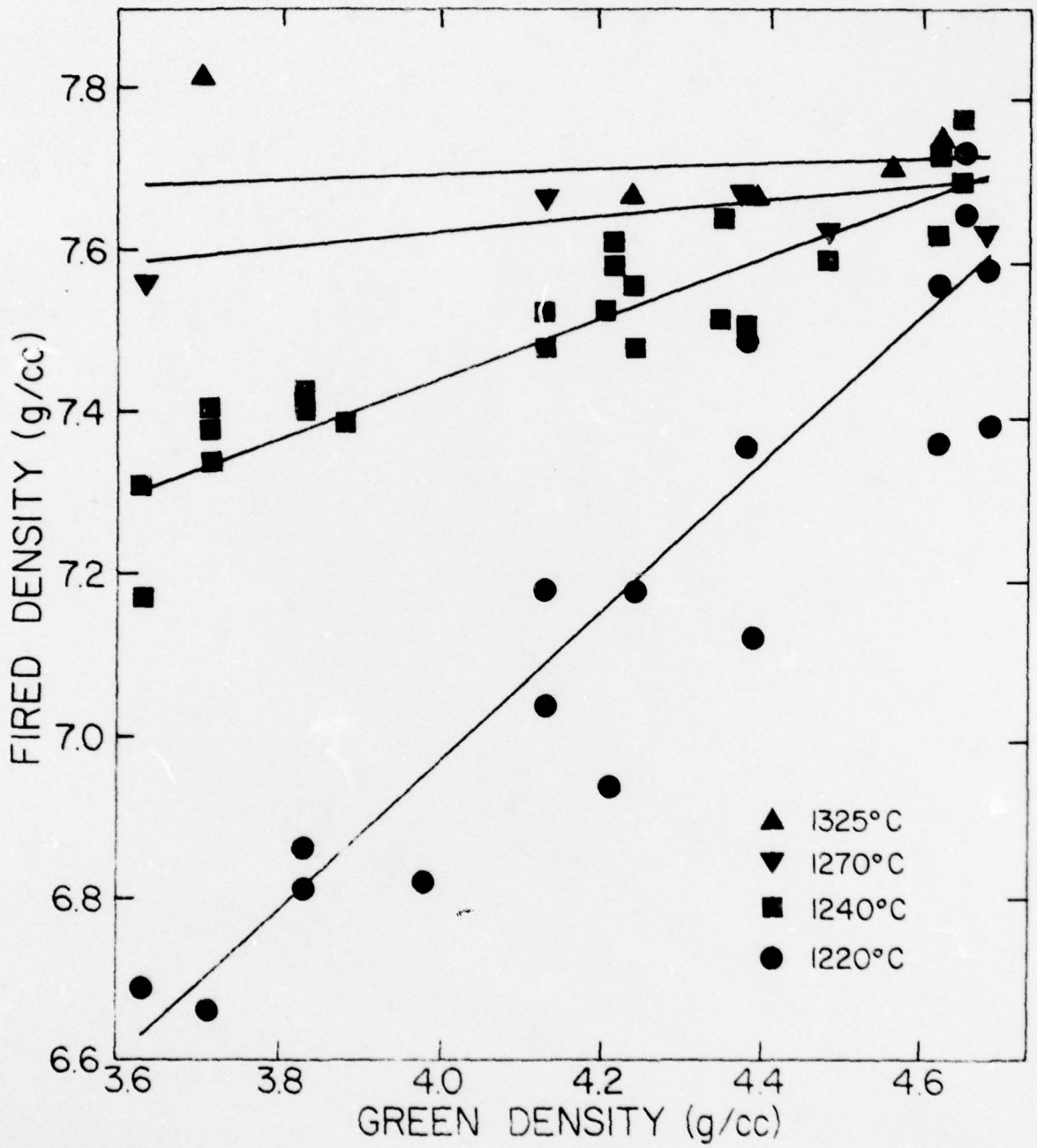

Fig. 5 Fired density vs green density for tapes with a 74/26 w/o powder/organic ratio fired at 1220, 1240, 1270, and 1325°C with hold times of 1.5 hours.

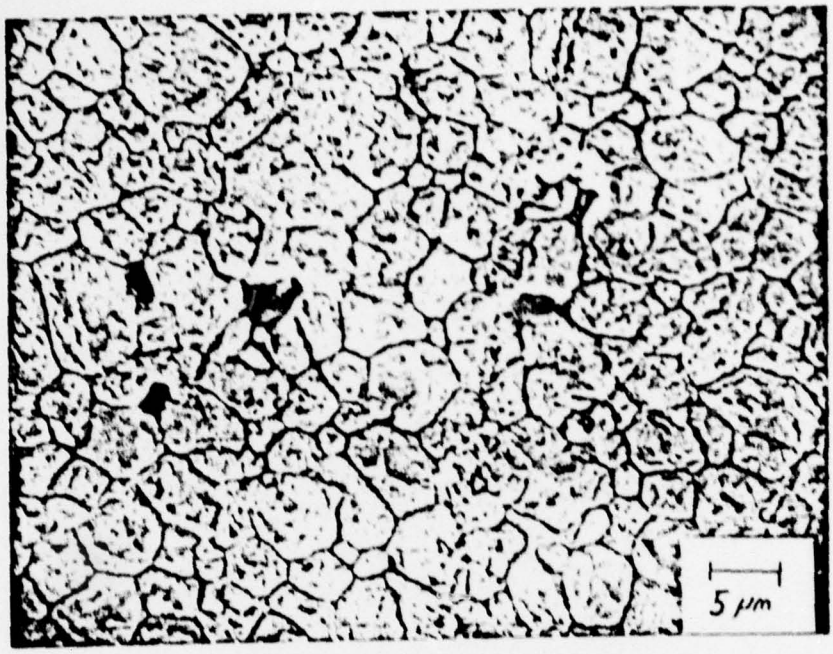

Fig. 6a. Micrograph of PZT-401, 74 wt% tape (4.6 g/cc green density) fired at 1220°C, 1.5 hours.

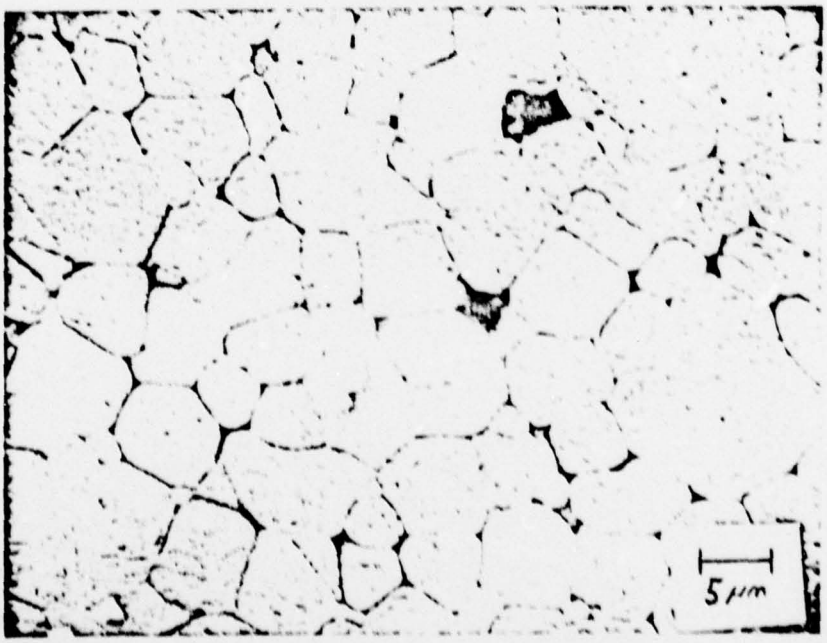

Fig. 6b. Micrograph of PZT-401, 74 wt% tape (4.6 g/cc green density fired at 1325°C, 1.5 hours.

Table III. Typical Values of Dielectric Constant (K) on Tan δ and Piezoelectric Coefficient d_{33} for PZT Samples Fired to Maximum Densities.

Firing Temperature	Dielectric Constant(K)*	Tan δ	d_{33}† ($\times 10^{12}$ n/c)
1220°C	1213	.0045	216
1240°C	1386	.0086	361
1270°C	1406	.0240	273
1325°C	1431	.0234	385
1300-1330°C††	1350		290

* Dielectric constant determined using Hewlett Packard (Model 4270A) Automatic Capacitance Bridge at 1KHz.

† Piezoelectric coefficients determined using Berlincourt (Model 3300 d_{33} Meter at 100 Hz.

†† Ultrasonic Inc. commercial data for PZT-401 fired 1300-1330°C (.5-1.5 hrs).

3. SUMMARY AND CONCLUSIONS

In this work we have shown that post casting pressing can be used to increase the as-cast density of green tape.

It has further been established that over a wide range of firing conditions a linear relation exists between the green and fired density of the tapes.

At present the exact reasons for the relationship and the significance of the convergence to a point are not clear to the authors.

The microstructure of the fired tape, the permittivity and d_{33} values are not much affected by the pressing process. Both the microstructure and electrical properties are comparable to those of parts produced from pressed discs.

An interesting point, however, is the fact that tape casting has a pronounced effect on the sintering kinetics of the PZT.

Discs of PZT-401 pressed to green densities of 4.7 gm/cc will not fire to the 7.7 gm/cc density at temperature below about 1320°C using the same firing schedule as used for the tape cast parts. Tape cast parts of somewhat lower green density will attain this density when fired at 1220°C.

Preliminary particle size and surface area measurements show little difference between the as received PZT powders and the powders in the slip used to cast the tape. It is difficult to speculate about the causes of the increased powder reactivity in the tapes without a more thorough characterization of the powders.

At present work is in progress to extend the green density-fired density data to both higher and lower values of green density.

An effort will be made to use current sintering models to explain the linear relationship of the green and fired densities.

Additional work is planned on the characterization of the powders in the slip and an analysis of sintering will be made in attempt to explain the enhanced sintering that occurs for the tape cast parts.

References

1. Howett, G.N., R.G. Breckenridge and J.M. Brownlow, "Fabrication of Thin Ceramic Sheets for Capacitors," J. Am. Cer. Soc. 30(8)237-42 (1947).

2. Shanefield, D.J. and R.E. Mistler, "Manufacture of Fine-Grained Alumina Substrates for Thin Films," Western Electric Engineer 15(8)26-31 (1971).

3. J. Lebiedzik, R.G. Burke, S. Troutman, G.G. Johnson, Jr. and E.W. White. "New Methods for Quantitative Characterization of Multiphase Particulate Materials Including Thickness Measurement," Scanning Electron Microscopy, Part 1, 26-33 (1973).

4. R.E. Runk and M.J. Andrejco, "A Precision Tape Casting Machine for Fabricating Thin Organically Suspended Ceramic Tapes," Am. Cer. Soc. Bull. 54 (2) 199-200 (1975).

Unclassified

SECURITY CLASSIFICATION OF THIS PAGE (When Data Entered)

REPORT DOCUMENTATION PAGE		READ INSTRUCTIONS BEFORE COMPLETING FORM
1. REPORT NUMBER	2. GOVT ACCESSION NO.	3. RECIPIENT'S CATALOG NUMBER
4. TITLE (and Subtitle) CERAMIC PIEZOELECTRIC TRANSDUCERS		5. TYPE OF REPORT & PERIOD COVERED Annual Summary Report Jan. 1, 1977 to Dec. 31, 1977 6. PERFORMING ORG. REPORT NUMBER
7. AUTHOR(s) L.E. Cross, J.V. Biggers, R.E. Newnham		8. CONTRACT OR GRANT NUMBER(s) N00014-76-C-0515
9. PERFORMING ORGANIZATION NAME AND ADDRESS Materials Research Laboratory The Pennsylvania State University University Park, PA 16802		10. PROGRAM ELEMENT, PROJECT, TASK AREA & WORK UNIT NUMBERS
11. CONTROLLING OFFICE NAME AND ADDRESS Office of Naval Research Ballston Tower Arlington, VA 22217		12. REPORT DATE 13. NUMBER OF PAGES 150
14. MONITORING AGENCY NAME & ADDRESS(if different from Controlling Office) Dr. A.M. Diness, Room 619 Ballston Tower, 800 N. Quincy Street Arlington, VA 22217		15. SECURITY CLASS. (of this report) Unclassified 15a. DECLASSIFICATION/DOWNGRADING SCHEDULE

16. DISTRIBUTION STATEMENT (of this Report)

Approved for Public Release; Distribution Unlimited

17. DISTRIBUTION STATEMENT (of the abstract entered in Block 20, if different from Report)

18. SUPPLEMENTARY NOTES

19. KEY WORDS (Continue on reverse side if necessary and identify by block number)

Piezoelectric, Ceramic, Transducer, Ferroelectric, Electrostrictive, Dielectric

20. ABSTRACT (Continue on reverse side if necessary and identify by block number)

This report documents work performed during the period January 1 to December 31, 1977 under joint ONR-DARPA sponsorship. This period covers the second year of a three year program focused upon the tasks associated with the development of new and improved materials for ceramic piezoelectric transducers, and with improving the understanding of the processing and properties of present PZT ceramics.

(Over)

Next page →

DD FORM 1 JAN 73 1473 EDITION OF 1 NOV 65 IS OBSOLETE
S/N 0102-014-6601

Unclassified

SECURITY CLASSIFICATION OF THIS PAGE (When Data Entered)

A major part of the effort has been concerned with the development of new techniques for the fabrication of diphasic ceramic and ceramic:plastic composites and with investigation of the manner in which local and macroscopic symmetry and phase interconnection (connectivity) controls the coupled elasto-electric (piezoelectric) and thermo-elasto-electric (pyroelectric) properties of the composite. Replicating a natural microstructure of desired connectivity, a new type of flexible ceramic elastomer composite has been developed which exhibits g_{33} constants over an order of magnitude larger than PZT and has interesting potential for many passive voltage generation applications such as in hydrophones and towed arrays.

Tape casting (doctor blade) methods are being used to explore a wide range of potentially interesting lamellar heterogeneous systems with ferroelectric, antiferroelectric and interleaved electrode configurations. New pretreatments of the cast tapes are being studied to equalize shrinkage in the different compositions during firing and poling and property studies are now in progress for a number of these new composite systems.

Electrostriction transducers in the ferroelectric relaxor family $Pb_3MgNb_2O_9$:$PbTiO_3$ have been studied, and in cooperation with Corning Research Center extruded multi-element transducer structures incorporating these materials are being investigated.

The ADAGE computer graphics faciilty at Penn State is being used to develop a family of Elastic Gibbs functions for the PZT solid solution system and to study the full three dimensional polarization surfaces in the vicinity of the morphotropic phase boundary.

Processing studies have been performed on PZT and on various relaxor ferroelectric formulations. Preparation, calcining, fabrication and densification procedures have had to be developed both for conventional single phase, and for the more unusual diphasic systems presently under study.